Western University

Scholarship@Western

Electronic Thesis and Dissertation Repository

1-26-2022 9:00 AM

The Influence of Frontal and Axial Plane Deformities on Contact Mechanics during Squatting: A Finite Element Study

Yidan Xu, *The University of Western Ontario*

Supervisor: Willing, Ryan T., *The University of Western Ontario*
A thesis submitted in partial fulfillment of the requirements for the Master of Engineering Science degree in Mechanical and Materials Engineering

Follow this and additional works at: https://ir.lib.uwo.ca/etd

Part of the Biomechanical Engineering Commons

Recommended Citation

Abstract

Knee Osteoarthritis (KOA) is a degenerative joint disease and a leading cause of disability worldwide. Lower limb malalignment was a risky factor leading to KOA, altering the load distributions. This study aimed to study the influence of knee deformities on knee contact mechanics and knee kinematics during squatting. A full-leg squat FE model was developed based on general open-source models and validated with in vivo studies to investigate the outputs under frontal malalignment (valgus 8° to varus 8°) and axial malalignment (miserable malalignment 30°). As a result, Varus-aligned and miserable aligned models increased medial tibiofemoral force and lateral patellar contact pressures, while the valgus-aligned model increased lateral tibiofemoral force medial patellar contact pressures with no effects on total contact loads. The Model with a higher medial force ratio (medial force/total force) induced a higher internal tibial rotation. In conclusion, we recommended that patients with knee malalignment be taken care of alignments in both frontal and axial planes.

Keywords

Summary for Lay Audience

Knee Osteoarthritis (KOA) is a degenerative joint disease and a leading cause of disability around the world. Lower limb malalignments in the frontal and axial planes were risky factors leading to KOA, as it altered the force and stress distributions. To date, the influence of malalignment on load and stress distributions has not been investigated in both joints: tibiofemoral and patellofemoral joints using computational studies.

This study aimed to study the influence of knee malalignment in the frontal plane and axial plane on knee contact mechanics in tibiofemoral and patellofemoral joints and knee kinematics during a typical daily activity—squatting. To achieve this, a full-leg squat FE model was developed based on an open-source FE model and a general musculoskeletal model and validated with in vivo studies using parametric studies. Then, the model was used to investigate the outputs under frontal malalignment ranging from valgus 8° to varus 8°and axial malalignment with combined 30° femoral anteversion and 30° external tibial torsion (miserable malalignment). As a result, varus-aligned and miserable aligned models increased medial force while the valgus-aligned model decreased medial force. In contrast, malalignments showed no effects on total contact force. In addition, the model with a greater Q-angle (quadriceps angle) increased the lateral patellar contact pressures, while the model with a lower Q-angle increased the medial patellar contact pressures. According to rotational kinematics in results, models with a higher medial force ratio (medial force/total force) induced higher internal tibial rotations. In conclusion, we recommended that patients with knee malalignment be taken care of alignments in both frontal and axial planes.

Co-Authorship Statement

Chapter 1: Yidan Xu − wrote manuscript

Ryan Willing − reviewed manuscript

Chapter 2: Yidan Xu − wrote manuscript

Ryan Willing − reviewed manuscript

Chapter 3: Yidan Xu − study design, data collection, interpreted results, wrote manuscript

Ryan Willing − study design, interpreted results, reviewed manuscript

Chapter 4: Yidan Xu − study design, data collection, interpreted results, wrote manuscript

Ryan Willing − study design, interpreted results, reviewed manuscript

Chapter 5: Yidan Xu − wrote manuscript

Ryan Willing − reviewed manuscript

Acknowledgments

First and foremost, I would like to express many thanks to my supervisor Prof. Ryan Willing. You were always supportive and super patient whenever I faced problems or felt lost. Thanks to your assistance and guidance, I finished my FE simulations and thesis writing.

Special thanks to the Open Knee development team and the study of Spencer Wangerin from Cal Poly. Your contributions to the open-source finite element knee joint at SimTk database played a vital role in this study.

Lastly, I would like to thank my mom and dad. Although you have no idea about knee biomechanics and what I am studying, you always encourage and love me.

Table of Contents

List of Tables

List of Figures

List of Appendices

Chapter 1

1 Introduction

1.1 Problem

Knee Osteoarthritis (KOA) is a degenerative joint disease and a leading cause of disability in the United States and around the world [1]. Significantly, KOA affects 37.4% of adults over 60 years old [2] and has been more prevalent since the mid-20th century [3]. The medical treatment of KOA resulted in approximately $81 billion in 2003 and affected over 46 million people in America [4]. Generally, KOA affects two joints - the tibiofemoral joint and patellofemoral joint - and develops slowly over 10-15 years, interfering with daily and work activities [5]. Population studies have identified that KOA results from local mechanical factors acting primarily on articular cartilage, which is susceptible to excessive stress [6-8]. In the development of KOA, cartilage breaks down and subsequently degenerates, causing pain, stiffness or poor mobility. Malalignment of the knee joint substantially alters the load distribution, increasing stress on the medial or lateral compartment and thus inducing the initiation and progression of KOA [10-12]. Therefore, knee joint malalignment is considered as a critical risk factor for KOA onset and progression, possibly associated with other risk factors including age, obesity, genetics and knee laxity [9]. Generally, knee malalignment can happen for many reasons. In some instances, an individual can be born with the situation or it can develop due to diseases, trauma and knee injury [32]. It can also develop over time due to previous surgery [20].

According to previous studies [10,14-15], populations with varus and valgus aligned knees have a higher risk of KOA in the medial and lateral compartment, respectively. Furthermore, torsional deformity (i.e., internal tibial rotation) has been observed with greater varus alignment and knee varus moment during walking, which implies concentrated loading on the medial condyle, leading to medial KOA progression [13]. Malalignment in the coronal and axial plane may also affect ligament strain/stress, inducing ligamentous laxity and knee instability. Knee instability has previously been identified as a risk factor to the onset and progression of OA as knee instability shifts

loaded locations towards unsuitable areas [9]. In these areas, cartilage is more likely to degenerate [6, 19].

Clinically, interventions that correct the excessive loading resulting from knee malalignment such as osteotomies have been performed to treat KOA and relieve pain [16,17]. High tibial osteotomy (HTO) and distal femoral osteotomy (DFO) are effective treatments for medial KOA and lateral KOA, respectively. In addition, rotational osteotomies are treatments for patients with axial plane knee deformities. When a patient with KOA suffers from pain and develops functional limitations, total knee replacement (TKR) is considered to alleviate pain and restore joint function [18]. Frontal alignment in TKA has been shown to be correlated to loosening incidence of prosthesis components, so accurate alignment is a crucial factor for the prevention of loosening [23, 24]. The axial alignment in TKA has been proven to affect the stress distribution and knee kinematics [30, 31]. Typically, surgeons aim for ideal alignment following osteotomies or TKR to maximize osteotomy or implant survival and restore knee functions. Finite element analysis (FEA) with a knee joint model may be useful to identify the influence of different alignment in the coronal and axial planes on knee biomechanics.

1.2 Previous Work

In vivo, the magnitude of contact forces and moments has been measured to analyze the effect of knee deformity during static or dynamic loading [20, 21]. Kutzner et al. measured the contact force value, medial/lateral force ratio and knee moments during single-leg and double-leg support activities using an instrumented total knee arthroplasty (TKA). The varus-valgus alignment angle of patients after TKA surgery was measured using full-leg radiographs to analyze the effect of alignment on contact ratio. Increased medial condyle load was observed in knees with varus alignment [20]. Krackow et al. assessed the knee moments of twenty-four subjects *in vivo* during gait and determined that subjects with tibial rotation deformities had varus alignment and higher varus moments which implies higher medial loading [21]. Direct measurement of contact loading is challenging and limited to a small number of subjects with instrumented TKA. Furthermore, the influence of knee alignment deformities on distributions of contact stress in knee cartilage and ligament forces/strains cannot be identified *in vivo*. However,

in combination with *in vivo* data, musculoskeletal models can investigate the altered stress distributions and ligament forces under variation in the coronal plane alignment and ligament properties during gait [22]. Similarly, in combination with *in vivo* data from subjects during self-selected speed walking, subject-specific finite element models have been used to demonstrate that varus aligned knees put higher stress on the medial compartment while valgus aligned knees put higher stress on the lateral compartment [24]. *In vitro*, the same conclusions have demonstrated varus aligned knees had a higher contact pressure in the medial compartment [25, 26] and varus-valgus malalignment alters knee kinematics [27]. To validate these *in vitro* studies, a scaled musculoskeletal model estimated the effect of variations in alignment on contact stress distributions and ligament strains [29]. In combination with *in vitro* data, a forward-dynamic computational model during a squatting motion was used in this study to estimate the effect of variation in axial plane alignment on ligament strains as well as muscle forces and joint kinematics [28]. In addition, some computational models have studied the isolated effect of alignment on the knee contact force and stress distributions while other factors were controlled for, such as gender, age, weight and height [22, 28, 29].

Previous studies mostly focused on the influence of malalignment during walking. To date, the literature still lacks examples of application of finite element (FE) models to estimate the influence of malalignment in the coronal and axial plane on contact mechanics, especially during squatting. Thus, the FE model in this study was used to predict the contact force, distributions of stress in the tibial and patellar cartilage under coronal and axial plane deformities during a dynamic squatting motion.

1.3 Objectives

The objectives of this thesis were to (1) develop a full leg squat model based on an open-source finite element model and (2) predict the effect of coronal and axial plane knee deformities using the full leg squat FE model. To achieve these objectives, the OpenKnee model was modified to a full leg model using the coordinates of added parts from a musculoskeletal model by reorganizing boundary conditions, constraints and load scenarios. Then, the full leg model was used to perform parametric analysis during squatting and validated with previously published literature. Finally, the altered

3

distributions of contact load and stress and magnitude of muscle force under variations in the coronal and axial plane deformities were investigated using the full leg squatting model. We assumed that the full leg model after parametric analysis and validation was in neutral alignment. It was hypothesized that (1) varus aligned knees would induce a higher medial force ratio; (2) femoral anteversion and external tibial torsion would result in higher stress on lateral patella cartilage.

References

[1] Oliveria SA, Felson, D. T., Reed, J. I., Cirillo, P. A., Walker, A. M. Incidence of symptomatic hand, hip, and knee osteoarthritis among patients in a health maintenance organization. *Arthritis and rheumatism*. 1995;38:1134-1141.

[2] Heidari B. Knee osteoarthritis prevalence, risk factors, pathogenesis and features: Part i. *Caspian J Intern Med*. 2011;2(2):205-212.

[3] Wallace IJ, Worthington S, Felson DT, et al. Knee osteoarthritis has doubled in prevalence since the mid-20th century. *Proc Natl Acad Sci U S A*. 2017;114(35):9332-9336.

[4] Yelin E, Murphy L, Cisternas MG, Foreman AJ, Pasta DJ, Helmick CG. Medical care expenditures and earnings losses among persons with arthritis and other rheumatic conditions in 2003, and comparisons with 1997. *Arthritis Rheum*. 2007;56(5):1397-1407.

[5] Roos EM, Arden NK. Strategies for the prevention of knee osteoarthritis. *Nat Rev Rheumatol*. 2016;12(2):92-101.

[6] Andriacchi TP , Favre J. The Nature of In Vivo Mechanical Signals That Influence Cartilage Health and Progression to Knee Osteoarthritis. *Curr Rheumatol Rep* 2014;16:463–70.

[7] Pelletier JP, Martel-Pelletier J, Howell DS. Etiopathogenesis of osteoarthritis. In: Koopman WJ, ed. *Arthritis and Allied Conditions: A Textbook of Rheumatology*. Baltimore, Md: Williams & Wilkins; 1997:1969-1984.

[8] Sharma L, Song J, Felson DT, Cahue S, Shamiyeh E, Dunlop DD. The Role of Knee Alignment in Disease Progression and Functional Decline in Knee Osteoarthritis. *JAMA*. 2001;286(2):188–195.

[9] Issa SN, Sharma L. Epidemiology of osteoarthritis: an update. *Curr Rheumatol Rep*. 2006;8(1):7-15.

[10] Sharma L, Song J, Felson DT, Cahue S, Shamiyeh E, Dunlop DD. The role of knee alignment in disease progression and functional decline in knee osteoarthritis. *JAMA*. 2001;286(2):188-195.

[11] Cerejo, R., D. D. Dunlop, S. Cahue, D. Channin, J. Song, and L. Sharma. The influence of alignment on risk of knee osteoarthritis progression according to baseline stage of disease. Arthritis Rheum. 46:2632–2636, 2002.

[12] Ford, K. R., G. D. Myer, and T. E. Hewett. Valgus knee motion during landing in high school female and male basketball players. Med. Sci. Sports Exerc. 35:1745–1750, 2003.

[13] Krackow KA, Mandeville DS, Rachala SR, Bayers-Thering M, Osternig LR. Torsion deformity and joint loading for medial knee osteoarthritis. *Gait Posture*. 2011;33(4):625-629.

[14] Sharma L. The role of varus and valgus alignment in knee osteoarthritis. *Arthritis and rheumatism.* 2007;56(4):1044-1047.

[15] Moisio K, Chang A, Eckstein F, Chmiel JS, Wirth W, Almagor O, et al. Varus-valgus alignment reduced risk of subsequent cartilage loss in the less loaded compartment. *Arthritis Rheum.* 2011;63:1002–9.

[16] Akizuki S, Shibakawa A, Takizawa T, Yamazaki I, Horiuchi H. The long-term outcome of high tibial osteotomy: a ten- to 20-year follow-up. *J Bone Joint Surg Br*. 2008;90(5):592-596.

[17] Delgado ED, Schoenecker PL, Rich MM, Capelli AM. Treatment of severe torsional malalignment syndrome. *J Pediatr Orthop*. 1996;16(4):484-488.

[18] Medical Advisory Secretariat. Total knee replacement: an evidence-based analysis. *Ont Health Technol Assess Ser*. 2005;5(9):1-51.

[19] Chaudhari AMW, Briant PL, Bevill SL, Koo S, Andriacchi TP . Knee kinematics, cartilage morphology, and osteoarthritis after ACL injury. *Med Sci Sports Exerc*. 2008;40:215–22.

[20] Kutzner I, Bender A, Dymke J, Duda G, von Roth P, Bergmann G. Mediolateral force distribution at the knee joint shifts across activities and is driven by tibiofemoral alignment. *Bone Joint J*. 2017;99-B(6):779-787.

[21] Krackow KA, Mandeville DS, Rachala SR, Bayers-Thering M, Osternig LR. Torsion deformity and joint loading for medial knee osteoarthritis. *Gait Posture*. 2011;33(4):625-629.

[22] Smith CR, Vignos MF, Lenhart RL, Kaiser J, Thelen DG. The Influence of Component Alignment and Ligament Properties on Tibiofemoral Contact Forces in Total Knee Replacement. J Biomech Eng. 2016;138(2):021017.

[23] Jeffery RS, Morris RW, Denham RA. Coronal alignment after total knee replacement. *J Bone Joint Surg Br*. 1991;73(5):709-714.

[24] Yang NH, Nayeb-Hashemi H, Canavan PK, Vaziri A. Effect of frontal plane tibiofemoral angle on the stress and strain at the knee cartilage during the stance phase of gait. *J Orthop Res*. 2010;28(12):1539-1547.

[25] Agneskirchner JD, Hurschler C, Wrann CD, Lobenhoffer P. The effects of valgus medial opening wedge high tibial osteotomy on articular cartilage pressure of the knee: a biomechanical study. *Arthroscopy*. 2007;23(8):852-861.

[26] Riegger-Krugh C, Gerhart TN, Powers WR, Hayes WC. Tibiofemoral contact pressures in degenerative joint disease. *Clin Orthop Relat Res*. 1998;(348):233-245.

[27] Sobczak S, Dugailly PM, Baillon B, et al. In vitro biomechanical study of femoral torsion disorders: effect on femoro-tibial kinematics. *Clin Biomech (Bristol, Avon)*. 2012;27(10):1011-1016.

[28] Thompson JA, Hast MW, Granger IF, Piazza SJ, Siston RA. Biomechanical effects of total knee arthroplasty component malrotation: A computational simulation. *J Orthop Res.* 2011;29:969–75.

[29] Van Rossom S, Wesseling M, Smith CR, et al. The influence of knee joint geometry and alignment on the tibiofemoral load distribution: A computational study. *Knee.* 2019;26(4):813-823.

[30] Maderbacher, G, Baier, C, Springorum, H. R, Maderbacher, H, Birkenbach, A. M, Benditz, A, Keshmiri, A. Impact of axial component alignment in total knee arthroplasty on lower limb rotational alignment: an in vitro study. *The journal of knee surgery.* 2017;30(04), 372-377.

[31] Moewis, P., Checa, S., Kutzner, I., Hommel, H., & Duda, G.N. Physiological joint line total knee arthroplasty designs are especially sensitive to rotational placement – A finite element analysis. *PLoS ONE.* 2018;13.

[32] Gruskay JA, Fragomen AT, Rozbruch SR. Idiopathic Rotational Abnormalities of the Lower Extremities in Children and Adults. *JBJS Rev.* 2019;7(1):e3.

2 Background

2.1 Knee structure and functions

The knee was formerly considered as a hinge joint, but it is a much more complex structure with numerous ligaments in conjunction with muscles crossing the joint. The knee joint works along with the hip and ankle joints to move and support the body during daily activities. The knee complex is necessary to allow for the alternate actions of mobility and stability. Thus, the knee should be regarded as consisting of two articulations within one capsule: the tibiofemoral joint and the patellofemoral joint. The tibiofemoral joint is between the femoral condyles and the meniscus, as well as the tibial plateaus, while the patellofemoral joint is between the patella and femur.

The patella is the biggest sesamoid bone in the human body and articulates with the femoral sulcus at the anterior part of the distal femur (Figure 2.1.1b) by the patellar tendon and quadriceps tendon (Figure 2.1.1a). The patellar tendon originates from the inferior border of the patella and travels distally to the tibial tubercle. The patellar tendon also travels proximally, wrapping the patella and merges with the quadriceps tendon at the superior anterior area of the patella. Loads on the quadriceps tendon are transmitted to the tibia through the patellar tendon.

(a)   (b)
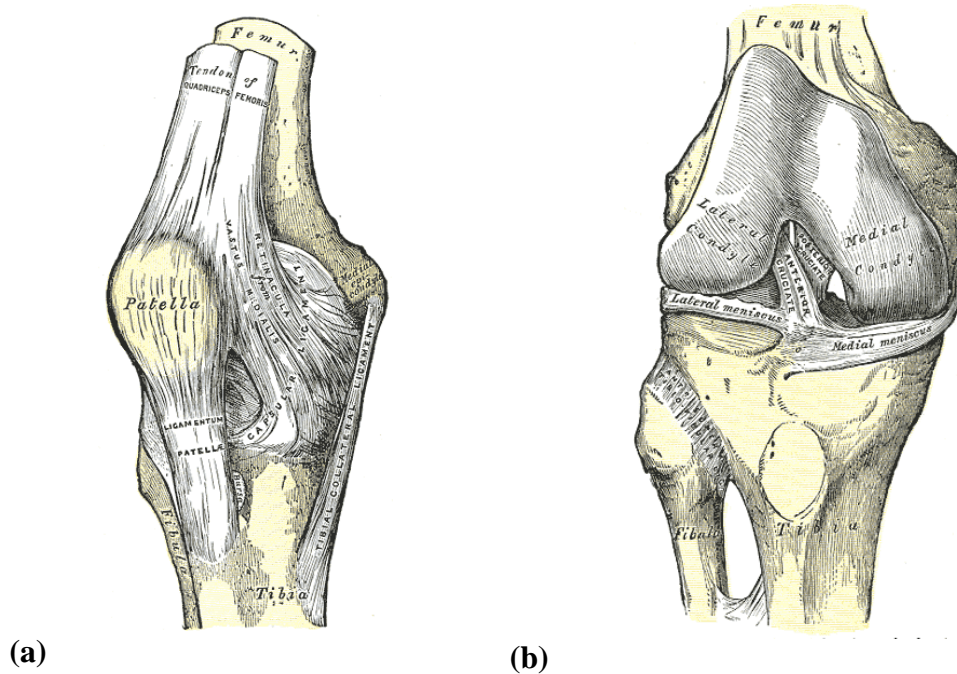
Figure 2.1.1: Anterior view of the right knee joint: (a) with patella and muscles, (b) without patella and muscles (adapted from Gray 1924) [4] (Image use permitted by Creative Commons (https://creativecommons.org/publicdomain/mark/1.0/))

The ends of the distal femur are separated posteriorly by a gap, also called the intercondylar notch, whereas it is an intact bone in the anterior aspect. The medial condyle has a greater radius of curvature and is larger than the lateral condyle [1]. The ends of the proximal tibia are also split by a rough area and two bony spines [4]. The ends of each bone have articular cartilage covering the articulating surfaces. The articular cartilage is a porous solid allowing synovial fluid to permeate it. The articular cartilage and meniscus transmit loads in the tibiofemoral joint, while synovial fluid lubricates the cartilage to reduce wear [2]. The meniscus decreases the load and stress on the articular surface as well as the tibial plateau by increasing the contact area [3]. The meniscus are a pair of C-shaped fibril soft tissues (Figure 2.1.2) lying in the gap between the articular cartilage of the femur and tibia. The motion of the meniscus is restrained by multiple ligaments, such as transverse ligament, posterior meniscofemoral ligament and deep MCL connecting to the surrounding structures, so the meniscus will not be squeezed out under a large compressive load.
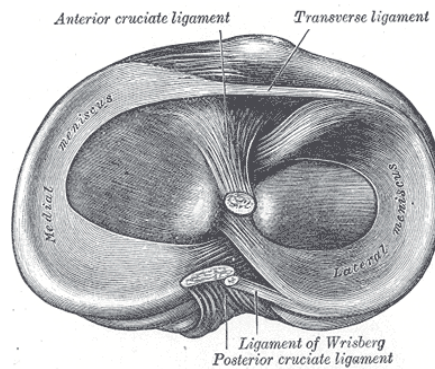
Figure 2.1.2: The top view of the meniscus (adapted from Gray 1924) [4]

(Image use permitted by Creative Commons

(https://creativecommons.org/publicdomain/mark/1.0/))

The femur and tibia are connected by various ligaments. There are four primary ligaments in the tibiofemoral joint. The anterior cruciate ligament (ACL), posterior cruciate ligament (PCL), medial collateral ligament (MCL) and lateral collateral ligament (LCL), each playing an essential role in knee rotation and displacement. The cruciate ligaments are situated at the middle of the joint and cross each other like the letter X. The anterior ligament (ACL) is responsible for restraint of the anterior translation (anterior shear) of the tibia with respect to the femur, whereas the posterior ligament (PCL) provides the primary restraint in posterior translation (posterior shear) of the tibia. Both cruciate ligaments have a role in restraining adduction and abduction rotations and can guide the rotation of the tibia. The medial collateral ligament (MCL) originates from the medial femoral condyle and inserts into the proximal tibia. The deep part of the MCL is inserted into the medial border of the medial meniscus (Figure 2.1.2). The MCL is primarily responsible for resisting valgus rotation. The lateral collateral ligament (LCL) originates from the lateral femoral condyle and travels distally to the fibular head. The LCL plays a critical role in resisting varus rotation.

2.2 Frontal plane Tibiofemoral joint alignment

The tibiofemoral angle is an alignment parameter for the lower limb. The tibiofemoral angle is formed by the intersection of the anatomical axis of the femur and the mechanical axis of the knee. The anatomical axis of the femur (Figure 2.2.1) is defined as

the line that is medially directed from the distal femur to the proximal femur end [5]. The anatomical axis of the tibia is the line directed from the center of the knee joint to the center of the ankle.
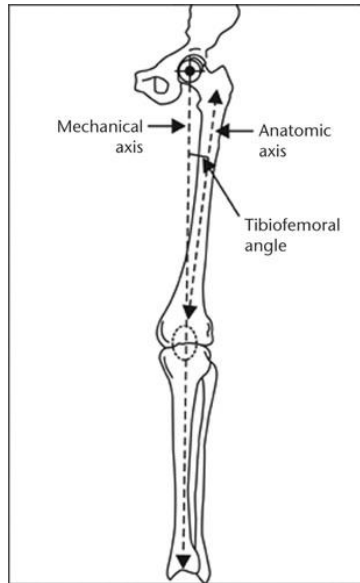
Figure 2.2.1: The tibiofemoral angle is the intersection angle between the mechanical axis and anatomical axis. (adapted from Waterson 2014) [5] (Image use permitted by Creative Commons (https://creativecommons.org/licenses/by/4.0/))

The mechanical axis is defined as the weight-bearing axis of the lower extremity, which passes from the center of the hip to the center of the ankle [5]. In neutral alignment, the mechanical line should pass through the center of the knee between the intercondylar tubercles [8] or within a slight deviation from it. Excessive deviation of the mechanical line to the medial or lateral side of the knee has been taken to indicate the lower extremity is in varus or valgus rotation (Figure 2.2.2) [9].
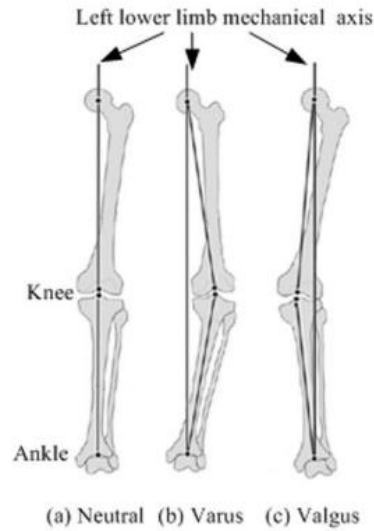
Figure 2.2.2 Frontal malalignment: (a) Neutral aligned knees (b) Varus aligned knees; (c) Valgus aligned knees. (adapted from Xing 2010) [90] (Image use permitted by © 2011 IEEE)

A standard tibiofemoral angle deviation is approximately 3 degrees in healthy patients [6-7], so the femur is angled up to ± 3 degrees off the mechanical axis, creating a slight physiological valgus or varus angle at the knee. When the tibiofemoral angle is greater than 3 degrees, valgus aligned knees exist, also described as genu valgum ("knock kneed"). When the tibiofemoral angle is less than 3 degrees, the resulting abnormal knees are called genu varum ("bow legged"). Deviation of the tibiofemoral angle implies excessive loading on the medial or lateral compartment of the knee [8]. The standard deviation in tibiofemoral angle in osteoarthritis patients is 8 degrees [7]. During double-leg support, the mechanical axis can simply be defined as the line travelling the ground reaction forces up. Therefore, loads through the knee are distributed equally to the medial compartment and lateral compartment. When a deviation of the mechanical axis to the medial or lateral side exists, the deviation increases the compressive load on the medial or the lateral compartment. Abnormally excessive loading on the cartilage can cause damage [11-12], leading to subsequent knee osteoarthritis (KOA). Also, local biomechanical factors can lead to KOA progression due to abnormal loading conditions [10]. Therefore, frontal plane malalignment is associated with the initiation and progression of KOA [13-15]. According to a previous study [15], populations with varus

aligned knees have higher risks of medial KOA, while people with valgus alignment have higher risks of lateral KOA.

2.3 Axial plane lower-extremity alignment

In the axial plane, torsional deformities of the femur or tibia can be measured, as shown in Figure 2.3.1. The femoral version (FV) is the angle between the femoral neck axis and the posterior condylar axis (PCL) [71-73]. If the angle value is positive, the femoral neck axis falls anterior to the PCL, which is called anteversion. Tibial torsion (TT) is the angle between the proximal tibial line and the bimalleolar line [72-73], with a positive value indicating the relative external rotation of the distal tibia to the proximal tibia.
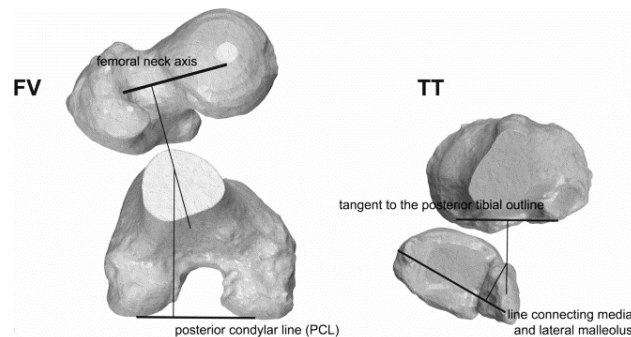
Figure 2.3.1: 3D models of measuring the rotational angles of femur or tibia in the axial plane. FV: femoral version. TT: tibial torsion (Adapted from León-Muñoz 2021 [73]) (Image use permitted by Creative Commons (https://creativecommons.org/licenses/by/4.0/))

Malrotation is quantified and documented by previous clinical examinations, which is helpful for correlative osteotomies. Previous literature [74-78] has reported a wide range of normal femoral anteversion values from 6° to 24° and external tibial torsion values from 26° to 35°, which are measured with CT, as summarised in Table 2.3.1 below. However, standard values are still controversial according to reported angle differences in previous studies [89]. Eckhoff et al. reported that patients with femoral anteversion greater than 23° suffered from anterior pain, while those with femoral anteversion of 18° were pain-free in the control group [74].

Table 2.3.1: Summary of normative rotation values in the axial plane

Resource	Number	Age/years	Femoral anteversion	Tibial torsion
[74]	20	Adult	18°±7°	—
[75]	40	20-40	11.6°±3.5°	26°±4.2°
[76]	10	20-64	12.4°±3.8°	—
[77]	50	Adult males	6.5°±7.7°(R) 5.8°±8.4°(L)	30.9°±7.1°(R) 29.1°±6.9°(L)
[78]	355	Adult	24.1°±17.4°	34.9°±15.9°

Furthermore, a patient with combined excessive femoral anteversion and outward tibial torsion is described as having miserable malalignment [84,85]. In miserable malalignment, the squinting patellae (inward facing patellae) can be observed with the foot facing forward, while external tibial torsion can be seen with the patellae anterior (Figure 2.3.2). Also, extreme outward tibial torsion can be seen when a patient with miserable malalignment externally rotates their hips [85]. As a result, the typical symptom for axial plane malalignment in patients is anterior knee pain, since femoral anteversion and external tibial torsion increase patella tilt and subluxation, resulting in higher lateral patellar contact pressure and forces [74,79]. Also, both femoral anteversion and external tibial torsion result in a higher Q-angle, which is the angle of intersection between the pull line of the quadriceps and the line from the tibial tubercle to the mid-point of the patella, leading to a larger lateral force on the patella [81, 82]. However, this influence may diminish as the flexion angle increases [83] as the tibia rotates internally with knee flexion. Except for anterior knee pain and patellar mal-tracking, patients with rotational malalignment of the femur and tibia experience hip and ankle pain [89]. Therefore, rotational osteotomy has been recommended by previous studies [80, 84, 86, 87, 89] to relieve pain for patients with femoral anteversion and external tibial torsion. According to [80], the typical corrective angles are 25° and 30° in the femur and tibia, respectively. Similarly, the average corrective angle in the proximal tibia is 26° in [86].

Figure 2.3.2 Miserable malalignment patient. A: the squinting patellae (inward facing patellae) can be observed with the foot facing forward; B: external tibial torsion can be seen with the patellae anterior (Adapted from Bruce et al. 2004) [85] (Image use permitted by Wolters Kluwer Health, Inc)

Furthermore, rotation deformities have been proven to be correlated with higher knee adduction moments, which are indirect measurement of medial condyle force. Patients with medial knee osteoarthritis (KOA) have been found to have higher torsion deformity and higher knee varus moments during gait analysis [85]. External tibial torsion is positively associated with knee adduction moment [86] in subjects with moderate KOA. In addition, linear relationships between the frontal alignment and the rotational alignment of the distal femur and tibial torsion were reported in León-Muñoz et al. [73] and Bruce et al. [85] among patients with KOA.

2.4 Biomechanics of squatting

Squatting is a typical knee-straining posture and known as a risk factor for knee osteoarthritis (OA) [16]. Some occupations, including mining, construction, and manufacturing, require workers to keep their knees bending or frequent squatting [17-18] while athletes such as catchers have to squat repetitively when playing baseball or training [20]. As a result, these people are more likely to suffer from KOA [19]. McMillan et al. (2005) concluded that prolonged or frequent squatting, considered job risk factors, doubles the risk of KOA in the general population. In addition, squatting is a typical posture during daily living, such as going to the toilet and washing in the Middle East and Asian countries [21]. Therefore, an improved and comprehensive understanding of contact mechanics and knee kinetics during squatting is meaningful and supportive for

sports physicians, rehabilitation therapists and researchers [22]. Over the past few decades, numerous studies have been carried out to understand the biomechanics of the knee during squatting or weight-bearing activity using experiments or computational methods [23-29].

A typical free body diagram of the squatting motion [30] is shown in Figure 2.4.1. The flexion moment at the knee is equal to body weight (W) multiplied by the moment arm (d). The moment arm is defined as the perpendicular distance from the center of the knee joint to the weight-bearing axis. As the flexion angle (θ) increases, the moment arm increases, so the magnitude of the flexion moment (M) becomes greater.

$$d = L \cdot \sin(\theta/2)$$
$$M = W \cdot d$$
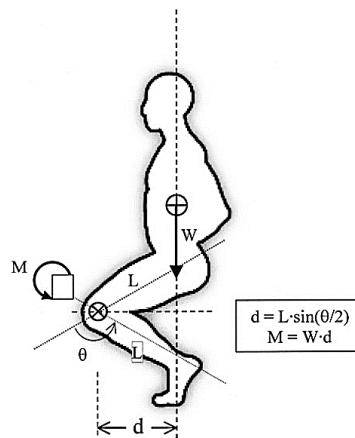
Figure 2.4.1: Free body diagram of moments during squatting. W: body weight; L: length of the leg; θ: flexion angle; d: moment arm; M: flexion moment (adapted from Cohen 2011) [30] (Image use permitted by SAGE)

As the knee flexes and extends, the patella is pulled superiorly by the quadriceps tendon and is pulled inferiorly by the patellar tendon. However, the patella does not function as a simple pulley because the pull force is equal on both ends of the simple pulley. On the contrary, the tension in the quadriceps tendon is larger than the tension in the patellar tendon [31]. The combination of these two tensions generates compressive force on the femoral cartilage (Figure 2.4.2). As the knee flexes, the magnitude of the compressive force will increase [32]. The tendon force produces a flexion moment which equilibrates the body moment during squatting (Figure 2.4.1).
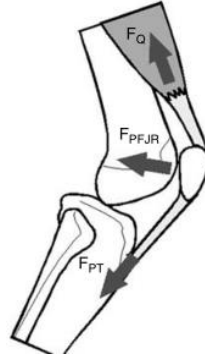
Figure 2.4.2: The compressive force (F_{PFJR}) is the combination of the quadriceps tendon force (F_Q) and patellar tendon force (F_{PT}). As the knee flexion angle increases, the magnitude of the compressive force will increase (adapted from Sanchis-Alfonso 2006) [91] (Image use permitted by Springer Nature)

Contact force can be measured by various methods such as models or instrumented implants. Models non-invasively determine contact forces based on measured kinematics, anthropometrics, and ground reaction forces and calculated kinetics [33]. Figure 2.4.3 shows the model used to calculate tibiofemoral joint forces by Smith et al. (2008). This method is non-invasive and low-cost but makes numerous assumptions, such as the line of actions of muscle forces and contact tibiofemoral forces are parallel to the long axis of femur in the frontal plane (Figure 2.4.3), and the angles of patellar tendon and hamstring with respect to the long axis of tibia were assumed to be constants. Instrumented implants collect data directly and are more accurate. However, instrument implants are invasive and not used widely.
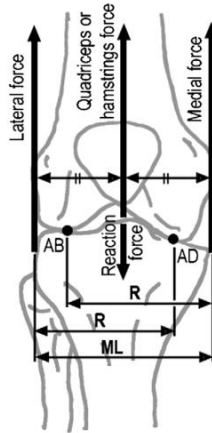
Figure 2.4.3: The force contributions for calculation of the contact force in the frontal plane (adapted from Smith 2008) [33] (Image use permitted by Elsevier)

2.5   Computational modelling in biomechanics

Although experimental methods can be used to examine knee joint mechanics, they are expensive and time-consuming when using a large number of specimens. Also, the scenarios and outputs of the experiment are limited. Thus, computational modelling has played an essential role in comprehensively understanding joint mechanics [34]. Computational models can obtain information that is difficult or impractical to test in experiments. There are two popular types of computational modelling methods in biomechanics: musculoskeletal modelling and finite element modelling. Musculoskeletal modelling is able to calculate the joint internal loads and contact forces by using experimentally obtained 3D motion and ground reaction forces. These forces provide an estimate of excessive loading, implying the risk of the initiation or progression of OA. However, musculoskeletal modelling cannot provide details of the stress and strain in soft as well as hard tissues, while the finite element model can [35].

Finite element models have been widely used to quantify specific stresses and strains in different tissues [36]. Finite element models typically reconstruct the subject-specific geometries of tissues along with their realistic material properties. Although the manual segmentation of the complex geometry from CT or MR images is comparatively time-consuming, the reconstructed model assigned with specific material properties increases

the fidelity of biomechanics of the joint in the finite element method. Compared to the musculoskeletal model, which linearly scales a general model to make a subject-specific model, the finite element model can be more accurate and patient-specific. However, compared to the finite element model, the musculoskeletal model is more computationally efficient [37] since it is based on rigid body mechanics.

Based on different characteristics, model developers can choose either of the computer models or combine them. For example, using the combined scaled musculoskeletal model and subject-specific finite element model to examine the initiation and progression of OA during gait or walking [38, 39]. By applying the force, moment, translation and rotation exported from the musculoskeletal model as boundary conditions, the finite element model can quantify the detailed changes in stresses, strains and fluid pressures in specific tissues.

2.6   OpenKnee Model

2.6.1 Geometry and Mesh Development

The finite element (FE) model comes from the partially validated three-dimensional whole knee-joint model from the OpenKnee project by Erdemir et al. at SimTK.org [40, 41]. In this model, geometries (.IGES files) were reconstructed from magnetic resonance images (MRI) generated by a 1.0 Tesla extremity MRI scanner (Orthone, ONI Medical Systems Inc, Wilmington MA). During scans, the knee was in full extension. Enhanced contrast for articular cartilages and ligaments was provided by the scanning technique [42], which is a 3D incoherent gradient-echo sequence with fat suppression, Repetition Time (TR) $= 30\ ms$, Echo Time (TE) $= 6.7\ ms$, Field of View (FOV) $=$ $150\ mm\ \times 150\ mm$, Flip Angle 200°, Slice Thickness $= 1.5\ mm$. The total scan time is approximately 18 minutes in 3 planes: frontal, sagittal, and axial. Geometries included two generations: Generation 1 included tibiofemoral joints, and Generation 2 included patellofemoral joints. Generation 1 consists of bones (distal femur, proximal tibia), cartilage (tibial, femoral), menisci (medial and lateral), cruciate ligaments (anterior and posterior), and collateral ligaments (medial and lateral). Generation 2 consists of the patella, patellar cartilage and patellar tendon. After merging two generations of the

OpenKnee model, knee components are shown, as in Figure 2.6.1. The donor of the cadaver here was a 70 year old female (77.1 kg, 1.68 m). Table 2.6.1 shows the specimen details.
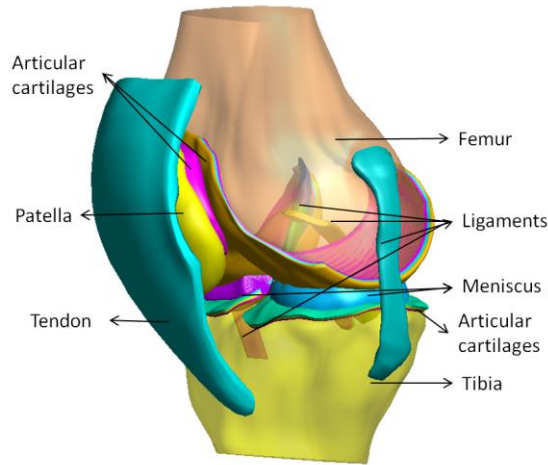
Figure 2.6.1: OpenKnee model components labelled.

Table 2.6.1: Specimen Details

Side	Right
Donor Age	70 years
Donor Estimated Body Weight	170 lbs (77.1 kg)
Donor Height	5'6" (1.68 m)
Donor Gender	Female
Donor Cause of Death	Pneumonia/Cancer

The mesh was generated using TrueGrid (XYZ Scientific, Livermore, CA) based on the three-dimensional models from MRI. All soft tissues were meshed using hexahedral elements, while the bones were quadrilateral shell elements. The meshed model contained 103,360 nodes and 86,544 elements in total. A Mesh convergence study was performed considering the articular cartilage mesh because of the research focus on contact mechanics [41]. This study confirms that model predictions are not a function of mesh density.

Furthermore, the meshed model could be readily imported into FEBio for pre-processing and simulation. FEBio is an implicit, nonlinear finite element solver that is specifically designed for applications in biomechanics [43]. In this study, simulations were set to

conduct quasi-static analysis in FEBio, in which the inertial response of the system was ignored.

2.6.2 The Coordinate System in OpenKnee Model

The coordinate system of the OpenKnee model is consistent with the widely accepted coordinates defined by Grood and Suntay [44]: the x-axis is the flexion axis; the y-axis is the anterior-posterior axis; the z-axis is the mechanical axis. The coordinates originate at the mid-point of the medial and lateral condyle. The quadriceps angle (Q-angle) of this model was defined as 14.1 degrees [45]. The Q-angle is the interaction angle between the line from the anterior superior iliac spine (ASIS) to the mid-point of the patella and the line from the tibial tubercle to the mid-point of the patella. The 14.1 degree angle was achieved by rotating the model 5.3 degrees since the initial Q-angle was 8.8 degrees in the original coordinates (same as MRI coordinates).

2.6.3 Material Properties

The bones (tibia, femur and patella) are considered rigid bodies due to their high stiffness compared to other soft tissues in the knee [46-48]. The rigid body is implemented in FEBio by defining the center of mass that is a reference point for all other nodes of the rigid body. The motions (rotations and translations) of the reference point describe all kinematics of the bone as a rigid body. In this way, no strain and stress occur within the rigid body. Thus, the number of equations is significantly reduced in the simulation.

Cartilage is viscoelastic in nature. However, compared to the viscoelastic time constant of cartialge (1500 s) [49], the loading time in this study was shorter. Therefore, all articular cartilages (femoral, tibial and patellar) are considered as linear and isotropic elastic material with Young's modulus of $E = 15\ MPa$ and a Poisson ratio of $\mu = 0.475$, similar to previous studies [50, 51]. A nearly incompressible Neo-Hookean material was chosen to define cartilages. The parameters for cartilages are shown in Table 2.6.2. In FEBio, setting C_2 in Mooney-Rivlin (uncoupled) material [52] to zero can use Neo-Hookean material, with the strain energy function as follows:

21

$$\Psi = C_1(\tilde{I}_1 - 3) + C_2(\tilde{I}_2 - 3) + \frac{K}{2}(\ln J)^2 \tag{1}$$

Where,

C_1 and C_2: Mooney-Rivlin material coefficients.

*by setting C_2 to zero, the ground substance is Neo-Hookean material.

$\tilde{I}_1$ and $\tilde{I}_2$: Invariants of the deviatoric right Cauchy-Green deformation tensor.

K: Bulk modulus

J: Determinant of the deformation gradient tensor

Table 2.6.2: Material parameters for cartilage

C_1(MPa)	C_2(MPa)	K(MPa)
2.54	0	100

Although menisci is viscoelastic, similar to cartilage, menisci is reasonably defined as a homogeneous and transversely isotropic material with the circumferential modulus $E_1 = 125\ MPa$, radial modulus E_2 and compressive modulus E_3, both equal to $27.5\ MPa$ [53]. In FEBio, the material called Fung Orthotropic material was used. The material constants are shown in Table 2.6.3 below.

Table 2.6.3: Material constants for the meniscus

E_1	E_2	E_3	ν_{12}	ν_{23}	ν_{31}	G_{12}	G_{23}	G_{31}	c^*	K^*
125	27.5	27.5	0.1	0.33	0.1	2.0	12.5	2.0	1.0	10.0

*Currently, K and c have no effect on material behavior. They are set for FEBio syntax compliance.

Each horn of the meniscus was attached to the tibial plateau via tension-only linear springs to simulate horn attachments, as shown in Figure 2.6.2. Each node (88 nodes on each horn) on the horn face was connected to the corresponding node on the tibial plateau. The total stiffness of each horn was approximately 2000 N/mm, and each spring stiffness was 22.73 N/mm [50].
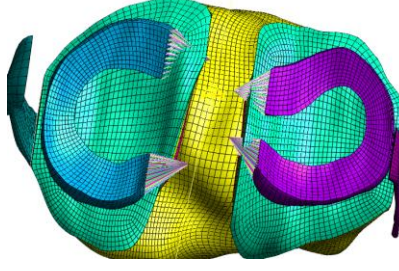
Figure 2.6.2: The top view of the meniscus

Anatomically, ligaments are highly anisotropic due to their fibrous alignment in diversity. Cruciate ligaments (ACL and PCL), collateral ligaments (MCL and LCL) and patellar tendons are defined as closely incompressible, transversely isotropic hyperelastic materials. This type of material represents the collagen behaviour of the ligaments, which offers primary resistance to tensile loading [55]. Collagen fibers are mostly aligned to the long axis of the ligaments. Thus, the fiber orientations of ligaments and tendon in this model were modelled across their longitudinal axis. The material called uncoupled transversely isotropic Mooney-Rivlin was chosen, including a Neo-Hookean ground substance and fiber component as the following strain energy function [52]:

$$W = \Psi + F(\tilde{\lambda}) \tag{2}$$

With

$$\tilde{\lambda}\frac{\partial F}{\partial \tilde{\lambda}} = \begin{cases} 0 & \tilde{\lambda} < 1 \\ C_3(e^{C_4(\tilde{\lambda}-1)} - 1) & 1 \le \tilde{\lambda} < \lambda_m \\ C_5 + C_6\tilde{\lambda} & \tilde{\lambda} \ge \lambda_m \end{cases} \tag{3}$$

Where,

Ψ: The equation shown in Eq.(1)

C_3: Exponential stresses scale

C_4: Rate of uncramping fibers

C_5: Elastic modulus of the straightened fibers

λ_m: Stretch where the fibers start to be straightened.

The material parameters for the ligaments and the tendon agreed with previous studies [46, 54], as shown in Table 2.6.4.

Table 2.6.4: Material parameters for the ligaments and tendons

	C_1	C_2	C_3	C_4	C_5	λ_m	K
ACL	1.95	0	0.0139	116.22	535.039	1.046	146.41
PCL	3.25	0	0.1196	87.178	431.063	1.035	243.9
MCL	1.44	0	0.57	48	467.1	1.063	793.65
LCL	1.44	0	0.57	48	467.1	1.063	793.65
PT*	2.75	0	0.065	115.89	777.56	1.042	206.61

*Quadriceps tendon and patellar tendon are a whole model in the OpenKnee model.

The medial patellofemoral ligament (MPFL) [56-58] and lateral patellofemoral ligament (LPFL) [59] were modelled as two tension-only springs. The stiffness of the MPFL was 50 N/mm [57, 58] in total and 25 N/mm for each. The stiffness of the LPFL was 16 N/mm [60] in total and 8 N/mm for each.

2.6.4 Contact Definitions

Soft tissues (ligaments, tendons and articulations) were attached to the bones by defining the rigid boundary condition in FEBio. In this formulation, the nodes on the attached surface were defined as a rigid-node set and the node set was attached to a rigid body. Thus, all the degrees of freedom on the attached faces of the ligaments (tendons) or articulations were constrained to the reference point of the corresponding rigid body.

A frictionless, finite sliding contact formulation was defined for all articulations, which is well-established by previous studies [46, 50]. This condition was achieved by defining a two-pass, sliding-elastic penalty algorithm in FEBio [52]. The two-pass algorithm in FEBio could resolve the potential mismatches of mesh quality, so the master and slave surface definition is arbitrary. In the two-pass algorithm, first surface A is the master surface while surface B is the slave surface, and next surface A is the slave surface while surface B is the master surface. The average value of the two integrals was set to be the contact integrals. The penalty algorithm calculated the contact tractions that prevented the two interfaces from penetrating based on the penalty factor. Convergent contact was

achieved by prescribing a penalty factor of 1 MPa/mm, so it was used for all contact definitions.

Thirteen contact pairs were defined to represent physiological mechanical interactions between femoral cartilage and tibial cartilage surfaces (both lateral and medial parts), between patellar cartilage and femoral cartilage surfaces, between meniscus and femoral cartilage surfaces (both lateral and medial parts), between meniscus and tibial cartilage surfaces (both medial and lateral parts), between ACL and PCL, between MCL and tibia, between LCL and tibia, between MCL and femur, between LCL and tibia and between quadriceps tendon and femoral cartilage.

Contact force is defined as the net contact force across the contact interface, which is evaluated by integrating the contact traction over the contact surface. Contact traction vectors are evaluated at contact surface faces.

2.6.5 Previous Studies

A passive flexion simulation was conducted with the OpenKnee model to illustrate the ability of the model to predict joint kinematics and soft-tissue deformations [68, 69]. To compare simulation data with published experimental data, the tibia was fixed while the femur was flexed up to 100 degrees. Furthermore, the remaining rotations and translations of the joint model were left unconstrained during the simulation. The loading conditions were the same as the previous study by Wilson et al. (2000), in which 15 knee specimens were tested [67]. The rotations of the femur and the translations of the tibial insertion of the anterior cruciate ligament (ACL) were examined in the simulation and compared with the experimental data. The overall agreement between predicted and experimental data was reasonable. In conclusion, this model has the potential to examine the effect of a major structure on coupled movements of the knee and tissue deformations by changing ligament properties or removing a structure.

The OpenKnee model has been used to examine the effect of meniscectomy on joint movements and cartilage deformations [68, 70]. In a simulation, the femur was prescribed a flexion angle of 45 degrees under a 100 N compressive load, while the remaining rotations and translations of the joint were set free. Under these loading

conditions, the simulations were conducted with an intact knee model and with the knee model removing the medial and lateral meniscus. In the experiment, the concentrated contact regions and increased deformations at central tibial cartilage in the model with meniscectomy were observed as expected. This simulation shows that the OpenKnee model can be used to study the impact of the clinical intervention.

Anterior cruciate ligament (ACL) deformations have been examined by simulating an anterior drawer test with the OpenKnee model [68, 71]. The anterior drawer test is simulated by fixing the tibia and applying a 100 N posterior force on the femur, while the knee joint is under 0 and 30 degrees of flexion. In the simulation, the translation of the knee and the deformation of the ACL were compared with the experimental data from the specimen used for the development of the OpenKnee model. This simulation allowed the OpenKnee model to examine the soft tissue mechanical functions with desired loading conditions.

Wangerin et al. (2013) developed an FE model based on the OpenKnee model to predict osteochondral tissue stress and strain during the stance phase of gait [41]. In the simulation, the loading boundary conditions were decided by a published OpenSim model, which was developed from a specimen with a similar height to the specimen used for the OpenKnee model. The model was validated by comparing the predicted timing and locations of maximum contact parameters (contact area, contact pressure and strain) with published studies.

2.6.6 Theory of in situ strains in FEBio

In situ strains (or stresses) usually exists *in vivo* in biological soft tissues such as ligaments, tendons and muscles. These strains (or stresses) can be relieved by cutting or removing tissues from the body. After cutting or removal of the tissues, the retraction of the living tissue can be observed, yielding a stress-free configuration. Computational geometries of the soft tissues are usually obtained *in vivo*, and thus, considering them as stress-free is not reasonable. Previous studies have demonstrated that these strains are essential to the stability of the joints [46, 61]. Therefore, initial strains of soft tissues in the computational model are necessary to obtain predictive joint mechanics accurately.

The framework implemented in FEBio aims to apply pre-strain directly on the initial reference configuration without the knowledge of the stress-free configuration. To achieve this, the framework (Figure 2.7.1) is based on the theory proposed by Johnson and Hoger (1995) [63]. The total elastic deformation gradient F_e is defined to describe the deformation from the stress-free to the current loaded configuration. F_e is determined by a multiplicative decomposition,

$$F_e = FF_P \tag{4}$$

Where F is the gradient of the deformation by applying load on reference configuration, and F_P is the deformation gradient of local mapping $\varphi(X)$ from the stress-free to reference configuration, F_P is also called the pre-strain gradient.
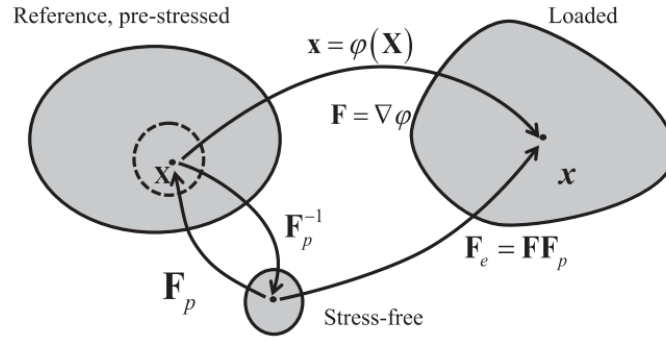
Figure 2.7.1: The relationship between stress-free configuration, reference configuration under initial strain, and current loaded configuration (adapted from Maas 2016 [62]) (Image use permitted by Elsevier)

By defining an initial estimate of F_P, it is possible to obtain the total deformation gradient F_e. This is convenient for soft tissues, like ligaments. As it is challenging to obtain the complete pre-strain gradient of ligaments from experiment data, therefore, when measuring a ligament strain, fiber stretch λ_p is usually measured [64-66]. But assumptions are necessary to estimate the special form of the pre-strain gradient $F_P(\lambda_p)$ according to Weiss et al. (2005) [64]. It is assumed that the material is incompressible and the fiber stretch is along the direction of the fibers. Also, it is assumed that the material is transversely isotropic and fiber-dominated under load. Therefore, with the

initial fiber stretch and satisfied assumptions, the pre-strain gradient can be calculated as follows:

$$F_P = Q \begin{bmatrix} \lambda_p & 0 & 0 \\ 0 & \lambda_p^{-1/2} & 0 \\ 0 & 0 & \lambda_p^{-1/2} \end{bmatrix} Q^T \tag{5}$$

Where Q is the rotation matrix between the local and the global coordinate frame.

However, the drawback of this pre-strain gradient approach is the distortion of geometry in the current state due to assumptions, which implies that the strains in the current configuration are not accurately prescribed [46, 64]. Therefore, the framework in FEBio provides an iterative algorithm updating the pre-strain gradient and updating rules eliminating distortion [62].

References

[1] Smith PN, Refshauge KM, Scarvell JM: Development of the concepts of knee kinematics. Arch Phys Med Rehabil 84:1895, 2003.

[2] C. R. Ethier and C. A. Simmons, Introductory Biomechanics: From Cells to Organisms. Cambridge: Cambridge University Press, 2007

[3] Messner K, Gao J: The menisci of the knee joint. Anatomical and functional characteristics, and a rationale for clinical treatment. J Anat 193 (Pt 2):161, 1998.

[4] Gray, Henry. Anatomy of the Human Body. Philadelphia: Lea & Febiger, 1924.

[5] Waterson H B, Philips J R A, Mandalia V I, Toms A D. Thou shalt not varus: still applicable in total knee arthroplasty? *Bone & Joint*.2014;3(3)

[6] Bellemans J, Colyn W, Vandenneucker H, Victor J. The chitranjan ranawat award. *Clin Orthop Relat Res*. 2012;470(1):45-53. doi:10.1007/s11999-011-1936-5

[7] Cooke D, Scudamore A, Li J, Wyss U, Bryant T, Costigan P. Axial lower-limb alignment: comparison of knee geometry in normal volunteers and osteoarthritis patients. *Osteoarthritis Cartilage*. 1997;5(1):39-47. doi:10.1016/s1063-4584(97)80030-1

[8] Johnson F, Leitl S, Waugh W . 1980. The distribution of load across the knee. J Bone Joint Surg 67-B:346–349.

[9] George MJ. Knee Surgery - Reconstruction and Replacement. 2019

[10] Jackson BD, Wluka AE, T eichtahl AJ, et al: Reviewing knee osteoarthritis—A biomechanical perspective. J Sci Med Sport 7:347, 2004.

[11] Quinn, T. M., R. G. Allen, B. J. Schalet, P. Perumbuli, and E. B. Huniker. Matrix and cell injury due to sub-impact loading of adult bovine articular cartilage explants: effects of strain rate and peak stress. J. Orthop. Res. 19:242–249, 2001.

[12] Kerin, A. J., M. R. Wisnom, and M. A. Adams. The compressive strength of articular cartilage. Proc. Inst. Mech. Eng. H 212:273–280, 1998.

[13] Cerejo, R., D. D. Dunlop, S. Cahue, D. Channin, J. Song, and L. Sharma. The influence of alignment on risk of knee osteoarthritis progression according to baseline stage of disease. Arthritis Rheum. 46:2632–2636, 2002.

[14] Ford, K. R., G. D. Myer, and T. E. Hewett. Valgus knee motion during landing in high school female and male basketball players. Med. Sci. Sports Exerc. 35:1745–1750, 2003.

[15] Sharma, L., J. Song, D. T. Felson, S. Cahue, E. Shamiyeh, and D. D. Dunlop. The role of knee alignment in disease progression and functional decline in knee osteoarthritis. JAMA 286:188-195, 2001

[16] Ditchen DM, Ellegast RP, Gawliczek T, Hartmann B, Rieger MA. Occupational kneeling and squatting: development and validation of an assessment method combining measurements and diaries. *Int Arch Occup Environ Health*. 2015;88(2):153-165.

[17] Reid CR, Bush PM, Cummings NH, McMullin DL, Durrani SK. A review of occupational knee disorders. *J Occup Rehabil.*2010;20(4):489-501.

[18] Ditchen DM, Ellegast RP, Gawliczek T, Hartmann B, Rieger MA. Occupational kneeling and squatting: development and validation of an assessment method combining measurements and diaries. *Int Arch Occup Environ Health*. 2015;88(2):153-165.

[19] Bernard TE, Wilder FV, Aluoch M, Leaverton PE. Job-related osteoarthritis of the knee, foot, hand, and cervical spine. *J Occup Environ Med.* 2010;52(1):33-38.

[20] McElroy MJ, Riley PM, Tepolt FA, Nasreddine AY, Kocher MS. Catcher's Knee: Posterior Femoral Condyle Juvenile Osteochondritis Dissecans in Children and Adolescents. *J Pediatr Orthop.* 2018;38(8):410-417.

[21] Hemmerich A, Brown H, Smith S, Marthandam SSK, Wyss UP. Hip, knee, and ankle kinematics of high range of motion activities of daily living. J Orthop Res 2006;24:770–81.

[22] Escamilla RF. Knee biomechanics of the dynamic squat exercise. *Med Sci Sports Exerc*. 2001;33(1):127-141.

[23] Hale R, Green J, Hausselle J, Saxby D, Gonzalez RV. Quantified in vitro tibiofemoral contact during bodyweight back squats. *J Biomech*. 2018;79:21-30.

[24] Elias, J.J., Wilson, D.R., Adamson, R., Cosgarea, A.J. Evaluation of a computational model used to predict the patellofemoral contact pressure distribution. *J. Biomech.* , 2004 ;37, 295–302.

[25] Ali AA, Shalhoub SS, Cyr AJ, et al. Validation of predicted patellofemoral mechanics in a finite element model of the healthy and cruciate-deficient knee. *J Biomech*. 2016;49(2):302-309.

[26] Barink M, De Waal Malefijt M, Celada P, Vena P, Van Kampen A, Verdonschot N. A mechanical comparison of high-flexion and conventional total knee arthroplasty. *Proc Inst Mech Eng H*. 2008;222(3):297-307.

[27] Zelle J, Barink M, De Waal Malefijt M, Verdonschot N. Thigh-calf contact: does it affect the loading of the knee in the high-flexion range?. *J Biomech*. 2009;42(5):587-593.

[28] Besier TF, Gold GE, Beaupré GS, Delp SL. A modeling framework to estimate patellofemoral joint cartilage stress in vivo. *Med Sci Sports Exerc*. 2005;37(11):1924-1930.

[29] Gu W, Pandy M. Direct Validation of Human Knee-joint Contact Mechanics Derived From Subject-specific Finite-element Models of the Tibiofemoral and Patellofemoral Joints [published online ahead of print, 2019 Dec 1]. *J Biomech Eng*. 2019;10.1115/1.4045594.

[30] Cohen ZA, Roglic H, Grelsamer RP, et al. Patellofemoral stresses during open and closed kinetic chain exercises. An analysis using computer simulation. *Am J Sports Med*. 2001;29(4):480-487.

[31] Grelsamer RP, Weinstein CH. Applied biomechanics of the patella. *Clin Orthop Relat Res*. 2001;(389):9-14. doi:10.1097/00003086-200108000-00003

[32] Huberti, H.H., Hayes, W.C., 1984. Patellofemoral contact pressures. The influence of q&angle and tendofemoral contact. *J. Bone Joint Surg*. Am. 66, 715–724.

[33] Smith SM, Cockburn RA, Hemmerich A, Li RM, Wyss UP. Tibiofemoral joint contact forces and knee kinematics during squatting. *Gait Posture*. 2008;27(3):376-386.

[34] Kazemi M, Dabiri Y, Li LP. Recent advances in computational mechanics of the human knee joint. *Comput Math Methods Med.* 2013;2013.

[35] Nicholas Ali and Gholamreza Rouhi. Barriers to predicting the mechanisms and risk factors of non-contact anterior cruciate ligament injury. *The Open Biomedical Engineering Journal*. (4):178 189, 2010.

[36] Erdemir A, Besier TF, Halloran JP, et al. Deciphering the "Art" in Modeling and Simulation of the Knee Joint: Overall Strategy. *J Biomech Eng*. 2019;141(7):0710021-07100210.

[37] Trent M Guess, Hongzeng Liu, Sampath Bhashyam, and Ganesh Thiagarajan. A multibody knee model with discrete cartilage prediction of tibio-femoral contact mechanics. *Computer methods in biomechanics and biomedical engineering*. 16(3):256 270,2013.

[38] Halonen KS, Dzialo CM, Mannisi M, Venäläinen MS, de Zee M, Andersen MS. Workflow assessing the effect of gait alterations on stresses in the medial tibial cartilage - combined musculoskeletal modelling and finite element analysis. *Sci Rep*. 2017;7(1):17396.

[39] Shu L, Yamamoto K, Yao J, et al. A subject-specific finite element musculoskeletal framework for mechanics analysis of a total knee replacement. *J Biomech*. 2018;77:146-154.

[40] Erdemir A. Open Knee: Open Source Modeling and Simulation in Knee Biomechanics. *J Knee Surg*. 2016;29(2):107-116.

[41] Wangerin, S. Development and validation of a human knee joint finite element model for tissue stress and strain predictions during exercise. 2013

[42] B. Borotikar, "Subject-specific computational models of the knee to predict anterior cruciate ligament injury, Doctoral Dissertation," Cleveland State University, Dec. 2009.

[43] Maas SA, Ellis BJ, Ateshian GA, Weiss JA. FEBio: finite elements for biomechanics. *J Biomech Eng*. 2012;134(1):011005.

[44] E. S. Grood and W. J. Suntay, "A joint coordinate system for the clinical description of three-dimensional motions: application to the knee," Journal of Biomechanical Engineering, vol. 105, no. 2, pp. 136-144, May. 1983.

[45] L. Herrington and C. Nester, "Q-angle undervalued? The relationship between Q-angle and medio-lateral position of the patella," Clinical Biomechanics (Bristol, Avon), vol. 19, no. 10, pp. 1070-1073, Dec. 2004.

[46] Peña E, Calvo B, Martínez MA, Doblaré M. A three-dimensional finite element analysis of the combined behavior of ligaments and menisci in the healthy human knee joint. J Biomech. 2006;39(9):1686-1701.

[47] G. Li, O. Lopez and H. Rubash, "Variability of a three-dimensional finite element model constructed using magnetic resonance images of a knee for joint contact stress analysis," Journal of Biomechanical Engineering, vol. 123, pp. 341-346, 2001.

[48] M. Bendjaballah, A. Shirazi-Adl and D. Zukor, "Biomechanics of the human knee joint in compression: reconstruction, mesh generation, and finite element analysis," The Knee, vol. 2, no. 2, pp. 69-79, 1995.

[49] Armstrong CG, Lai WM, Mow VC. An analysis of the unconfined compression of articular cartilage. J Biomech Eng. 1984;106(2):165-173.

[50] Donahue, T. L. H., Hull, M. L., Rashid, M. M. & Jacobs, C. R. A finite element model of the human knee joint for the study of tibio-femoral contact. J Biomech Eng 124, 273–280 (2002).

[51] N. Yang, P. Canavan, H. Nayeb-Hashemi, B. Najafi and A. Vaziri. Protocol for constructing subject-specific biomechanical models of knee joint. Computer Methods in Biomechanics and Biomedical Engineering, vol. 13, no. 5, pp. 589-603, 2010.

[52] S. Maas, D. Rawlins, J. Weiss, and G. Ateshian. FEBio Finite Elements for Biomechanics: Theory Manual, 2010

[53] Yao J, Snibbe J, Maloney M, Lerner AL. Stresses and strains in the medial meniscus of an ACL deficient knee under anterior loading: a finite element analysis with image-based experimental validation. J Biomech Eng. 2006;128(1):135-141.

[54] Gardiner JC, Weiss JA. Subject-specific finite element analysis of the human medial collateral ligament during valgus knee loading. J Orthop Res. 2003;21(6):1098-1106.

[55] Weiss JA, Gardiner JC, Ellis BJ, Lujan TJ, Phatak NS. Three-dimensional finite element modeling of ligaments: technical aspects. Med Eng Phys. 2005;27(10):845-861.

[56] Nomura E, Inoue M, Osada N. Anatomical analysis of the medial patellofemoral ligament of the knee, especially the femoral attachment. Knee Surgery, Sport Traumatol Arthrosc. 2005;13(7):510-515.

[57] Kim KE, Hsu SL, Woo SL. Tensile properties of the medial patellofemoral ligament: the effect of specimen orientation. J Biomech. 2014;47(2):592-595.

[58] Criscenti G, De Maria C, Sebastiani E, et al. material and structural tensile properties of the human medial patello-femoral ligament. J Mech Behav Biomed Mater. 2016;54:141-148.

[59] Shah KN, DeFroda SF, Ware JK, Koruprolu SC, Owens BD. Lateral Patellofemoral Ligament: An Anatomic Study. Orthop J Sport Med. 2017;5(12):1-6.

[60] Merican AM, Sanghavi S, Iranpour F, Amis AA. The structural properties of the lateral retinaculum and capsular complex of the knee. J Biomech. 2009;42(14):2323-2329.

[61] Limbert G, Taylor M, Middleton J. Three-dimensional finite element modelling of the human ACL: simulation of passive knee flexion with a stressed and stress-free ACL. J Biomech. 2004;37(11):1723-1731.

[62] Maas SA, Erdemir A, Halloran JP, Weiss JA. A general framework for application of prestrain to computational models of biological materials. J Mech Behav Biomed Mater. 2016;61:499-510.

[63] Johnson, B.E., Hoger, A. The use of a virtual configuration in formulating constitutive equations for residually stressed elastic materials. J Elasticity. 1995;41:177–215.

[64] Weiss JA, Gardiner JC, Ellis BJ, Lujan TJ, Phatak NS. Three-dimensional finite element modeling of ligaments: technical aspects. Med Eng Phys. 2005;27(10):845-861.

[65] Ellis BJ, Lujan TJ, Dalton MS, Weiss JA. Medial collateral ligament insertion site and contact forces in the ACL-deficient knee. *J Orthop Res*. 2006;24(4):800-810.

[66] Lujan TJ, Lake SP, Plaizier TA, Ellis BJ, Weiss JA. Simultaneous measurement of three-dimensional joint kinematics and ligament strains with optical methods. *J Biomech Eng*. 2005;127(1):193-197.

[67] Wilson DR, Feikes JD, Zavatsky AB, O'Connor JJ. The components of passive knee movement are coupled to flexion angle. *J Biomech*. 2000; 33:465–473.

[68] Erdemir A. Open Knee: Open Source Modeling and Simulation in Knee Biomechanics. *J Knee Surg*. 2016;29(2):107-116.

[69] Erdemir, A., and Sibole, S. Open knee: capacity to reproduce passive joint kinematics. *23rd Congress of the International Society of Biomechanics*. 2011;7:3-7, 2011, Brussels, Belgium.

[70] Sibole, S., Bennetts, C., Borotikar, B., Maas, S., van den Bogert, A. J., Weiss, J. A. and Erdemir, A. Open knee: a 3D finite element representation of the knee joint. *34th Annual Meeting of the American Society of Biomechanics*. 2010;8:18-21, Providence, RI.

[71] Hernandez RJ, Tachdjian MO, Poznansk AK, Dias LS. CT determination of femoral torsion. *Am J Roentgenol*. 1981;137(1):97-101.

[72] Goutallier D, Van Driessche S, Manicom O, Ali ES, Bernageau J, Radier C. Influence of lower-limb torsion on long-term outcomes of tibial valgus osteotomy for medial compartment knee osteoarthritis. *J Bone Jt Surg - Ser A*. 2006;88(11):2439-2447.

[73] León-Muñoz VJ, Manca S, López-López M, Martínez-Martínez F, Santonja-Medina F. Coronal and axial alignment relationship in Caucasian patients with osteoarthritis of the knee. *Sci Rep*. 2021;11(1):1-8.

[74] Eckhoff DG, Montgomery WK, Kicoyne RF, et al. Femoral morphometry and anterior knee pain. *Clin Orthop*. 1994;302:64–68.

[75] Erkocak OF, Altan E, Altintas M, Turkmen F, Aydin BK, Bayar A. Lower extremity rotational deformities and patellofemoral alignment parameters in patients with anterior knee pain. *Knee Surg Sports Traumatol Arthrosc*. 2016;24(9):3011-3020. doi:10.1007/s00167-015-3611-y

[76] Kuo TY, Skedros JG, Bloebaum RD. Measurement of femoral anteversion by biplane radiography and computed tomography imaging: comparison with an anatomic reference. *Invest Radiol*. 2003;38(4):221-229. doi:10.1097/01.RLI.0000059542.90854.EF

[77] Seber S, Hazer B, Köse N, Göktürk E, Günal I, Turgut A. Rotational profile of the lower extremity and foot progression angle: computerized tomographic examination of 50 male adults. *Arch Orthop Trauma Surg*. 2000;120(5-6):255-258. doi:10.1007/s004020050459

[78] Clementz BG, Magnusson A. Fluoroscopic measurement of tibial torsion in adults. A comparison of three methods. *Arch Orthop Trauma Surg*. 1989;108(3):150-153. doi:10.1007/BF00934258

[79] Lee TQ, Anzel SH, Bennett KA, Pang D, Kim WC. The influence of fixed rotational deformities of the femur on the patellofemoral contact pressures in human cadaver knees. *Clin Orthop Relat Res*. 1994;302(302):69-74.

[80] Stevens PM, Gililland JM, Anderson LA, Mickelson JB, Nielson J, Klatt JW. Success of torsional correction surgery after failed surgeries for patellofemoral pain and instability. *Strateg Trauma Limb Reconstr*. 2014;9(1):5-12.

[81] Turner MS, Smillie IS. The effect of tibial torsion of the pathology of the knee. *J Bone Joint Surg*. 1981;63-B(3):396–398

[82] Powers CM. The Influence of Altered Lower-Extremity Kinematics on Patellofemoral Joint Dysfunction: A Theoretical Perspective. *J Orthop Sports Phys Ther*. 2003;33(11):639-646.

[83] Hvid I: The stability of the human patello-femoral joint. *Eng Med*. 12:55, 1983.

[84] James SL. Chondromalacia of the patella in the adolescent. In: Kennedy JC, ed. The Injured Adolescent Knee. Baltimore: Williams & Wilkins; 1979:205–251.

[85] Bruce WD, Stevens PM. Surgical Correction of Miserable Malalignment Syndrome. *J Pediatr Orthop*. 2004;24(4):392-396. doi:10.1097/00004694-200407000-00009

[86] Walton DM, Liu RW, Farrow LD, Thompson GH. Proximal tibial derotation osteotomy for torsion of the tibia: A review of 43 cases. *J Child Orthop*. 2012;6(1):81-85.

[87] Krackow KA, Mandeville DS, Rachala SR, Bayers-Thering M, Osternig LR. Torsion deformity and joint loading for medial knee osteoarthritis. *Gait Posture*. 2011;33(4):625-629.

[88] Huang C, Chan PK, Chiu KY, et al. Knee joint loadings are related to tibial torsional alignments in people with radiographic medial knee osteoarthritis. *PLoS One*. 2021;16(7):1-11.

[89] Gruskay JA, Fragomen AT, Rozbruch SR. Idiopathic Rotational Abnormalities of the Lower Extremities in Children and Adults. *JBJS Rev*. 2019;7(1):e3. doi:10.2106/JBJS.RVW.18.00016

[90] Xing Q, Theiss MM, Peng Q, Yang W, Li J, Chen JX. 3D automatic feature construction system for lower limb alignment. *2010 International Conference on Cyberworlds*. 2010;375-382.

[91] Sanchis-Alfonso, V., Ávila-Carrasco, C., Prat-Pastor, J.M., Atienza, C.M., Cuñat, E. (2006). Biomechanical Bases for Anterior Knee Pain and Patellar Instability. In: Sanchis-Alfonso, V. (eds) Anterior Knee Pain and Patellar Instability. Springer, London. https://doi.org/10.1007/978-0-85729-507-1_6

Chapter 3

3 The Development and Parametric Analysis of a full-leg squat model

3.1 Introduction

Sensitivity analysis in computational modelling is generally used to determine which parameters will make a significant difference in the behaviour of the model. Sensitivity analysis is an essential tool for model simplification, optimization design, robust design, decision-making, and simulation model validation [9, 10]. The analysis methods used for a simulation model varied due to different purposes, which implies that sensitivity analysis methods vary across different simulations for multidisciplinary fields, including engineering design (like aerospace and the electronics industry) and economics [11, 12]. The sensitivity analysis in this chapter is concerned about the variations of outputs, including load distribution, contact force, and muscle forces, due to varieties and uncertainty of input parameters, such as the lower limb alignment and *in situ* strains, which are subject-specific. Some of these inputs were influenced by modellers' assumptions or measurement unreliability. Thus, sensitivity analysis is used to study the influence of these uncertainties of inputs to inform the modeller about which inputs should be carefully used.

Previously, the results of contact force, stress, and force within ligaments were proven to be related to initial strains in ligaments [1, 48-50]. Models with subject-specific ligaments strains had fewer errors to experimental data compared to models with generic strains under laxity tests [50]. Also, the model an ACL initial strain is in a better agreement in resultant force with experimental data under flexion compared to the stress-free model [48].

In healthy patients, the standard deviation of neutral alignment is 3°, thus, the lower limb alignment from the musculoskeletal model was deviated in this chapter to investigate the varied outputs in the FE model, such as contact distribution. Moreover, the results were compared to published data, so errors in the models with different frontal alignments to the published data were reported. In addition, the contact forces in the patellofemoral and tibiofemoral joint were found to be correlated to the thickness and position of the patella

[21,24,39]. In [21], the tibiofemoral contact force was positively correlated to the moment arm of quadricep force. Also, a previous study [39] reported that both thickness and superior position of the patella are positively correlated to the patellofemoral contact force.

Therefore, the purposes of this chapter are: (1) to develop a full-leg squatting model using initial parameters; (2) to investigate the influence of *in situ* strains under valgus-varus torque; (3) to investigate the varieties of outputs, including force distribution in the tibiofemoral joint, total contact loads in the tibiofemoral joint and patellofemoral joint and muscle forces due to uncertainties of inputs, including *in situ* strains, tibiofemoral alignment in the frontal plane, patella thickness and superior patella during squatting; and (4) to compare the results in parametric studies with published data from previous studies and use desirable parameters to build a reference model for the next chapter.

3.2 Initial Model Development

3.2.1 Generic Model Modification

Based on a musculoskeletal model, the lower-extremity components were added to the FE model. Due to anatomy or numerical problems, modifications of LCL and lateral femoral cartilage in FE model were made to develop a full-leg squatting model with up to 90 degrees of flexion.

3.2.1.1 A Full Leg Model

To simulate a full-leg squat motion, more information about the lower leg of the subject was necessary to revise the FE model. However, the MRI of the OpenKnee model only includes the distal femur, proximal tibial, patella and the soft tissues among these three bones. Thus, a lower extremity musculoskeletal model was needed to determine the proximal insertion site of the quadriceps muscle, hip center, and ankle center (Figure 3.2.1).

Figure 3.2.1: The generic lower extremity musculoskeletal model (adapted from Lenhart 2015) [4] (Image use permitted by Springer Nature)

An OpenSim model from Lenhart et al. (2015) was selected due to the similar gender and height with the subject of the OpenKnee model [4]. So the coordinates of proximal quadriceps, hip center and ankle center derived from the musculoskeletal model were used in the FE model. Three rigid bodies were defined in the finite element model in FEBio software: hip center, ankle center and proximal quadriceps insertion. Their coordinates in OpenSim were adjusted to align with the coordinates in the finite model, where the origin of the global coordinates was the joint center. The proximal quadriceps insertion was connected to the end of the 3D quadriceps tendon mesh by a linear spring (k=15,000 N/mm) to simulate the quadriceps [1]. The 3D quadriceps tendon mesh originated from the OpenKnee model (as explained in 2.6.1). In addition, to simulate the quadriceps wrapping around the femoral cartilage during flexion, the proximal edge of the 3D model of the quadriceps tendon was extruded along the normal direction with respect to the surface of the 3D-shaped quadriceps tendon. Moreover, the extruded model could improve the contact condition between the inner face of the quadriceps tendon and the femoral cartilage during squatting. When the knee squats over 40 degrees of flexion, the inner face of the quadriceps tendon starts contacting the femoral cartilage, wrapping around the femur during 40° to 90° squatting, as shown in Figure 3.2.2.

Contact between the quadriceps tendon and cartilage
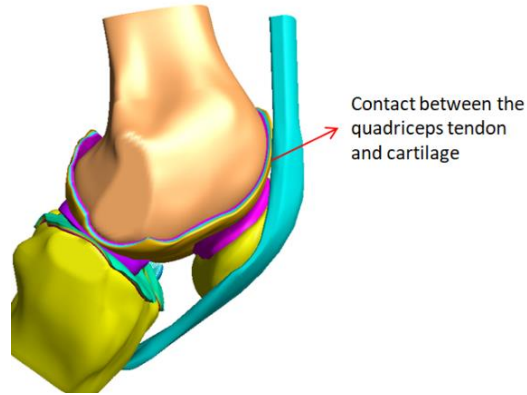
Figure 3.2.2: The FE knee model with extruded quadriceps tendon at 40 degrees of flexion, when the quadriceps tendon starts contacting the femoral cartilage.

3.2.1.2 Articular cartilages

When the flexion angle is greater than 80 degrees, a convergence problem occurs in the contact pairs between the femoral cartilage and lateral meniscus. In the weight-bearing flexion simulation, the lateral edge of the femoral cartilage curled up over 80 degrees of flexion, as shown in Figure 3.2.3. One reason for this was that the sharp corners of the lateral femoral cartilage and the inner part of the meniscus were not smoothing. According to the finite element contact guide [5], sharp corners in the target surface can result in convergence problems in a large sliding simulation. Another reason for convergence difficulties can be that the contact surface definition does not extend far enough to account for the expected motions of the contacting parts. Contact along the perimeter of the master surface should be avoided [6]. When a slave node falls off the master surface in one iteration, it could be trapped in contact in the next iteration. This phenomenon is known as chattering, which results in convergence problems. To solve this problem, the lateral surface of the femoral cartilage can be extended far enough to satisfy the sliding motions during the knee bend. The contact convergence problem was solved with the extended posterior area of the femoral cartilage and the contact pairs worked well at over 80 degrees of flexion. The refined lateral femoral cartilage and lateral meniscus at 90 degrees of flexion are shown in Figure 3.2.4.
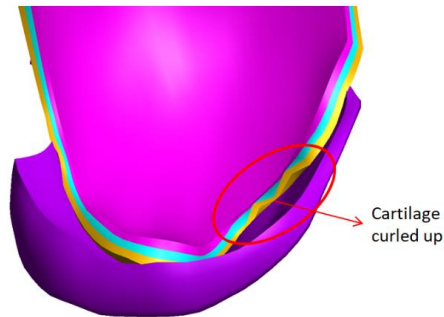
Figure 3.2.3: The initial femoral cartilage curled up over 80 degrees of flexion.
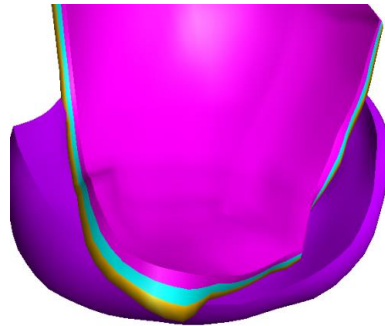
Figure 3.2.4: The refined lateral contact pair between femoral cartilage and meniscus at 90 degrees of flexion

3.2.1.3 LCL

Testing ten specimens with an average age of 61 years old (range from 50 to 71 years old), Meister et al. (2000) reported the mean measurement data of lateral collateral ligament (LCL) in full extension and the locations of femoral insertion [2], as shown in Figure 3.2.5. The average total length of the LCL from the most superior part of the femoral attachment to the most inferior part of the fibular attachment was 66.6 ± 6 mm (ranging from 55 to 72 mm). The location of the center of the femoral insertion of the LCL was determined by the value of line B (femoral attachment center to inferior lateral condyle border) and line C (femoral attachment center to posterior lateral condyle border) in Figure 3.2.5b, which equal 20.3 mm (ranging from 18 to 23 mm) and 19.5 mm (ranging from 16 to 23 mm), respectively.

(a)   **(b)**
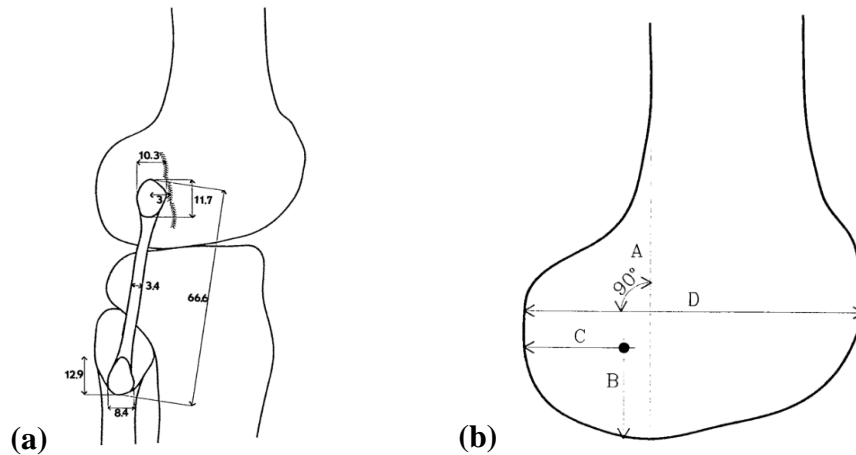
**Figure 3.2.5: Average measurement data of the LCL: (a) the average
dimensions of the LCL; (b) the locations of the femoral attachment. (Adapted
from Meister 2000) [2] (Image use permitted by SAGE)**

Espregueira-Mendes et al. (2005) also reported average data of the LCL from
measurements of 20 cadavers [3], with an average age of 50 years old (ranging from 35
to 64 years old). When the knee was in full extension, the mean length of the LCL was
63.1 mm, ranging from 55 to 71 mm. The location of the femoral attachment is shown in
Figure 3.2.6. The distance between the most inferior side of the femoral attachment and
the inferior articular surface of the lateral condyle was 22.7 mm (ranging from 18-33
mm). The distance between the most anterior side of the femoral attachment and the
posterior border of the lateral condyle was 31.8 mm (ranging from 28 to 36 mm). The
distance between the inferior side of the femoral attachment and the most posterosuperior
part of the lateral condyle was 12.9 mm (ranging from 10 to 18 mm)
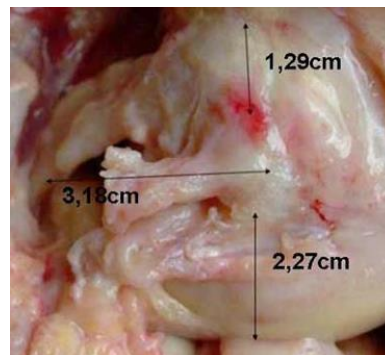
**Figure 3.2.6: The location of the femoral attachment. (Adapted from
Espregueira-Mendes 2005) [3] (Image use permitted by Springer Nature)**

According to the LCL anatomy, the geometry in the FE model was revised, as shown in Figure 3.2.7. The length of the LCL in the OpenKnee model was 30.05 mm, which is much lower than the published value in previous literature. Thus, the LCL was lengthened by maintaining the insertion site of the fibula as well as maintaining the angle between the longitudinal axis of LCL and the inferior-superior axis. After revision, the length of the LCL was 46.11 mm, while the distance between the inferior side of the femoral insertion face and the most inferior part of the lateral condyle was 20.61 mm. In addition, the distance between the anterior side of the femoral insertion face and the most posterior part of the lateral condyle was 24.2 mm.

(a)　　　　　　　　　　　　　(b)
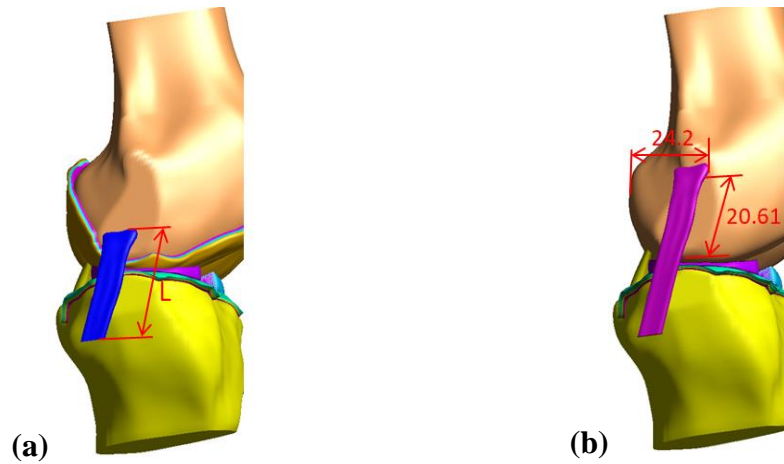
Figure 3.2.7: The dimension of the LCL: (a): the geometry of the LCL in the OpenKnee Model; (b): the dimension of the LCL after revision.

3.2.2 Loads and Boundary Conditions for Valgus-Varus Torque

To compare the model with pre-strain and the model without pre-strain, 10 Nm valgus torque and 10 Nm varus torque were simulated. This is because valgus-varus rotational kinematics play an important role in observing the influence of lower limb alignment in the frontal plane [49]. During the simulations (Figure 3.2.8), the femur was fixed while the tibia was only constrained in flexion-extension rotation and prescribed valgus or varus torque with respect to the femur. Otherwise, the tibia was free. The hip center and ankle center were locked rigidly to the femur and tibia, respectively. In addition, the proximal insertion of the quadriceps tendon was fixed while the patella was left unconstrained.
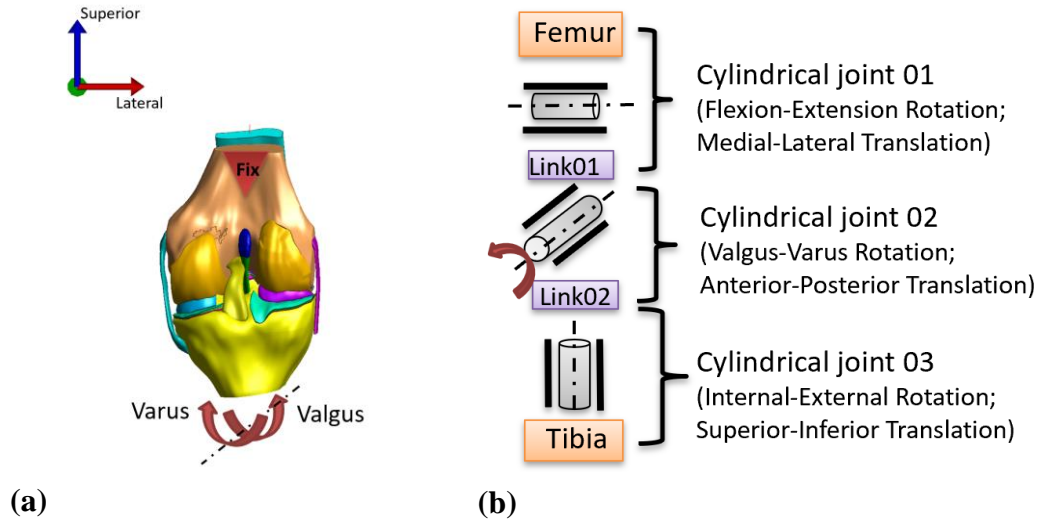
Figure 3.2.8 Boundary conditions descriptions for varus and valgus rotation. (a) Posterior view of the knee joint applied with varus and valgus torque on the tibia while the femur was fixed; (b) A series of cylindrical joints connecting femur and tibia. Each cylindrical joint allows one rotational degree of freedom about an axis and another translational degree of freedom along that axis.

3.2.3 Loads and Boundary Conditions for Squatting

Before applying loads, the pre-strain was applied to each ligament when the knee was in full extension. Thus, all loads were applied to the pre-strained knee joint, which is more realistic. In the squatting simulation, all rotations and translations of the femur were rigidly constrained, while the tibia and patella were left unconstrained. The hip center (a rigid body) was also rigidly locked with respect to the femur, preventing relative motions between them. Similarly, the ankle center (a rigid body) was rigidly locked to the tibia. In addition, the proximal end of the actuator (quadriceps tendon) was fixed except prescribed translation in the superior-inferior direction to change the length of the actuator. The model was not constrained.

During the simulations (Figure 3.2.9), the hip center was loaded with a gravitational force of 377.79N, which equals half the bodyweight of the donor (at a weight of 77.1 kg) for this finite element model. The gravitational force applied to the hip center was always

directed to the ankle center throughout the simulation. Before applying this gravitational force, the tibia was flexed at a slight angle (smaller than 10 degrees) by prescribing a flexion moment while the end of the actuator was fixed. Then, the gravitational force was incrementally applied by defining a linear load curve while removing the flexion moment. In this way, the knee model was approximately in balance while applying the gravitational force. This was helpful to avoid potential numerical problems.

The gravitational force was the only external force applied to the model and it generated a moment on the joint center since the end of the actuator (quadriceps tendon) was constrained. Thus, a resultant actuator force was produced by a counterbalance of the moment of gravitational force with the quadriceps tendon. Furthermore, compared to prescribed quadriceps muscle force in traditional squatting simulations, the quadriceps force was a resultant value in this study. After successfully applying the gravitational force, the model was in balance. The flexion angle was not prescribed during the next step, but the length of the actuator (quadriceps tendon) was changed. By increasing the length of the actuator (quadriceps tendon), the flexion angle increased as a result of the applied gravitational force.
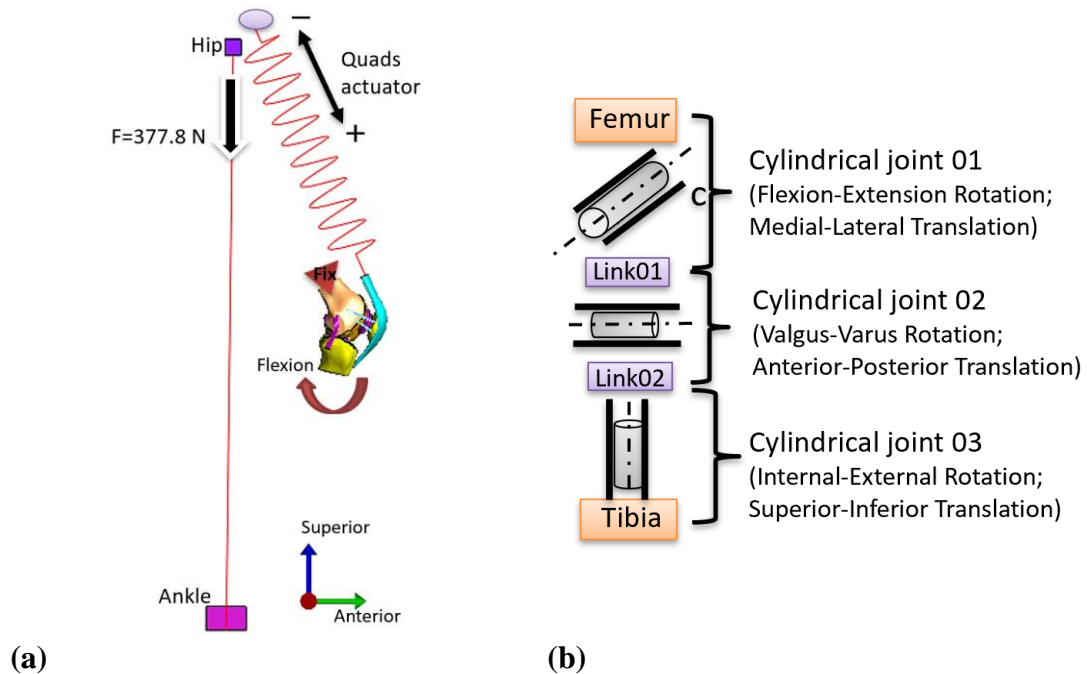

Figure 3.2.9 A full-leg squat model (a)Sagittal view of boundary conditions depictions. (b) A series of cylindrical joints connecting the femur and tibia.

44

3.3 Parametric Analysis Design Methods

In general, there are various approaches to performing sensitivity analysis. Commonly, sensitivity analysis is distinguished by how the inputs are conducted. The simplest and most common method for sensitivity analysis is one-at-a-time (OAT), which focuses on the difference of outputs resulting from deviations of the inputs from their normal values. Essentially, several input factors are of interest in sensitivity analysis, but only one parameter varies at a time during OAT analysis while other parameters are fixed at their normal values. However, the OAT approach cannot show the interactions between and across the input parameters [13]. Furthermore, the difficulty with this OAT method is that it is expensive and time-consuming. For example, when considering a situation with thirteen factors on three levels for each factor, the OAT method would require 3^{13} or 1,594,323 trials. As an alternative method, the Taguchi's method can provide an efficient way to process variance-based sensitivity analysis [14-16]. For example, the case with thirteen factors on three levels mentioned above could be conducted with only 27 trials using a classic orthogonal array $L_{27}(3^{13})$ with the Taguchi's method [17]. Also, this method requires that all the parameters are independent of each other, which means interactions among the parameters are significantly weak [16].

3.3.1 Design of *in situ* Strains Sensitivity Analysis

The initial strains for ligaments were defined as data from the previous study [1], as shown in Table 3.2.1. For the simulation without initial strains, the *in situ* strains were equal to 0%. The models with and without *in situ* strains were loaded in two scenarios: (1) 10 Nm valgus torque and (2) 10 Nm varus torque. The rotational kinematics and contact forces were compared between the pre-stressed and stress-free models under different loading scenarios.

Table 3.2.1: The initial strains defined in ligaments and tendons

ACL	PCL	MCL	LCL	PT	Resource
0.08	0.0	0.03	0.06	0.02	[1]

3.3.2 Design of Lower Limb Alignment Parametric Analysis

The inputs parameters of uncertainty were chosen to investigate the variation in tibiofemoral contact force distribution: the medial-lateral coordinate of hip center (MLHip), the medial-lateral coordinate of ankle center (MLAnkle), and the medial-lateral coordinate of the proximal center of quadriceps muscle (MLQuads), as shown in Figure 3.3.1. These parameters were taken from the OpenSim model, which was developed by a different specimen from the one used to develop the OpenKnee model. So, these parameters could disturb the lower limb frontal alignment in the initial model and influence the medial ratio of tibiofemoral contact force.
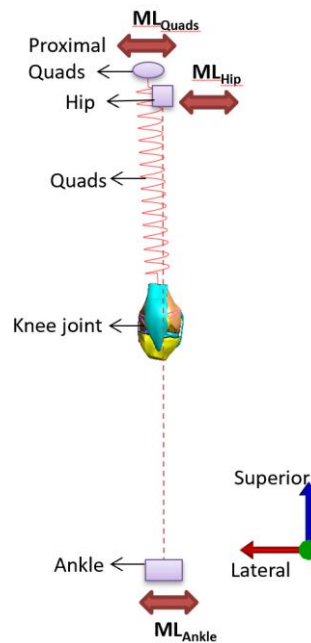
Figure 3.3.1 Frontal view of the full-leg FE model. The frontal alignment could be disturbed by varying the value of the medial-lateral coordinate of hip center (ML$_{Hip}$), the medial-lateral coordinate of ankle center (ML$_{Ankle}$), and the medial-lateral coordinate of the proximal center of quadriceps muscle (ML$_{Quads}$).

Sensitivity analysis was performed in this study using the Taguchi's method of orthogonal arrays, which analysts usually use in engineering designs of experiments and simulations [12,14-16]. This method was chosen for its reasonable number of trials and low computational cost. The chosen parameters of uncertainty were introduced as factors

in the Taguchi's method, which were independent of each other with no interactions. Seven levels were determined for each factor, which means a factor was changed from level one to seven. Each level for the factor had 5 mm medial translation as an increment. Therefore, the L49 matrix (Appendix a) was used for parametric study design in this model [18], which means that 49 different combinations were conducted in the simulation study. In Appendix a, the first combination shows that the coordinate of the hip center, proximal quadriceps insertion, and ankle center was translated medially 5 mm for each in the model. Since the parametric study aimed to examine the influence of the changed inputs of uncertainty on the outputs, the medial force ratio was output as the result of the Taguchi's method and compared to the experimental data from previous publications. A combination of the lowest RMSE between the predicted and experimental results was chosen to optimise the model parameters.

The medial contact force ratio (R_{mf}) in the tibiofemoral joint was output at every ten degrees of flexion from 20 to 90 degrees for each simulation in Appendix a. Then, the root-mean-square error (RMSE) between the predicted results in each simulation and the experimental results in the *in vivo* study by Kutzner et al. (2017) was calculated for each simulation, using the equation below:

$$RMSE = \sqrt{\frac{1}{N}\sum_{i=1}^{N}\left(R_{mf,i} - R_{k,i}\right)^2}$$

Where,

$R_{mf,i}$ is the predicted medial force ratio at the i-th increase ten degrees from 20 to 90 degrees of flexion in simulation.

$R_{k,i}$ is the experimental medial force ratio at the i-th increase ten degrees from 20 to 90 degrees of flexion in the study of Kutzner et al. (2017).

N is the total number of observations.

3.3.3 Design of Patella Thickness and Position Parametric Analysis

According to the free body diagram of moments during squatting (Figure 3.3.2), the moment produced by the bodyweight at a flexed position equals the moment produced by the reaction force of the quadriceps muscle [24]. The reaction force of the quadriceps muscle increased as the flexion lever arm increased since the lever arm of the quadriceps was assumed to be a constant. In a previous study [21], the negative relationship between the moment arm of quadriceps muscle force and the tibiofemoral contact force was reported during squatting. Therefore, the hypothesis was put forward in this study that the quadriceps muscle force will decrease as the moment arm of the quadricep force increases, resulting in tibiofemoral force decreasing. To observe the sensitivity of tibiofemoral contact force, the quadriceps moment arm can be increased by increasing patellar thickness. In addition, the length of the patellar tendon was increased to increase the patellar position superiorly. It was hypothesised that the quadriceps muscle force may be altered as the patellar position changed.
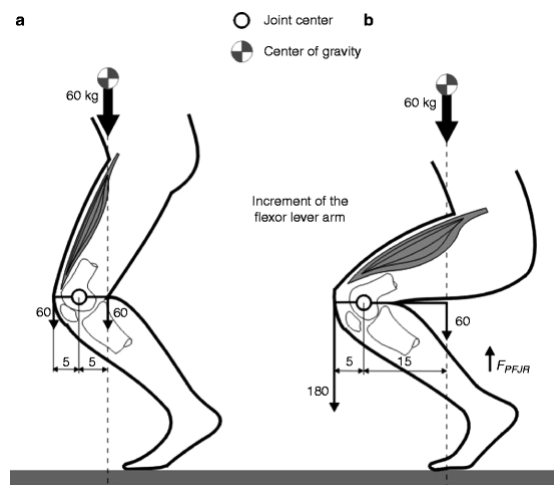
Figure 3.3.2: The free body diagram of moments during squatting. The reaction force of the quadriceps muscle force increased as the flexion lever arm of the body weight increased (Adapted from Sanchis-Alfonso 2006) [24] (Image permitted by Springer Nature)

The thickness of the patella (Figure 3.3.3a) in the initial model was measured in the axial view. The thickness of the patellar cartilage was included in the thickness of the patella, which corresponded with previous studies [26]. The length of the patellar tendon (Figure

3.3.3b) was defined as the distance from the tip of the patella apex to the proximal edge of the patellar tendon attached to the tibia [26]. Some previous studies reported the measurement of the patella and patellar tendon (PT) using MRI since MRI measurement has been proven to be accurate and reliable in estimating the geometry of the patella in its natural state [26-28]. A summary of these studies is shown in Table 3.3.1. In this table, the average length of the patellar tendon in [27] was 20 mm longer than the average value in [26] because the measurement in [27] used the distance from the tip of the patella apex to the distal edge of the patellar tendon attached to the tibia, while the measurement in [26] used the proximal edge of the patellar tendon attached to the tibia.
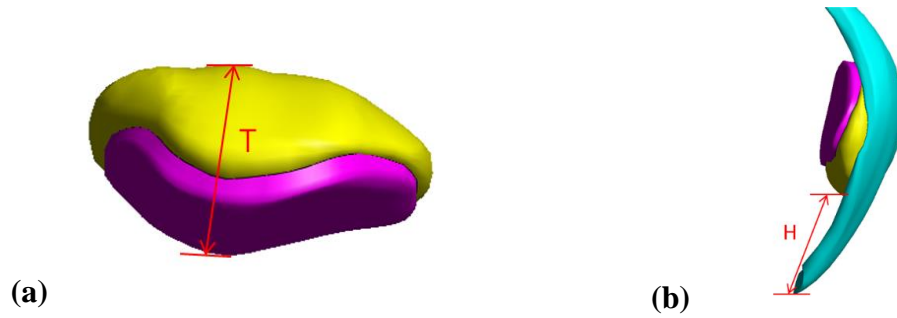

(a)   (b)

Figure 3.3.3: The measurement of the patella. (a): The thickness of the patella; (b): The longitudinal length of the patellar tendon.

Table 3.3.1: The reported patellar thickness and length of the patellar tendon

Resource	Mean patellar thickness (SD) / mm			Mean length of PT (SD) / mm		
	Total	Male	Female	Total	Male	Female
[26]	22.3 (1.9)	22.7 (1.8)	20.4 (1.2)	40.2 (4.2)	40.7 (4.2)	38.0 (3.4)
[27]	21.7 (1.3)	--	--	64.2 (4.4)	--	--
[28]	--	23.8 (1.4)	21.7 (1.4)	--	--	--

The patella thickness (T) and the longitudinal length of the patellar tendon (H) in the initial model were approximately 21 mm and 26 mm, respectively. In parametric study, T and H were increased one at a time by 5 mm and 10 mm, while always keeping the lower limb alignment in initial values. As a result, the outputs, including tibiofemoral contact force, patellofemoral contact force, quadriceps muscle force and patellar tendon force, were investigated and compared with data in the initial model and previous publications.

3.4 Result

3.4.1 Sensitivity to in situ strains

The relationship of torque and rotation angle is shown in Figure 3.4.1. In the pre-strain model, the torque-rotation response was apparently stiffer than the model without pre-strain.
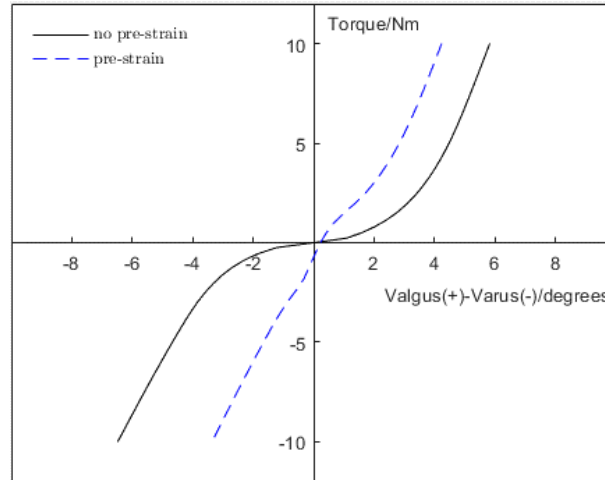

Figure 3.4.1: Valgus-varus rotation angles under 10 Nm torque for the simulation with pre-strain and without pre-strain.

Compared to the previous literature [7, 8], the torque-rotation response under 10 Nm valgus and varus torque in the model with pre-strain was more reasonable (Figure 3.4.2). In a previous study, Wan et al. (2013) examined laxity tests and ligament stress using a reconstructed 3D FE model with three different types of material for ACL, in which the model for the second type was the same as that in this study [7]. Under 10 Nm varus torque, the difference of varus angle between the study of Wan et al. (2013) and this study was 0.3 degrees. In addition, the FE model with non-linear springs as ligaments was used to examine laxity tests and collateral ligament contributions by Bendjaballah et al. (1997) [8]. As a result of this literature, the valgus rotation angle under 10 Nm valgus torque had a 0.6 degrees difference with the pre-strain model in this thesis.
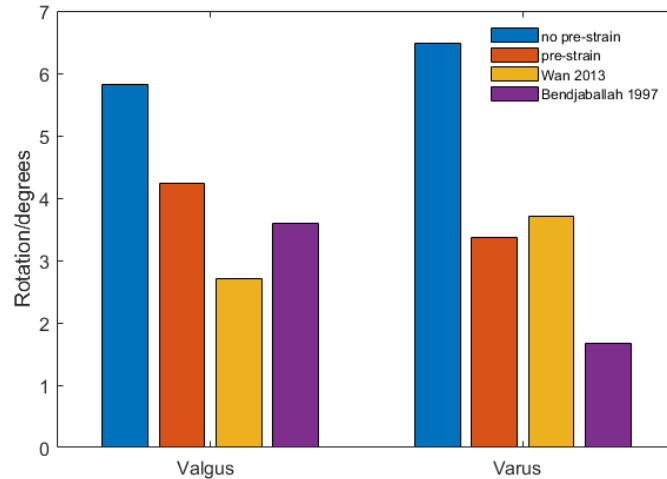
Figure 3.4.2: Valgus and varus rotation angles under 10 Nm torque in this study and previous literature [7,8].

The root mean square error (RMSE) under 10 Nm varus and valgus torque were calculated based on the data in this study and in the previous literature. As shown in Table 3.4.1, RMSE values in the pre-strain model were much lower than the values in the model without pre-strain. The pre-strain model resulted in the lowest errors in valgus rotation (1.2 degrees) and varus rotation (1.2 degrees).

Table 3.4.1: RMSE differences between this study and previous literature

Rotation [degrees]	No pre-strain model	Pre-strain model
Valgus rotation	2.7	1.2
Varus rotation	3.9	1.2

Average contact forces in lateral cartilage under valgus torque and medial cartilage under varus torque were examined in models with pre-strain and without pre-strain, as shown in Figure 3.4.3. In both valgus and varus torque simulations, average contact forces increased significantly in the pre-strain model, compared to the no pre-strain model. Therefore, joint responses, including rotation-torque response and contact force change, were significantly different in the model with pre-strain and without pre-strain. As a result, the model without pre-strain was too lax under valgus-varus rotations. However, the model with pre-strain could restore the physiological fidelity of the knee joint.
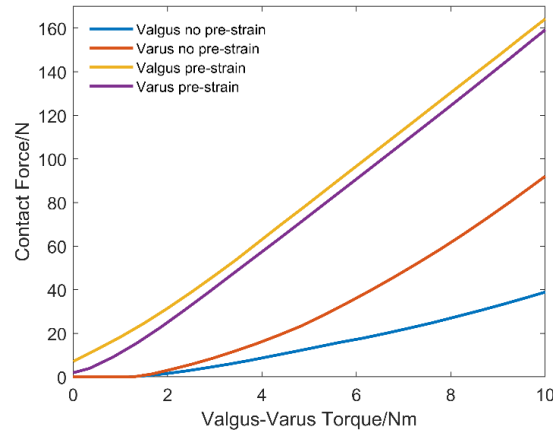
Figure 3.4.3: The average contact force under 10 Nm valgus and varus torque in the model with pre-strain and without pre-strain.

3.4.2 Sensitivity to lower limb alignment

Appendix a reports the medial force ratio (R_{mf}) in the tibiofemoral joint for each simulation at every ten degrees of flexion from 20 to 90 degrees. Appendix b reports RMSE and the average difference for each simulation. Box plots of RMSE and the average difference of hip, quadriceps and ankle at each offset are shown in Figure 3.4.4 and Figure 3.4.5. The red line of each box shows the median of each group. As suggested by the Taguchi's method [11,14,15], these results enabled the experimental designers to decide the optimal sequence for the design problem. For each factor, we can choose the offset value with the lowest median. Thus, the optimal sequence based on Figure 3.4.5 was reported in Appendix c.
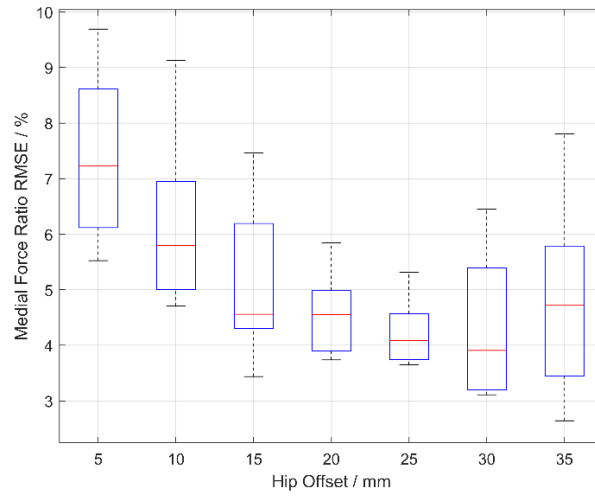
(a)
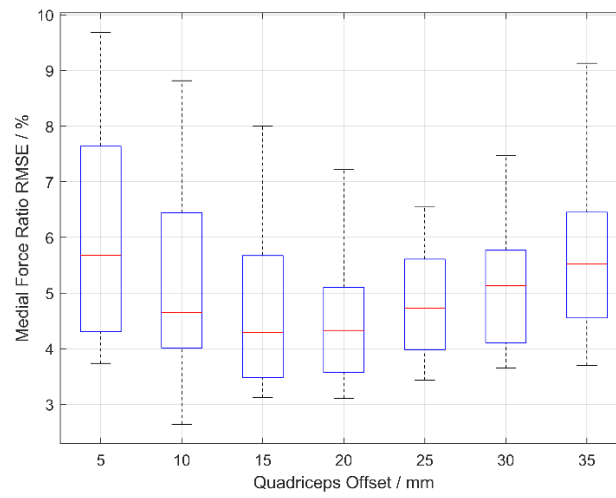
(b)
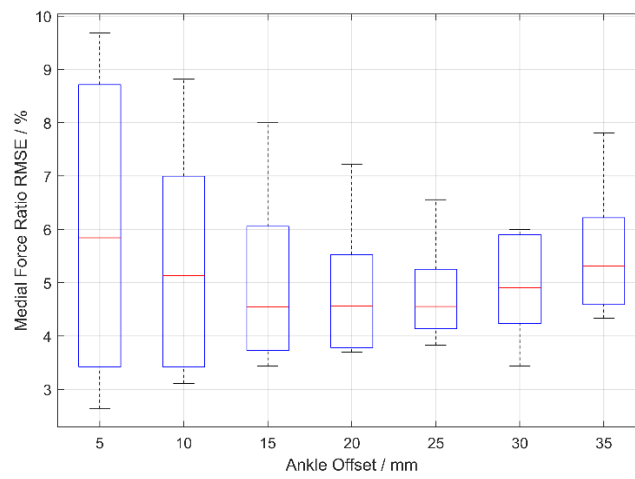
(c)

Figure 3.4.4: Box plots of RMSE of the hip (a), quadriceps (b) and ankle (c) at different offsets.
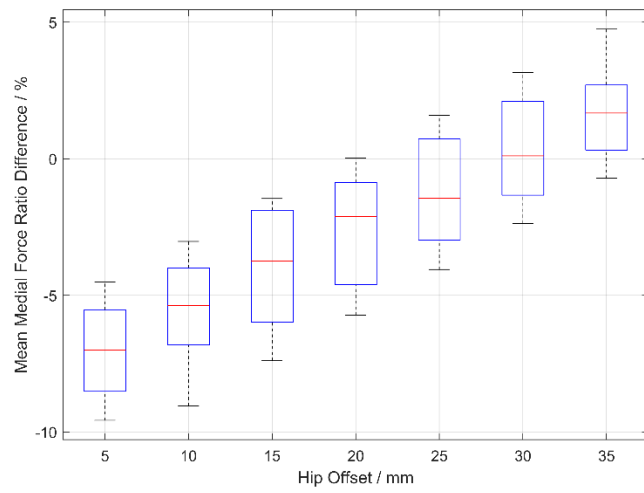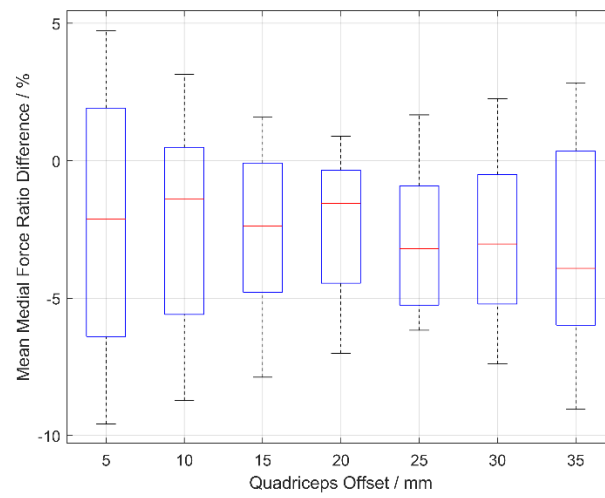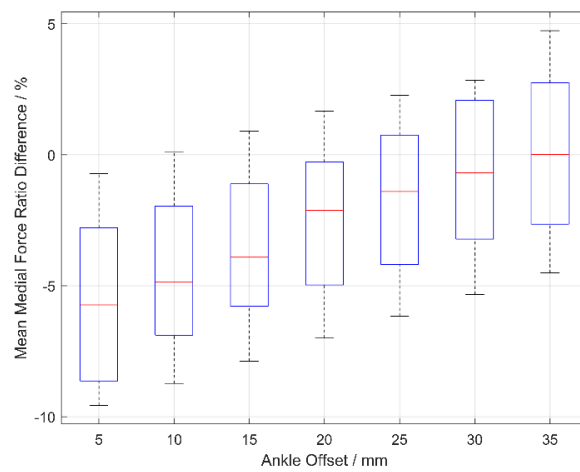
(a)

(b)

(c)

Figure 3.4.5: Box plots of the average difference of hip (a), quadriceps (b) and ankle (c) at different offsets.

Appendix c reports the series of the offset level, which is the optimal choice of each factor (hip, quadriceps and ankle), since each has the lowest median value of RMSE and thus better fit the experimental data. Furthermore, a graphical representation identifying the optimum situation readily is depicted in Figure 3.4.5 to emphasize the result. The lowest median value of RMSE was at 30 mm medial offset of the hip, at 15 mm medial offset of the quadriceps, and at 15 mm medial offset of the ankle. However, this optimal sequence is not among the combinations in Appendix a. So, a new simulation was planned and the results of this sequence, including average difference and RMSE between the data in this model and in publications are shown in Appendix c.

The values of average difference for each simulation are shown in Appendix b and Figure 3.4.5. The smallest value (close to zero) of the median of the average difference was at 30 mm offset of the hip, at 20 mm offset of the quadriceps and 35 mm offset of the ankle. However, this optimal sequence is not included in Appendix a and was planned for a new simulation. Thus, the results of this sequence are reported in Appendix b. In addition, according to Figure 3.4.5b, the results of the average difference were not significantly affected by variations in quadriceps offset, although the offset of 20 mm provides the best choice.

The optimal sequence and the corresponding results compared to previous experiments are shown in Appendix c. The optimal sequence with the lowest RMSE was included in the validated model as the baseline model in the next chapter. The validated baseline model was used to study the influence of the altered knee joint alignment in the frontal and axial plane. The medial force ratios in the model with the chosen optimal sequence during squatting are shown in Figure 3.4.6, compared with data in the initial model and the experiments by Kutzner et al. (2017) [19]. The medial force ratios during squatting in the initial model had significant differences from the data in previous studies. At 30 degrees of flexion, the difference in medial force ratio between the initial model and the experiment data is -14%, while it is 1.6% between the model with the optimal sequence and the experiment data. During squatting, the RMSE between the initial model and the experiment data was 11.9, while it was 2.3 between the model with the optimum sequence and the *in vivo* data. Also, the average difference to the experiment data

decreased from -11.61 in the initial model to -0.46 in the model with optimum alignment sequence.
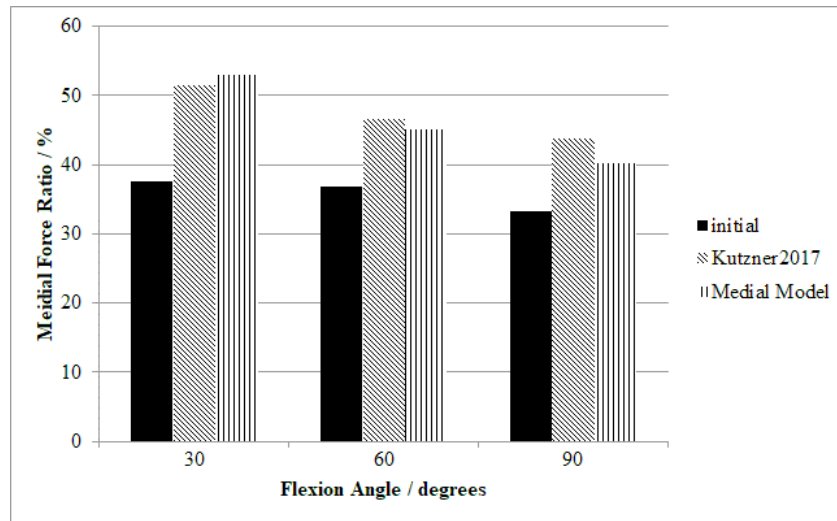

Figure 3.4.6: The medial force ratios at 30, 60 and 90 degrees of flexion in the initial model, the model with optimal sequence and experiments by Kutzner et al. (2017)

Figure 3.4.7 shows the linear regression analysis between the medial force ratio in the tibiofemoral joint and the different offsets of hip, quadriceps, and ankle at 20 and 90 degrees of flexion. For the hip, the coefficient of determination (R^2) was 0.6071 at 20 degrees and 0.7758 at 90 degrees. For the quadriceps, the coefficients of determination (R^2) at 20 and 90 degrees of flexion were both less than 0.01, which shows that the medial quadriceps offsets corresponded poorly with the medial force ratio. For the ankle, the coefficient of determination was 0.3845 at 20 degrees and this decreased to 0.0546 at 90 degrees of flexion. Therefore, the correlation between the offset value and the medial force ratio increased for the hip as the flexion angle increased, while it decreased for the ankle as the flexion angle increased.

Figure 3.4.8 shows the correlation between the total tibiofemoral contact force and the different offsets of hip, quadriceps and ankle at 20 and 90 degrees of flexion. For the hip, the coefficients of determination (R^2) were 0.2817 and 0.0009, respectively, which implies that, as the flexion angle increased, the offsets of the hip corresponded poorly with the total contact force in the tibiofemoral joint. For the quadriceps, values of R^2

56

ranged from 0.0018 to 0.0227, which implies a poor correlation both at low and high flexion angles. For the ankle, the values of R^2 were 0.6882 at 20 degrees and 0.9889 at 90 degrees of flexion, with both showing a strong correlation between the ankle offsets and the total contact force in the tibiofemoral joint.
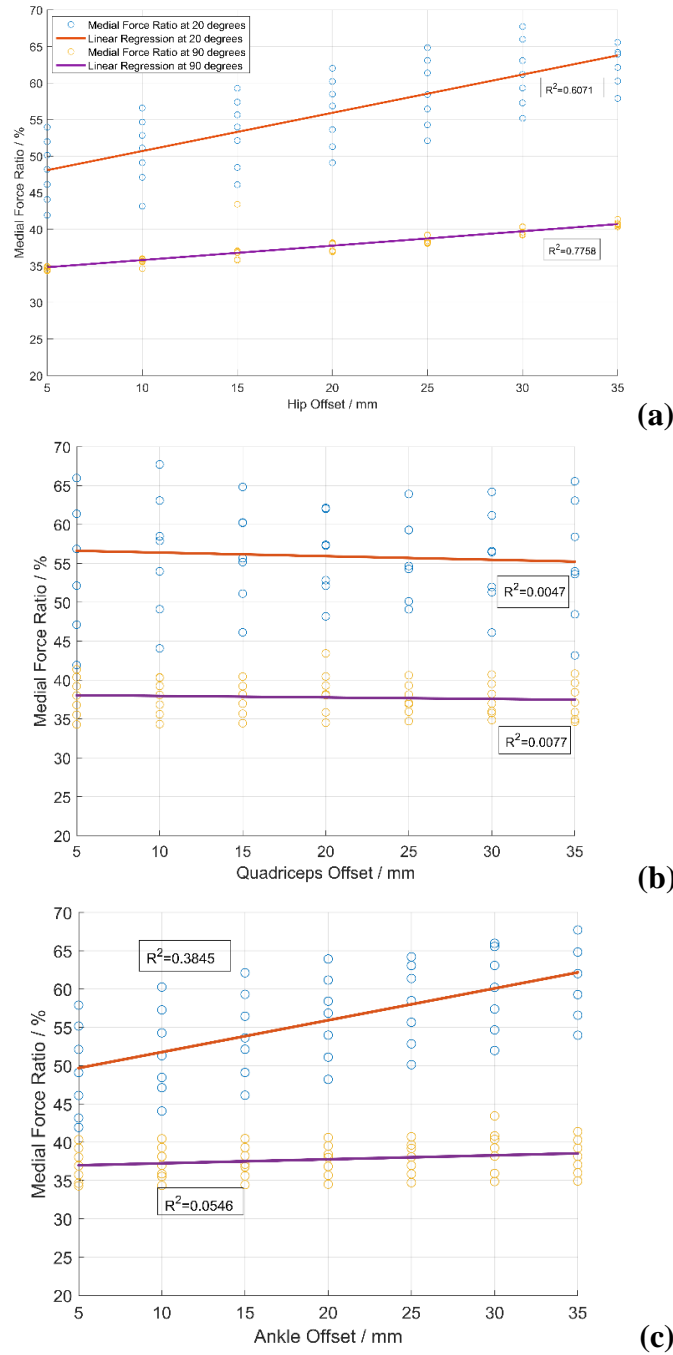

Figure 3.4.7: Linear regression analysis between the medial force ratio in the tibiofemoral joint and the offsets of the hip (a), quadriceps (b) and ankle (c).
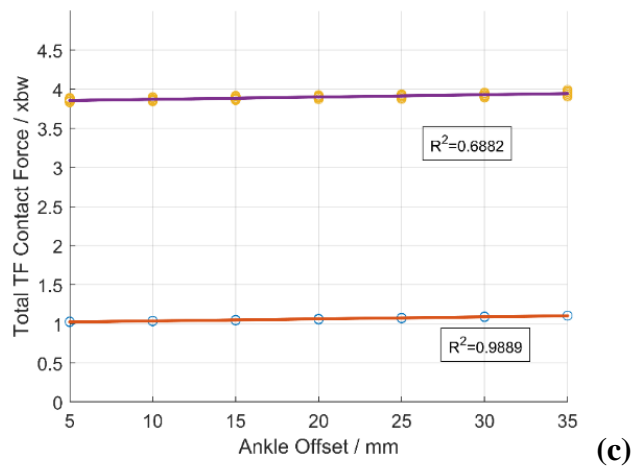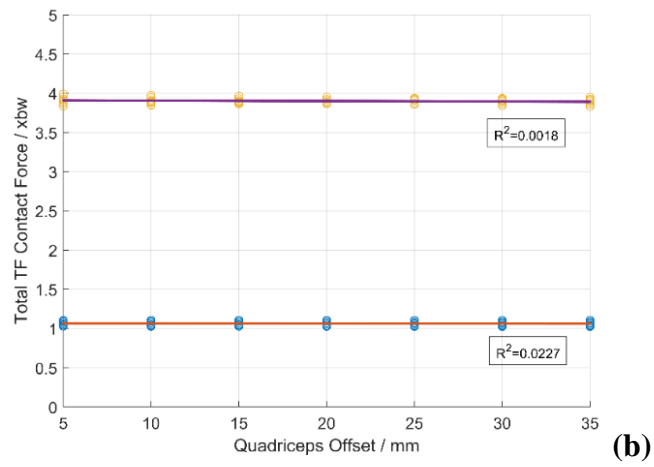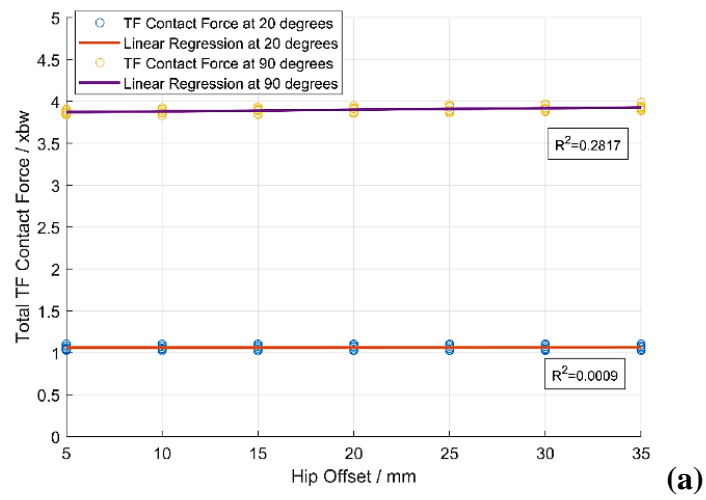
Figure 3.4.8: Linear regression analysis between the total tibiofemoral contact force and the offsets of the hip (a), quadriceps (b) and ankle (c).

3.4.3 Sensitivity to Patella Thickness and Position

Figure 3.4.9 shows total tibiofemoral contact force normalized to bodyweight during squatting in this study and data from the previous literature [19, 21-23]. The magnitude of the total TF contact force in the initial model increased from 1.02 to 3.82 times bodyweight (BW) as the flexion angle increased from 20 to 90 degrees. The values of the TF contact force in the initial model were higher than the values from the literature, and the difference between them increased as the flexion angle increased. The maximum difference between the TF force in the initial model and the literature [21] was 1.89 times bodyweight at 90 degrees of flexion. In the parametric study, lengthening the patellar tendon and altering the model to optimal sequence had no effects on the magnitude of the total TF contact force. However, models with thickening patella had significantly decreased TF contact forces, which were closer to data in the previous literature [19, 21-23] with a difference between -0.53 to 1.26. Moreover, Figure 3.4.10 shows an inverse relationship between the magnitude of the TF contact force and the thickness of the patella.
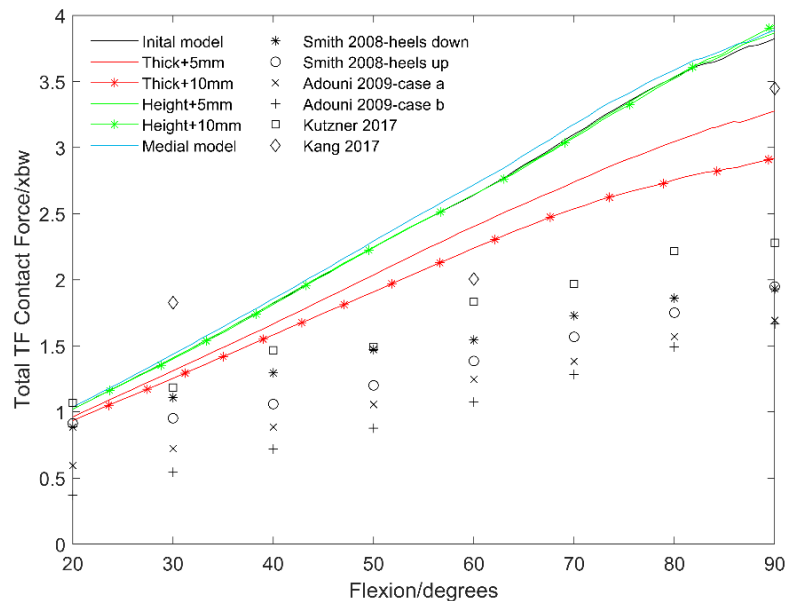

Figure 3.4.9: Total tibiofemoral contact forces normalized to bodyweight in the initial model, models with thickening patella by 5 mm and 10 mm, models with lengthening patellar tendon by 5 mm and 10 mm, model with optimal sequence, and models in previous publications [19, 21-23]

Figure 3.4.10 shows total patellofemoral contact force during squatting from 20 to 90 degrees of flexion from the FE model in this study and data extracted from the previous literature [22]. The model with the optimal sequence did not affect the PF contact force. In contrast, the model with a thickening patella and the model with a higher patella both increased the magnitude of PF contact force after 70 degrees of flexion during squatting.

Figure 3.4.10: Total patellofemoral contact force normalized to bodyweight in the initial model, models with thickening patella by 5 mm and 10 mm, models with lengthening patellar tendon by 5 mm and 10 mm, the model with optimal sequence, and in models in a previous publication [22]

Figure 3.4.11 shows the quadriceps tendon force during squatting from 20 to 90 degrees of flexion from the FE model in this study and data from the previous literature [22]. The model with increased patella thickness had decreased quadriceps tendon force, which is closer to the literature than the other models in this study. After 80 degrees of flexion during squatting, the quadriceps forces increased to larger than the value in the initial model.

Figure 3.4.11: The quadriceps tendon force normalized to bodyweight in the initial model, models with thickening patella by 5 mm and 10 mm, models with lengthening patellar tendon by 5 mm and 10 mm, the model with optimal sequence, and in models in a previous publication [22]

Figure 3.4.12 shows the patellar tendon force during squatting from 20 to 90 degrees of flexion from the FE model in this study and data from the previous literature [22]. The magnitudes of patellar tendon force from the models in this study were lower than the data from the literature. The model with the optimal sequence and the model with higher patella did not affect the value of patellar tendon force. In contrast, the model with thickening patella significantly decreased the magnitude of the patellar tendon force.
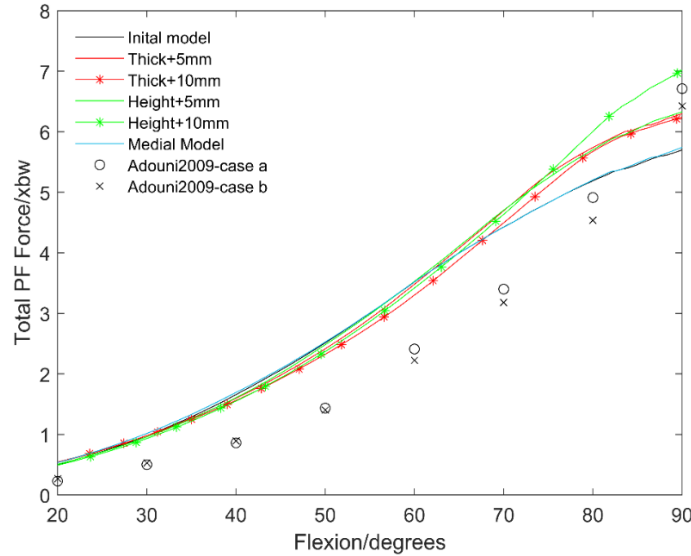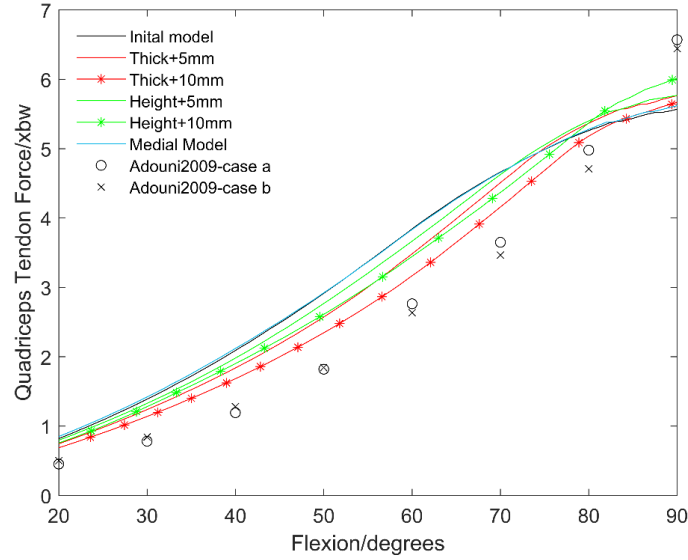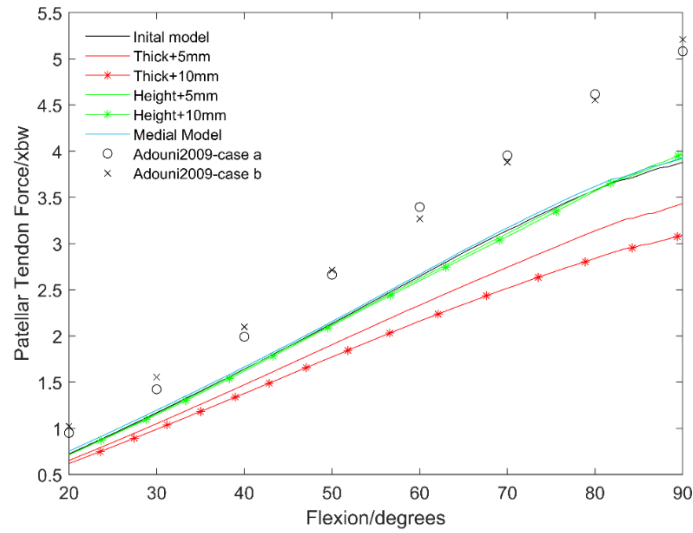
Figure 3.4.12: The patellar tendon force normalized to bodyweight in the initial model, models with thickening patella by 5 mm and 10 mm, models with lengthening patellar tendon by 5 mm and 10 mm, the model with optimal sequence, and in models in a previous publication [22]

3.5 Discussion

To develop a full-leg squatting model, we combined the modified finite element knee joint model and the coordinates of the hip center, ankle center and proximal quadriceps insertion point from a musculoskeletal model. The parametric analysis in this chapter was concerned about the variations of outputs, including contact force distribution, total contact forces and muscle forces under variations of inputs parameters such as *in situ* strains, frontal alignment, patella thickness and position, which are subject-specific. The model with *in situ* strains was compared with the model without *in situ* strains under valgus and varus torque to study the influence of *in situ* strains on kinematics and contact force. In addition, the medial-lateral coordinates of the hip center, ankle center and proximal quadriceps insertion point were offset medially to investigate the sensitivity of tibiofemoral contact force distribution to frontal alignment during squatting. Also, patella thickness and patellar tendon length were increased to explore the variations in total contact forces in both tibiofemoral and patellofemoral joint and muscle forces. The results were compared with previous studies in terms of tibiofemoral contact force,

62

patellofemoral contact force, medial force ratio in the tibiofemoral joint, quadriceps force and patellar tendon force. The validated model with more reasonable parameters than the initial model was applied to study the effect of knee deformities in the next chapter.

Using parametric analysis, this study reports that the relationship between the tibiofemoral contact force distribution and frontal knee joint alignment is linear (Figure 3.4.7). However, the frontal plane alignment had weak effects on the total tibiofemoral contact force (Figure 3.4.8). The same trends were found in previous studies [29, 30]. The RMSE to the *in vivo* data decreased from 11.89 to 2.33 after changing the alignment to the optimum sequence in the parametric study (Figure 3.4.6). In *in vivo* measurement, Kutzner et al. (2017) collected the medial and lateral forces in tibiofemoral joints from patients with instrumented knee implants during single-leg and double-leg support activities. The patients in this test had an average frontal alignment of 3° varus, which has been proven to be a neutral alignment in healthy patients.

Furthermore, the sensitivity of medial tibiofemoral contact force ratio to altered hip center, ankle center and proximal quadriceps center was quantified separately in this study. Increasing the medial coordinates of the hip center and ankle center implies increasing the varus angle of the femur mechanical axis (center of the hip to center of the knee joint) and the tibia mechanical axis (center of the knee joint to the center of the talus), respectively. Also, increasing the medial coordinates of the proximal quadriceps center equals decreasing the Q-angle, which is similar to the previous experiments [31]. As a result, the hip center position in variations had a more significant effect on the tibiofemoral contact force distribution than the ankle center position in variations during squatting, especially at high flexion angle. At 90 degrees of flexion, no significant correlation was found between the ankle center medial offset and the medial force ratio, with a coefficient of determinant (R^2) equal to 0.0546. In addition, the correlations between the Q-angle and medial force ratio or total TF contact force were small (Figure 3.4.7b, Figure 3.4.8b). However, according to our knowledge, no previous ligament has observed the effect of femur mechanical axis angle, tibia mechanical axis angle and Q-angle separately. In some computational studies [1, 32], the femur mechanical axis and tibia mechanical axis have been rotated by half of the total valgus or varus angle for each

63

to examine the sensitivity of knee contact forces in medial and lateral condyles to the tibiofemoral alignment. In addition, some other computational studies have only altered the tibial abduction and adduction angle to simulate the different tibiofemoral alignment angles [29, 30]. Other studies have observed the influence of tibiofemoral alignment on contact forces based on subject-specific FE models [34] or *in vivo* experiments [19,35], where the tibiofemoral alignment angles were analyzed using standing full-extension legs *in vivo*, and they were unable to be altered for each subject.

In the parametric study, the medial force ratios in the models with different tibiofemoral alignment angles were compared with *in vivo* experiments [19,35]. Accordingly, the model with the lowest RMSE had a tibiofemoral alignment of 6.06º varus and a decreased Q-angle by 1.38º with respect to the initial model. According to a previous study [42], the standard deviation of Q-angle in healthy patients is roughly 5º. The RMSE in medial force ratio between the validated and initial models was 12.05 during squatting from 20 to 90 degrees of flexion. The medial force ratio at 90 degrees varied from 33.2% in the initial model to 40.34% in the validated model. *In vivo* measurements [19,35] reported the medial force ratio ranging from 29% to 53% during double-leg supported knee bends at the instant of peak resultant joint force in patients with a tibiofemoral alignment angle ranging from 7º varus to 4.5º valgus. With the same patients, [36] reported the maximum difference in peak medial contact force of approximately one-time bodyweight between patients with 6.5º varus and 4.5º valgus aligned knees during daily activities, including walking and squatting. With 500 healthy volunteers, a previous study [37] reported that 32% of men and 17% of women had a tibiofemoral alignment of 3º varus or more. Also, 73% of the 500 healthy volunteers had a tibiofemoral alignment angle between 3º valgus and 3º varus [37]. The same deviation of 3º in healthy participants was found in another study [38] and the author also reported that the standard deviation of tibiofemoral alignment was 8º in osteoarthritic patients.

The tibiofemoral contact force magnitude is sensitive to the thickness of the patella (Figure 3.4.9). As the flexion angle increased, so did the effect of this parameter in this study. Therefore, the maximum difference occurred at 90 degrees of flexion, where the TF contact force decreased by 0.9-times bodyweight. A similar correlation was also found in a

previous study [21], in which the TF contact force decreased as the moment arm of the quadricep muscle increased during squatting, and the effect was more substantial as the flexion angle increased. In addition, we observed the patellofemoral contact force magnitude increased (Figure 3.4.10) as the patella thickened after 70 degrees of flexion, where a maximum difference was 0.54-times bodyweight at 90⁰. This result follows the trends identified in the previous studies [39,46,47]. The sensitivity of PF contact force to patellar thickness was 0.41xbw/mm in [39], while the sensitivity of PF pressure to patellar thickness was approximately 10%/mm in [47]. In addition, according to [39], a 3 mm superior or inferior position of the patellar component led to a 5% increase or 16% decrease of PF contact force magnitude, respectively. Similarly, a 5mm superior position in this study led to a 9% increase in PF contact force magnitude (Figure 3.4.11).

In this study, the relative increase in the quadriceps force magnitude during 20 to 90 degrees squatting exceeded the associated increase in the patellar tendon force magnitude. Also, the patella tendon force ratio to the quadriceps force decreased as the flexion angle increased. The predicted muscle forces in this study agree with those in the previous literature [22, 40-41], and their ratio follows the trends in [22, 42, 44]. Thus, muscle forces are significantly sensitive to patellar thickness (Figure 3.4.11, Figure 3.4.12), leading to the ratio of patellar tendon force over the quadriceps force (F_{pt}/F_q) decreasing up to 0.15. In the 10 mm thickening patella model, the ratio (F_{pt}/F_q) was 0.9 at 20 degrees and 0.546 at 90 degrees. These ratios are in good agreement with the previous literature [22], where the ratio was 0.95 at 20⁰ and 0.39 at 90⁰. The tendency of this ratio (F_{pt}/F_q) during knee flexion confirms that the PF joint is not a simple pully [44,45] as the pull force is equal on both ends of the simple pulley. Although both tendon forces decrease as the patella thickness increases, the total PF contact force increases. According to Figure 2.4.2, this can result from a smaller angle between tendon forces vectors due to a thicker patella.

In summary, the model with the more varus tibiofemoral alignment (hip center medial offset 35 mm, ankle center medial offset 5 mm and the proximal quadriceps medial offset 10 mm) and with a 10 mm thickener patella was chosen as a reference model because it yielded the same trends as previous squatting studies.

3.6 Conclusion

This chapter aimed (1) to develop a full-leg model and (2) investigate the influence of the uncertainty inputs and validate the results with previously published data. The first aim was achieved by combining the general FE model from the OpenKnee project and the coordinates of the lower extremity (hip center, ankle center and proximal quadriceps insertion) from a musculoskeletal model to be a full-leg FE model. In addition, pre-strains were applied to the ligaments and muscle/tendons while keeping the knee full-extension before squatting. For the second aim, sensitivity analysis was performed to investigate outputs under the inputs (tibiofemoral alignment, patella thickness and patella superior-inferior position) in variations. Then, the outputs (total contact forces and medial force ratio in the tibiofemoral joint, total contact force in the patellofemoral joint, the quadriceps reaction force and patellar tendon resultant force) were validated by comparing trends with published trends from *in vivo* experiments and computational simulations during squatting. According to these results, tibiofemoral alignment strongly influenced the contact distributions while the patella thickness influenced the total contact force.The model with the lowest RMSE to the published data was chosen as the reference model to study the influence of the knee deformities (see Chapter 4). This suggests that the boundary conditions and lower extremity parameters we used in this full-leg squatting model were desirable and this model is appropriate to be applied as a reference.

References

[1] Smith CR, Vignos MF, Lenhart RL, Kaiser J, Thelen DG. The influence of component alignment and ligament properties on tibiofemoral contact forces in total knee replacement. *J Biomech Eng*. 2016;138(2). doi:10.1115/1.4032464

[2] Meister BR, Michael SP, Moyer RA, Kelly JD, Schneck CD. Anatomy and kinematics of the lateral collateral ligament of the knee. Am J Sports Med. 2000;28(6):869-878.

[3] Espregueira-Mendes, da Silva MV. Anatomy of the lateral collateral ligament: a cadaver and histological study. Knee Surg Sports Traumatol Arthrosc. 2006;14(3):221-228.

[4] Lenhart RL, Kaiser J, Smith CR, Thelen DG. Prediction and Validation of Load-Dependent Behavior of the Tibiofemoral and Patellofemoral Joints During Movement. Ann Biomed Eng. 2015;43(11):2675-2685.

[5] ANSYS contact technology guide. ANSYS Release 9.0.002114.© SAS IP, Inc.

[6] ABAQUS analysis user's manual version 6.6

[7] Wan C, Hao Z, Wen S. The effect of the variation in ACL constitutive model on joint kinematics and biomechanics under different loads: a finite element study. *J Biomech Eng*. 2013;135(4):041002.

[8] Bendjaballah MZ, Shirazi-Adl A, Zukor DJ. Finite element analysis of human knee joint in varus-valgus. *Clin Biomech (Bristol, Avon)*. 1997;12(3):139-148.

[9] French, S. Modelling, making inferences and making decisions: The roles of sensitivity analysis. *Top.* 2003;11: 229-251.

[10] Jack P.C. Kleijnen. Sensitivity analysis and related analyses: A review of some statistical techniques. *Journal of Statistical Computation and Simulation*. 1997;57:1-4, 111-142.

[11] Carino, C. Structural layout assessment by orthogonal array based simulation. *Mechanics Research Communications*. 2006;*33*(3), 292-301.

[12] Saltelli, A., Chan, K., Scott, E.M. Sensitivity analysis. *John Wiley & Sons Ltd.* 2006.

[13] Gunter, B. Statistically Designed Experiments. *Quality Progress*. 1990;(4): 74.

[14] Taguchi, G. Introduction to Quality Engineering: Designing Quality into Products and Processes. *Asian Productivity Organization*. 1986.

[15] Taguchi, G., Konishi, S. Orthogonal Arrays and Linear Graphs. *American Supplier Institute Inc., Dearborn, MI.* 1987.

[16] Phadke, S. M. Quality Engineering Using Robust Design. *Englewood Cliffs, N. J.: Prentice Hall.* 1989.

[17] Kacker RN, Lagergren ES, Filliben JJ. Taguchi's Orthogonal Arrays Are Classical Designs of Experiments. *J Res Natl Inst Stand Technol*. 1991;96(5):577-591.

[18] Hedayat, A.S., Sloane, N.J.A. and Stufken, J. *Orthogonal Arrays: Theory and Applications. Springer, New York.* 1999.

[19] Kutzner I, Bender A, Dymke J, Duda G, von Roth P, Bergmann G. Mediolateral force distribution at the knee joint shifts across activities and is driven by tibiofemoral alignment. Bone Joint J. 2017;99-B(6):779-787.

[20] Hale R, Green J, Hausselle J, Saxby D, Gonzalez RV. Quantified in vitro tibiofemoral contact during bodyweight back squats. J Biomech. 2018;79:21-30.

[21] Smith SM, Cockburn RA, Hemmerich A, Li RM, Wyss UP. Tibiofemoral joint contact forces and knee kinematics during squatting. *Gait Posture.* 2008;27(3):376-386.

[22] Adouni M, Shirazi-Adl A. Knee joint biomechanics in closed-kinetic-chain exercises. *Comput Methods Biomech Biomed Engin.* 2009;12(6):661-670.

[23] Kang KT, Koh YG, Jung M, et al. The effects of posterior cruciate ligament deficiency on posterolateral corner structures under gait- and squat-loading conditions: A computational knee model. *Bone Joint Res.* 2017;6(1):31-42.

[24] Sanchis-Alfonso, V., Ávila-Carrasco, C., Prat-Pastor, J.M., Atienza, C.M., Cuñat, E. (2006). Biomechanical Bases for Anterior Knee Pain and Patellar Instability. In: Sanchis-Alfonso, V. (eds) Anterior Knee Pain and Patellar Instability. Springer, London. https://doi.org/10.1007/978-0-85729-507-1_6

[25] Lenton GK, Bishop PJ, Saxby DJ, et al. Tibiofemoral joint contact forces increase with load magnitude and walking speed but remain almost unchanged with different types of carried load. *PLoS One.* 2018;13(11):e0206859. Published 2018 Nov 5.

[26] Yoo JH, Yi SR, Kim JH. The geometry of patella and patellar tendon measured on knee MRI. *Surg Radiol Anat.* 2007;29(8):623-628.

[27] Basso O, Johnson D., Amis A. The anatomy of the patellar tendon. *Knee surgery, sports traumatology, arthroscopy : official journal of the ESSKA.* 2001;9(1):2-5.

[28] Kim MH, Yoo MJ, Seo JB et al. Statistical analysis of the patellar thickness in adult by MRI. *J Korean Orthop Assoc.* 2005;40:646–651

[29] Saliba CM, Brandon SCE, Deluzio KJ. Sensitivity of medial and lateral knee contact force predictions to frontal plane alignment and contact locations. *J Biomech.* 2017;57:125-130. doi:10.1016/j.jbiomech.2017.03.005

[30] Adouni M, Shirazi-Adl A. Partitioning of knee joint internal forces in gait is dictated by the knee adduction angle and not by the knee adduction moment. *J Biomech.* 2014;47(7):1696-1703. doi:10.1016/j.jbiomech.2014.02.028

[31] Mizuno Y, Kumagai M, Mattessich SM, et al. Q-angle influences tibiofemoral and patellofemoral kinematics. *J Orthop Res.* 2001;19(5):834-840. doi:10.1016/S0736-0266(01)00008-0

[32] Lerner ZF, DeMers MS, Delp SL, Browning RC. How tibiofemoral alignment and contact locations affect predictions of medial and lateral tibiofemoral contact forces. *J Biomech*. 2015;48(4):644-650. doi:10.1016/j.jbiomech.2014.12.049

[33] Van Rossom S, Wesseling M, Smith CR, et al. The influence of knee joint geometry and alignment on the tibiofemoral load distribution: A computational study. *Knee*. 2019;26(4):813-823. doi:10.1016/j.knee.2019.06.002

[34] Yang N, Nayeb-Hashemi H, Canavan PK. The combined effect of frontal plane tibiofemoral knee angle and meniscectomy on the cartilage contact stresses and strains. *Ann Biomed Eng*. 2009;37(11):2360-2372. doi:10.1007/s10439-009-9781-3

[35] Bergmann G, Bender A, Graichen F, et al. Standardized loads acting in knee implants. *PLoS One*. 2014;9(1). doi:10.1371/journal.pone.0086035

[36] Trepczynski A, Kutzner I, Bergmann G, Taylor WR, Heller MO. Modulation of the relationship between external knee adduction moments and medial joint contact forces across subjects and activities. *Arthritis Rheumatol*. 2014;66(5):1218-1227. doi:10.1002/art.38374

[37] Bellemans J, Colyn W, Vandenneucker H, Victor J. The chitranjan ranawat award. *Clin Orthop Relat Res*. 2012;470(1):45-53. doi:10.1007/s11999-011-1936-5

[38] Cooke D, Scudamore A, Li J, Wyss U, Bryant T, Costigan P. Axial lower-limb alignment: comparison of knee geometry in normal volunteers and osteoarthritis patients. *Osteoarthritis Cartilage*. 1997;5(1):39-47. doi:10.1016/s1063-4584(97)80030-1

[39] Kebbach M, Darowski M, Krueger S, et al. Musculoskeletal multibody simulation analysis on the impact of patellar component design and positioning on joint dynamics after unconstrained total knee arthroplasty. *Materials (Basel)*. 2020;13(10). doi:10.3390/ma13102365

[40] Cohen ZA, Roglic H, Grelsamer RP, et al. Patellofemoral stresses during open and closed kinetic chain exercises. An analysis using computer simulation. *Am J Sports Med*. 2001;29(4):480-487. doi:10.1177/03635465010290041701

[41] Shelburne KB, Pandy MG. A dynamic model of the knee and lower limb for simulating rising movements. *Comput Methods Biomech Biomed Engin*. 2002;5(2):149-159. doi:10.1080/10255840290010265

[42] Ali AA, Shalhoub SS, Cyr AJ, et al. Validation of predicted patellofemoral mechanics in a finite element model of the healthy and cruciate-deficient knee. *J Biomech*. 2016;49(2):302-309. doi:10.1016/j.jbiomech.2015.12.020

[43] Herrington L, Nester C. Q-angle undervalued? The relationship between Q-angle and medio-lateral position of the patella. *Clin Biomech*. 2004;19(10):1070-1073. doi:10.1016/j.clinbiomech.2004.07.010

[44] Singerman R, Berilla J, Archdeacon M, Peyser A. In vitro forces in the normal and cruciate-deficient knee during simulated squatting motion. *J Biomech Eng*. 1999;121(2):234-242. doi:10.1115/1.2835109

[45] Grelsamer RP, Weinstein CH. Applied biomechanics of the patella. *Clin Orthop Relat Res*. 2001;(389):9-14. doi:10.1097/00003086-200108000-00003

[46] Hsu HC, Luo ZP, Rand JA, An KN. Influence of patellar thickness on patellar tracking and patellofemoral contact characteristics after total knee arthroplasty. *The Journal of arthroplasty*. 1996;11(1):69-80. doi:10.1016/S0883-5403(96)80163-X

[47] Tanikawa H, Tada M, Ogawa R, et al. Influence of Patella thickness on Patellofemoral pressure in total knee Arthroplasty. *BMC Musculoskelet Disord*. 2021;22(1):1-5. doi:10.1186/s12891-021-04175-y

[48] Limbert G, Taylor M, Middleton J. Three-dimensional finite element modelling of the human ACL: simulation of passive knee flexion with a stressed and stress-free ACL. *J Biomech*. 2004;37(11):1723-1731.

[49] Maas SA, Erdemir A, Halloran JP, Weiss JA. A general framework for application of prestrain to computational models of biological materials. *J Mech Behav Biomed Mater*. 2016;61:499-510. doi:10.1016/j.jmbbm.2016.04.012

[50] Naghibi Beidokhti H, Janssen D, van de Groes S, Hazrati J, Van den Boogaard T, Verdonschot N. The influence of ligament modelling strategies on the predictive capability of finite element models of the human knee joint. *J Biomech*. 2017;65:1-11. doi:10.1016/j.jbiomech.2017.08.030

Chapter 4

4 The influence of knee malalignment in the axial and frontal plane during squatting

4.1 Introduction

Deviations of knee alignment in the frontal plane have proven to be associated with potential risk for onset and progression of knee osteoarthritis (KOA) as they alter the contact stress distribution in the medial and lateral tibiofemoral compartments [1-4]. The same relationship has been found in the axial plane since the increased rotation of the tibia results in a greater knee adduction moment (KAM) [5-7]. Although KAM is the indirect measurement for medial condyle force, it has been found that greater KAM implies increased medial loading as a risk for medial KOA. Moreover, deviations of knee alignment in the axial plane result in anterior knee pain since femoral anteversion and tibial torsion result in the patella tilt and increased Q-angle leading to significantly greater lateral force in the patellofemoral joint [8-9].

Previously, *in vivo* measurements [10-11] have reported changes of over 20% in medial condyle loading in patients with alignments over 7° varus to 4.5° valgus. In computational studies, the predicted changes of over 50% bodyweight in medial and lateral loads over ±4° alignment range [12] and the change of -62% bodyweight in medial load over 8° valgus [13] have been reported. In addition, Van Rossom et al. [14] reported that tibiofemoral load distribution was significantly affected over ±15° coronal alignment range but minimally affected over ±15° rotation of the distal tibia. Whereas MacWilliams et al. [7] reported a linear relationship between rotations of the tibia in the transverse plane and internal valgus moment in patients with excessive tibial torsion during gait analysis. Similarly, a linear relationship was reported between the frontal alignment and the rotational alignment of the distal femur and tibial torsion in Huang et al. [6] in patients with KOA. Moreover, patella stress has been found to be significantly affected by the axial and frontal rotations of the femur and tibia [9, 15]. However, no previous studies to our knowledge have investigated the effect of alterations in alignment in the

frontal and axial plane on contact mechanics in both tibiofemoral and patellofemoral joints.

The primary aims of this chapter are to investigate the influence of deviations of alignment in the frontal and axial plane on (1) contact mechanics, including contact loads and stress distribution in both tibiofemoral and patellofemoral joints; (2) and kinematics in lower-extremity. It was hypothesized that (1) varus alignment will induce a higher medial force ratio while valgus alignment will induce a lower medial force ratio; (2) femoral anteversion and external tibial torsion will result in increased medial force ratio; and (3) femoral anteversion and external tibial torsion will lead to higher stress on the lateral patellar cartilage.

4.2   Method

4.2.1 Loads and Boundary Conditions of Squatting

The main components of the lower extremity FE model in this study are the hip joint, knee joint, and ankle joint. Both hip and ankle joints have three rotational degrees of freedom (DOFs). The spherical movements (Figure 4.2.1) in the hip and ankle joint are performed by three revolute joints in FEBio, consisting of flexion-extension (F-E), varus-valgus (V-V) and Internal-External (I-E). These rotational axes in revolute joints intersect at a fixed point, which is defined as the joint center. Three revolute joints to simulate the hip joint were built between the pelvis and femur components, while the revolute joints for simulating the ankle joint were built between the tibia and foot components. Moreover, the knee joint has three rotational DOFs and three translational DOFs, which are constrained by three cylindrical joints (Figure 4.2.2). These cylindrical joints are connections between the femur and tibia, whose joint axes interest at the joint center. Each cylindrical joint constrains motions between two rigid bodies to a rotation and translation about the joint axis. More specifically, the three cylindrical joints in the knee joint are composed of flexion-extension (F-E) rotation and medial-lateral (M-L) translation; valgus and varus (V-V) rotation and anterior-posterior (A-P) translation; and internal-external (I-E) rotation and inferior-superior (I-S) translation.
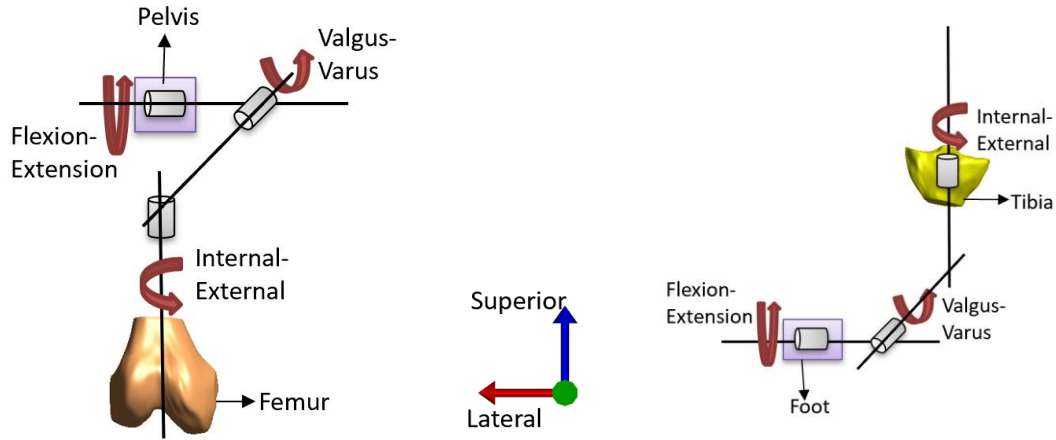
Figure 4.2.1 A series of revolute joints to simulate 3 rotational degrees of freedom (DOFs) in the hip (Left) and in the ankle (Right).
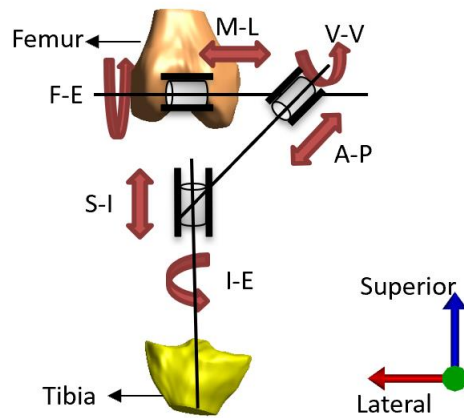
Figure 4.2.2 A series of cylindrical joints to simulate 6 degrees of freedom (DOFs) in the knee

In the FE squatting model (Figure 4.2.3), the femur was fixed while the tibia was free, although I-E rotation was constrained by a torsional spring (k=0.373 Nm/degree) at the ankle level to simulate the friction between the foot and the floor [16]. Similarly, the pelvis was constrained by a torsional spring to limit the internal-external rotation in some degrees relative to the femur. In addition, the foot was constrained by a prismatic joint to a translation relative to the pelvis component. The load of 378.09 N (equal to half bodyweight of the patient) was applied on the foot, pointing to the pelvis while the proximal quadriceps was fixed. So, the quadriceps tendon was in tension to balance the

moment resulting from the bodyweight. Furthermore, the model was not constrained but the patella was free to rotate and translate.

The flexion angle was not prescribed, while the length of the quadriceps tendon was. Increasing the quadriceps tendon length induced the flexion angle to increase because of the moment equilibrium of the bodyweight. Instead of the prescribed quadriceps force or kinematics, the quadriceps force resulted from the squatting simulation in this study, which is in agreement with some previous publications [16-17].
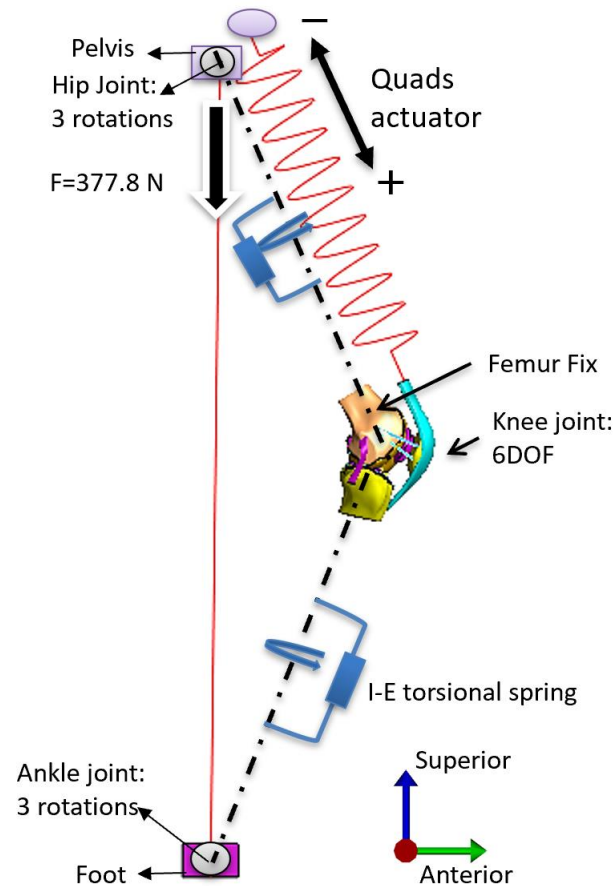
Figure 4.2.3 Boundary conditions for squatting

4.2.2 Knee deformity in the frontal plane and axial plane

A neutral knee alignment in the frontal plane is when the Hip-Knee-Ankle (HKA) angle is ± 3° varus-valgus [18-19]. The HKA angle is defined as the angle formed by the intersection of the mechanical axes of the femur and the tibia, which are defined as the line connecting the hip joint center and knee joint center and the line connecting the knee

joint center and ankle joint center, respectively. A deviation of the HKA is expressed with a positive value for varus alignment and a negative value for valgus alignment. The standard deviation of the HKA angle is 8° in osteoarthritic patients [19]. To investigate the influence of the frontal plane alignment, models were created in this study with different HKA alignments ranging from -8° valgus to +8° varus, at 4° increments. This was achieved by rotating the proximal part of the femur (hip joint center and proximal quadriceps) and distal part of the tibia (ankle joint center) by one half of the HKA alignment angle for each component while keeping knee joint geometry unchanged (Figure 4.2.4). Thus, HKA alignment angle equal to the summary of θ_{Hip} and θ_{Ankle}, according to Figure 4.2.4.
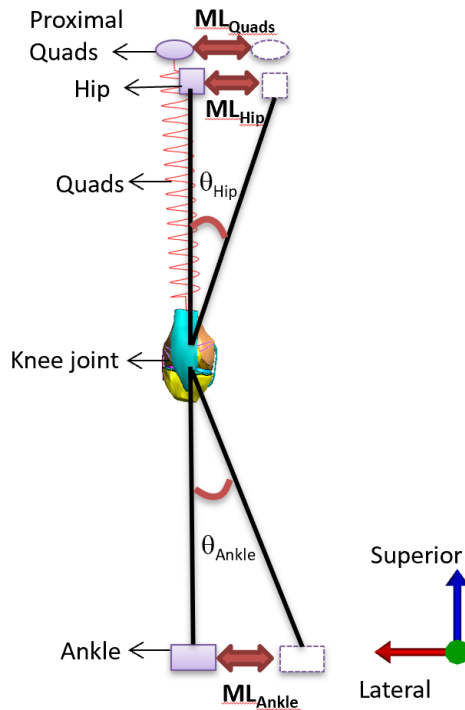
Figure 4.2.4 Frontal malalignment in FE model

The knee alignment in the axial plane was measured by the angle of femoral version (FV) and tibial torsion (TT) [20]. FV is the intersection angle between the femoral neck axis and the posterior condylar axis, while TT is the intersection angle between the proximal tibial line and the bimalleolar line. The reported average values of FV and TT in healthy adults measured with CT are in a wide range from 6° to 24° and from 26° to 35°, respectively [8, 24-29]. Although the exact normative values of FV and TT are

75

controversial [29], according to previous studies [9, 21, 29], osteotomies are employed for patients with increased inward femoral torsional deformity or outward tibial torsional deformity greater than 20°. The average corrective angles reported in a previous study were 25° in the femur and 30° in the tibia [29].

Moreover, a patient with combined excessive femoral anteversion, external tibial torsion, squinting patella, and increased Q-angle is defined as having miserable malalignment [22-23]. With miserable malalignment, the squinting patella (inwardly facing patella) can be observed with the foot facing forward (Figure 4.2.5), while external tibial torsion can be seen with the patella anterior.
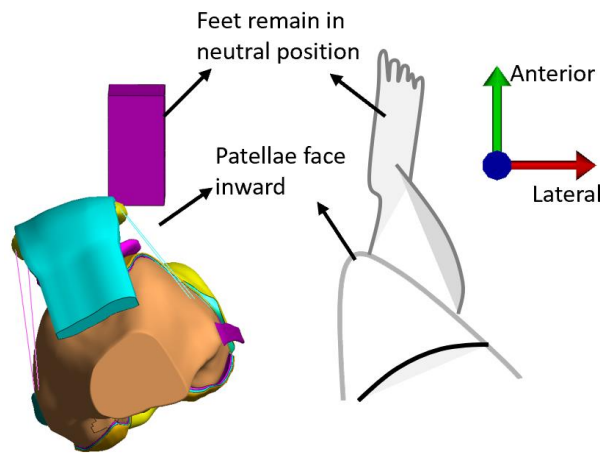
Figure 4.2.5 Top view of miserable malalignment (a combination of femoral anteversion and external tibial torsion) of FE model (Left) and simple figure (Right).

Although the specific angles of FV and TT in this model were unknown because the actual bone shape of the proximal femoral head and distal tibia did not exist in this FE model, the reported corrective angle for osteotomies in previous studies could be used in this study. Therefore, to simulate miserable malalignment, the distal femur and proximal tibia were simultaneously rotated inward by the averaged corrective angle of 30° (Figure 4.2.6), in line with the values reported in Stevens et al. [29]. In this way, the patella was facing inward while the foot was facing forward. To keep this posture during squatting for patients with miserable malalignment, the abduction-adduction (A-A) rotation of the

hip joint was constrained in some degrees by the A-A torsional spring with different levels of stiffness:

(1) Baseline 01 and Miserable 01: stiffness of 0.373 Nm/deg;

(2) Baseline 02 and Miserable 02: stiffness of 1.12 Nm/deg;

(3) Baseline 03 and Miserable 03: stiffness of 1.87 Nm/deg.

The flexion-extension axis of the knee joint was established using the midpoints of the medial and lateral condyles. The center of the knee joint was the midpoint between the medial and lateral condyles. The superior-inferior axis of the femur was established to be parallel to the femur shaft, while the anterior-posterior axis was established to be perpendicular to the other two axes.
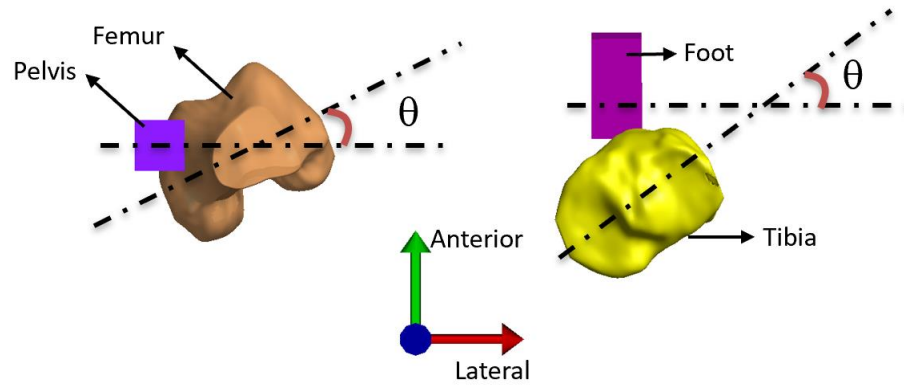
Figure 4.2.6 Top view of rotation angle (θ=30°) in the FE model between pelvis and femur (Left) and between foot and tibia (Right).

4.2.3 Data Analysis

To study the influence of frontal malalignment, contact stress distributions in both tibiofemoral and patellofemoral joints at 20, 45, and 90 degrees of flexion were plotted for the baseline model, 8° for the valgus-aligned model and 8° for the varus-aligned model. Moreover, the medial, lateral loads, and medial force ratio (medial load/total load) during squatting were reported for all frontal malalignment models and baseline model to study the force distribution in the tibiofemoral joint. Also, the total tibiofemoral and patellofemoral contact forces were plotted from 20° to 90°, at 10° increments for all models. In addition, the average difference and root mean square error (RMSE) between the frontal malalignment models and baseline model were calculated based on the medial

and lateral tibiofemoral forces at 10° increments (eight points) from 20 to 90 degrees of flexion.

To study the influence of axial malalignment (miserable malalignment), we compared the contact stress plots between the baseline and miserable malalignment models with the same torsional stiffness at adduction-abduction of the hip joint, in tibiofemoral and patellofemoral joints at 20°, 45° and 90°. Also, contact stress distributions in the tibiofemoral and patellofemoral joints were compared in the miserable malalignment models with different torsional springs at 20°, 45° and 90°. Furthermore, the rotational (adduction-abduction) kinematics of the hip joint were plotted over the flexion to study the influence of the stiffness value of the A-A torsional spring at the hip. To quantify the changes of force distribution, the medial contact force and lateral contact force were plotted during squatting. Also, the medial force ratio errors, including average error and RMSE in models with the same torsional stiffness, were calculated based on the values from 20° to 90° at 10° increments (eight points) for all models. The total tibiofemoral and patellofemoral contact forces were plotted from 20° to 90° at 10° increments for all models.

4.3   Results

4.3.1 The influence of knee deformity in the frontal plane

In the tibiofemoral joint, contact stress shifted to the lateral compartment in the valgus-aligned knee, while it shifted to the medial compartment in the varus-aligned knee during squatting (Figure 4.3.1). In the patellofemoral joint, the contact stresses were larger in the medial patellar cartilage in the varus-aligned knee, while they shifted to the lateral side in the valgus-aligned knee (Figure 4.3.2). The influence of malalignment on contact stress distribution was more significant at the lower flexion than at the higher flexion angle in both joints.

angle (°)	Plot bar	Valgus 8°	Baseline Model	Varus 8°
20°	2.71 — 0	Medial		lateral
45°	3.47 — 0			
90°	6.20 — 0		Posterior	
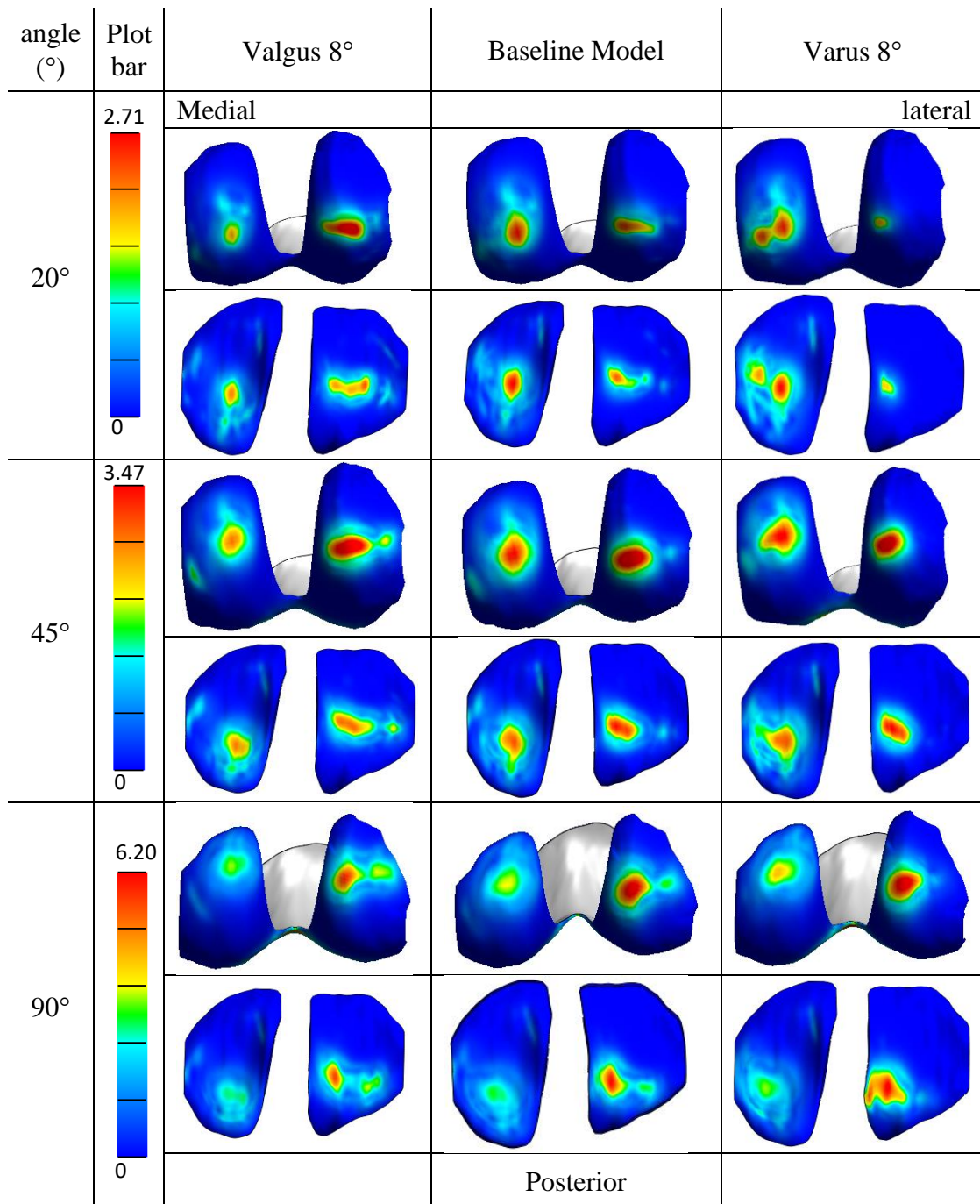
Figure 4.3.1: Contact stress distributions in the tibiofemoral joint during squatting at 20°, 45° and 90° in the baseline model, valgus 8° model and varus 8° model.
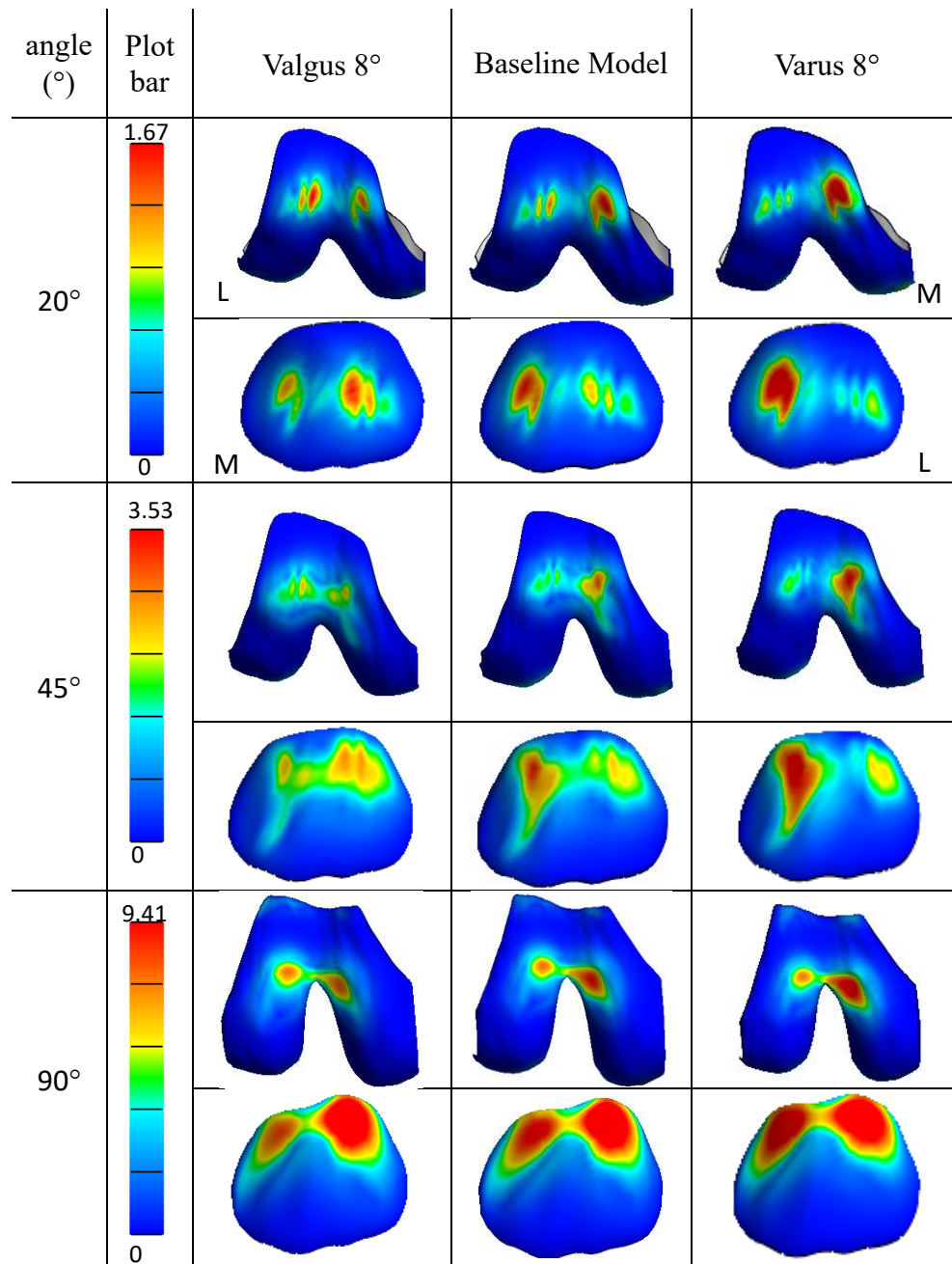
Figure 4.3.2: Contact stress distributions in the patellofemoral joint during squatting at 20°, 45° and 90° in the baseline model, valgus 8° model and varus 8° model.

Deviation of frontal plane alignment redistributed the medial and lateral force in the tibiofemoral joint (Figure 4.3.3 and Figure 4.3.4). Medial force magnitude increased as the valgus-aligned angle increased, while the lateral force magnitude decreased as the

varus-aligned angle increased. The medial force ratio was significantly different from the baseline model at a lower flexion angle. To be more specific, it decreased by 27% in the 8° valgus-aligned model and increased by 30% in the 8° varus-aligned model at 20 degrees of flexion.

(a)   (b)
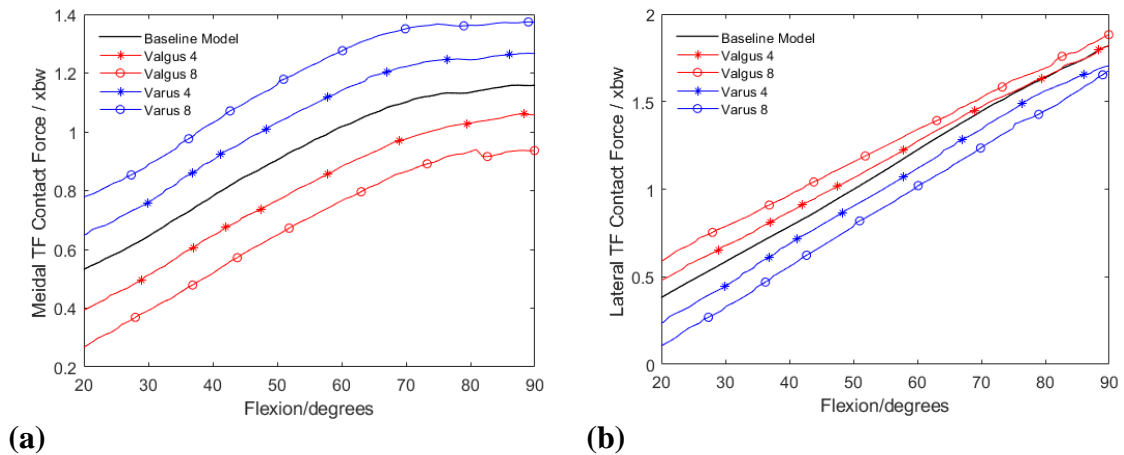
Figure 4.3.3: Medial (a) and lateral (b) tibiofemoral contact force during squatting in models with deviation of frontal alignment from 8° valgus to 8° varus, at 4° increments.
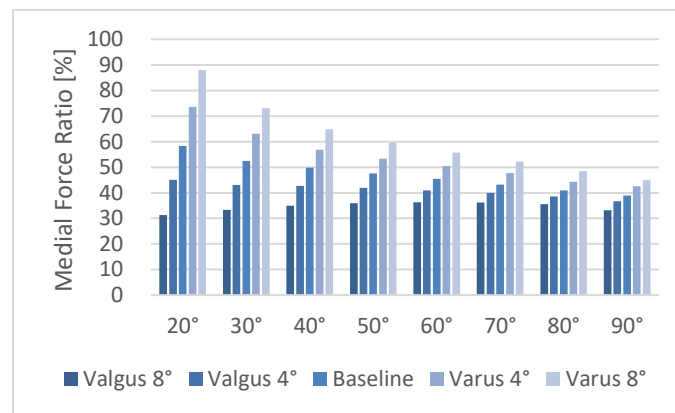
Figure 4.3.4: Medial force ratio (Medial force/Total force) in the baseline model and frontal plane malalignment models. Deviation of alignment from 8° valgus to 8° varus, at 4° increments.

Deviation of frontal plane alignment had a weak effect on total tibiofemoral contact force with errors within 0.1x bodyweight in low flexion angles and with errors around 0.15x

bodyweight after 70 degrees of flexion (Figure 4.3.5a). It also had a weak effect on total patellofemoral contact force with errors within 0.1x bodyweight during squatting from 20 to 90 degrees (Figure 4.3.5b).

Figure 4.3.5: Total tibiofemoral contact force (a) and Total patellofemoral contact force (b) in the baseline and frontal malalignment models. Deviation of alignment from 8° valgus to 8° varus, at 4° increments.
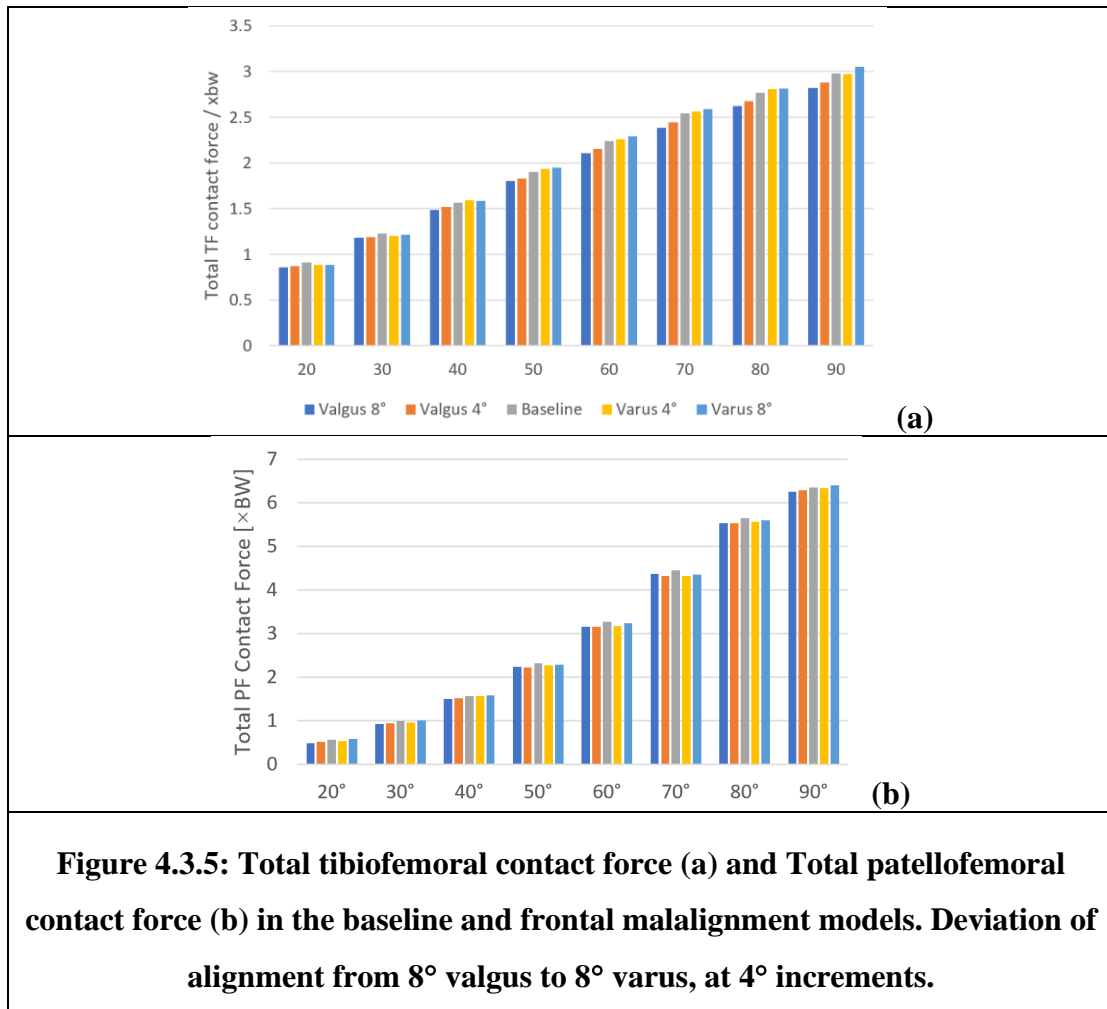
Specifying the difference of medial force ratio (medial load/total load) between the baseline model and frontal malalignment models in Table 4.3.1, the average difference during squatting from 20° to 90° was -1.5 %/deg in valgus-aligned knees and +1.7 %/deg in varus-aligned knees, while the RMSE was around 1.9 %/deg. The difference of medial force and lateral force between the baseline model and frontal malalignment models are shown in Table 4.3.1. In valgus-aligned knees, the medial force magnitude decreased by 0.03 BW/deg, while lateral force magnitude increased by 0.016 BW/deg. In varus-aligned knees, the medial force magnitude increased by 0.03 BW/deg, while the lateral force magnitude decreased by 0.027 BW/deg.

Table 4.3.1 Average difference and RMSE in frontal malalignment models

	Valgus 8°		Valgus 4°		Varus 4°		Varus 8°	
	Average Difference	RMSE	Average Difference	RMSE	Average Difference	RMSE	Average Difference	RMSE
Meidal force [×BW]	-12.47	14.33	-5.97	6.95	6.92	7.91	13.79	15.66
Lateral force [×BW]	0.13	0.15	0.05	0.06	-0.11	0.11	-0.21	0.22
Medial force ratio [%]	-12.47	14.33	-5.97	6.95	6.92	7.91	13.79	15.66

The varus alignment model significantly increased internal tibial rotation, while the valgus alignment model decreased internal tibial rotation (Figure 4.3.6b). However, the frontal plane malalignment had weak effects on knee adduction rotation, especially at a higher flexion angle (> 70°), as shown in Figure 4.3.6a.

(a)   (b)
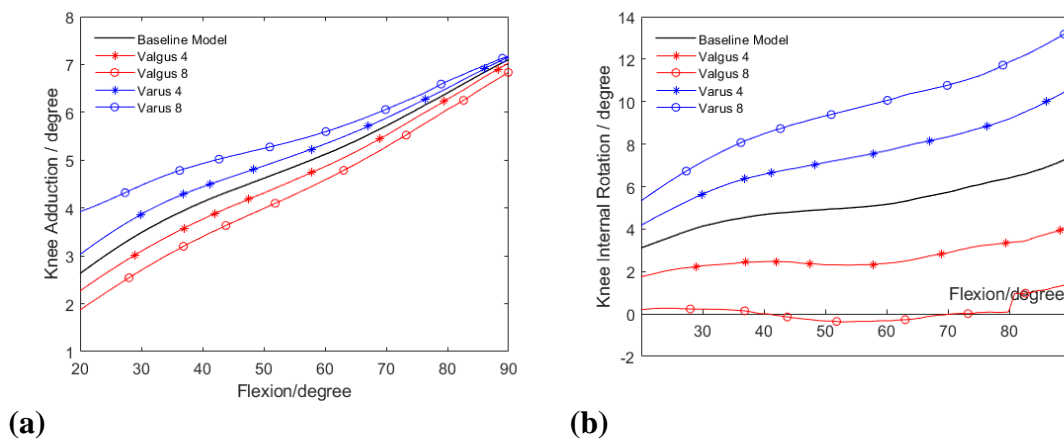
Figure 4.3.6: Knee joint adduction (a) and internal rotation (b) during squatting from 20 to 90 degrees in the baseline model and frontal malalignment model.

4.3.2 The influence of knee deformity in the axial plane

Miserable malalignment changed the contact stress in the tibiofemoral joint, with increased stresses in the medial compartment and decreased stresses in the lateral compartment compared to the baseline model (Figure 4.3.7a, Figure 4.3.8a, Figure 4.3.9a). The model with miserable malalignment had higher lateral patellar contact pressure (Figure 4.3.7b, Figure 4.3.8b, Figure 4.3.9b). Higher stiffness of the adduction-abduction torsional spring at the hip level induced more stress shift to the medial

compartment in the tibiofemoral joint, while it did not affect contact stress distribution in the patellofemoral joint (Figure 4.3.10). The hip adduction angle decreased as the stiffness of the torsional spring at the hip joint increased (Figure 4.3.11). This influence was significant in the miserable malalignment models, in which the model with the stiffness of 0.373 Nm/deg had adduction angles within 12 degrees while the model with a stiffness of 1.87 Nm/deg had abduction angles within 4 degrees.

Flexion angle (°)	Plot bar	Baseline 01	Miserable 01
20°	2.69 – 0		
45°	3.50 – 0		
90°	6.16 – 0		
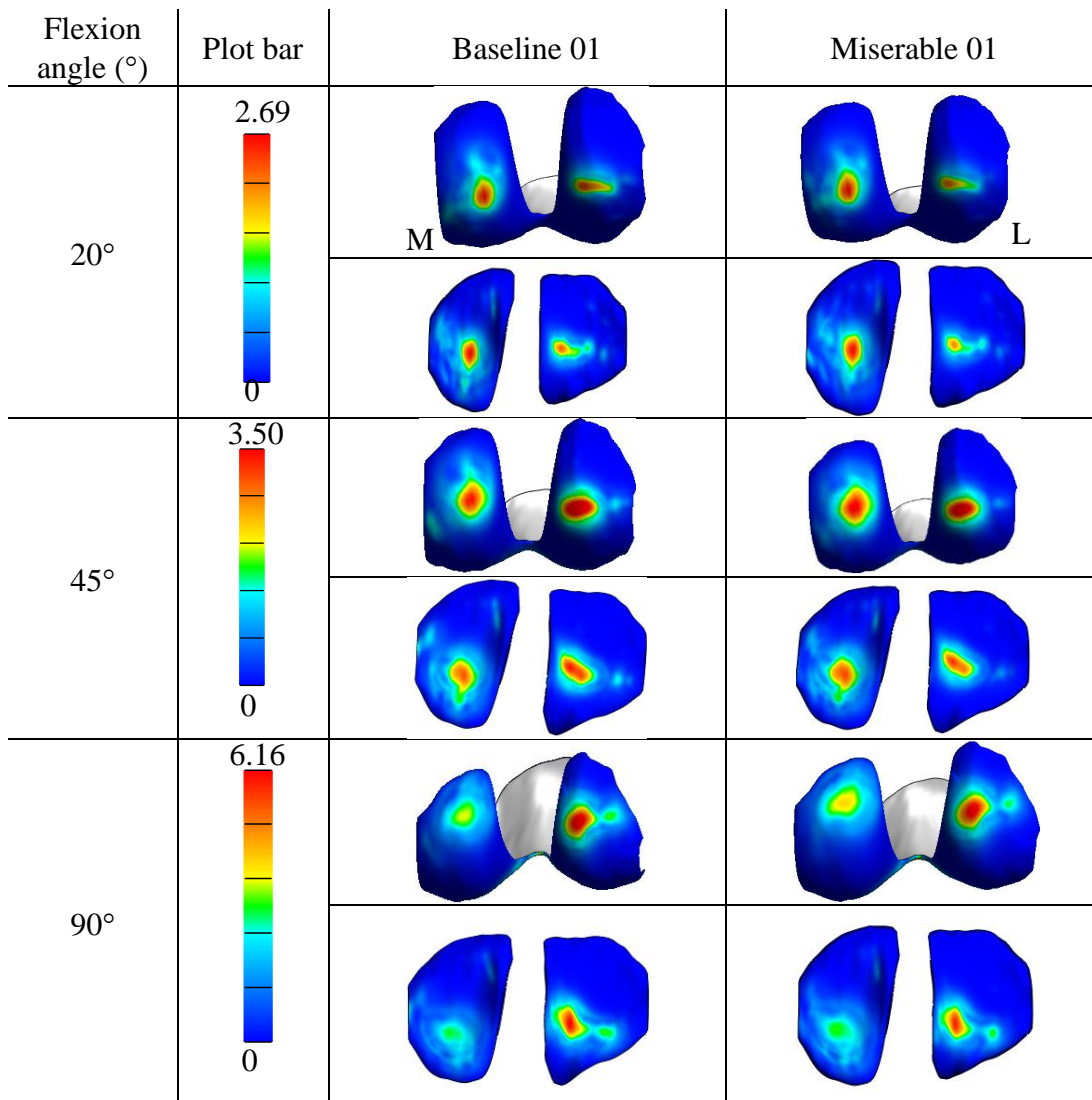
Figure 4.3.7a: Contact stress distributions in the tibiofemoral joint during squatting at 20°, 45° and 90° in the baseline model (Baseline 01) and miserable malalignment model (Miserable 01) with A-A hip torsional spring stiffness of 0.37 Nm/deg.

Flexion angle (°)	Plot bar	Baseline 01	Miserable 01
20°	1.66 — 0.01		
45°	3.57 — 0.02		
90°	9.47 — 0.04		
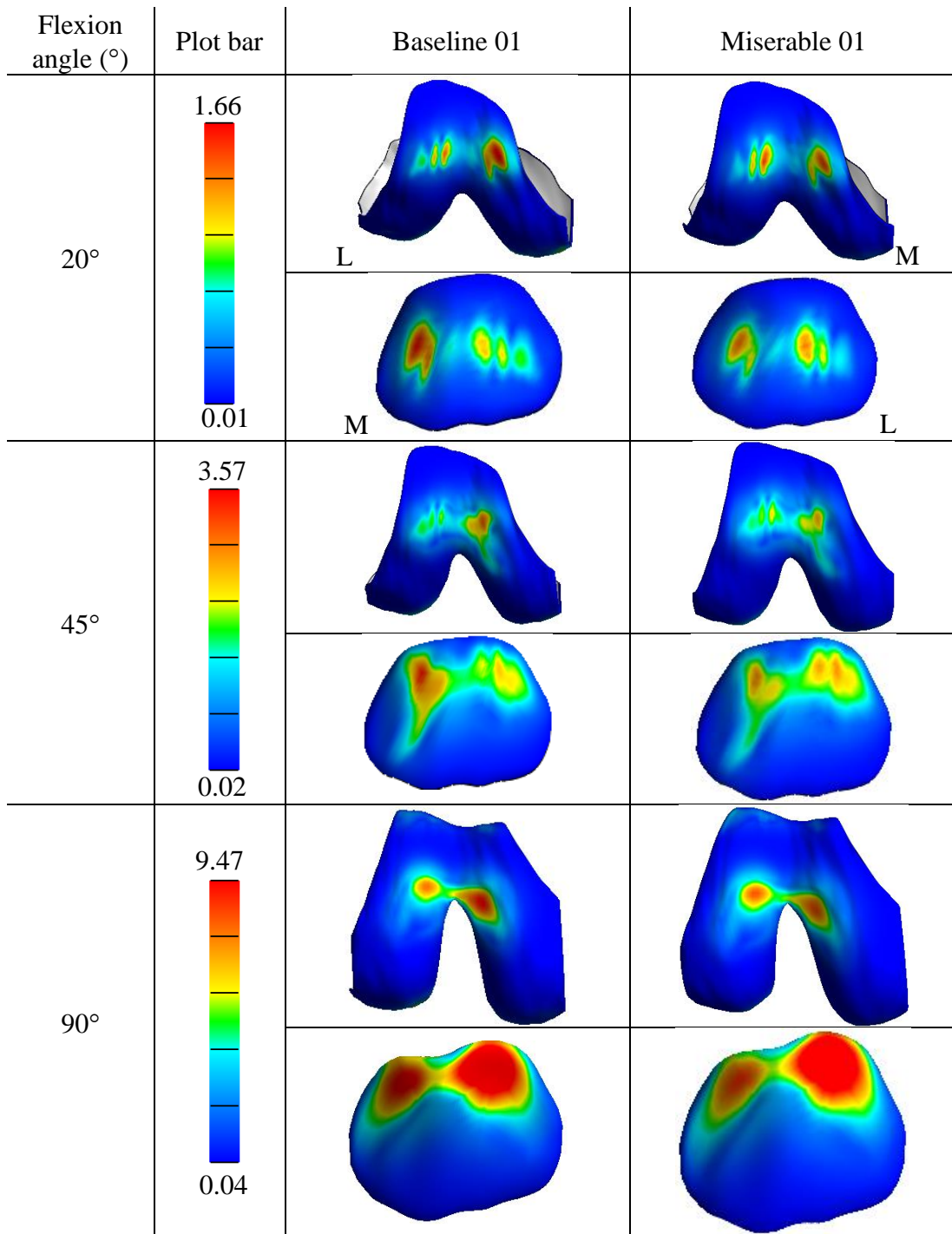
Figure 4.3.7b: Contact stress distributions in the patellofemoral joint during squatting at 20°, 45° and 90° in the baseline model (Baseline 01) and miserable malalignment model (Miserable 01) with A-A hip torsional spring stiffness of 0.37 Nm/deg.

Flexion angle (°)	Plot bar	Baseline 02	Miserable 02
20°	2.69 0		
45°	3.37 0		
90°	6.18 0		
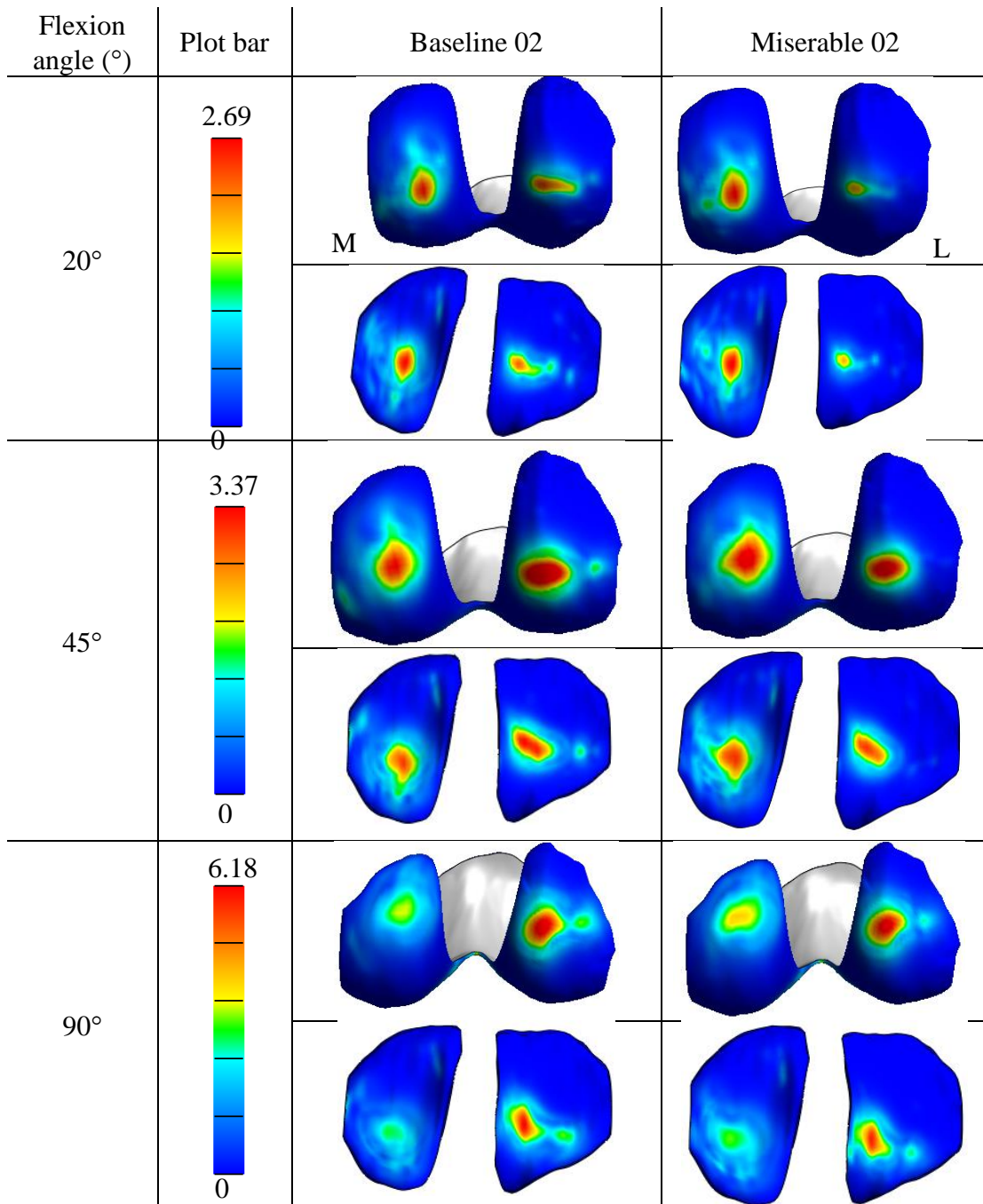
Figure 4.3.8a: Contact stress distributions in the tibiofemoral joint during squatting at 20°, 45° and 90° in the baseline model (Baseline 02) and miserable malalignment model (Miserable 02) with A-A hip torsional spring stiffness of 1.12 Nm/deg.
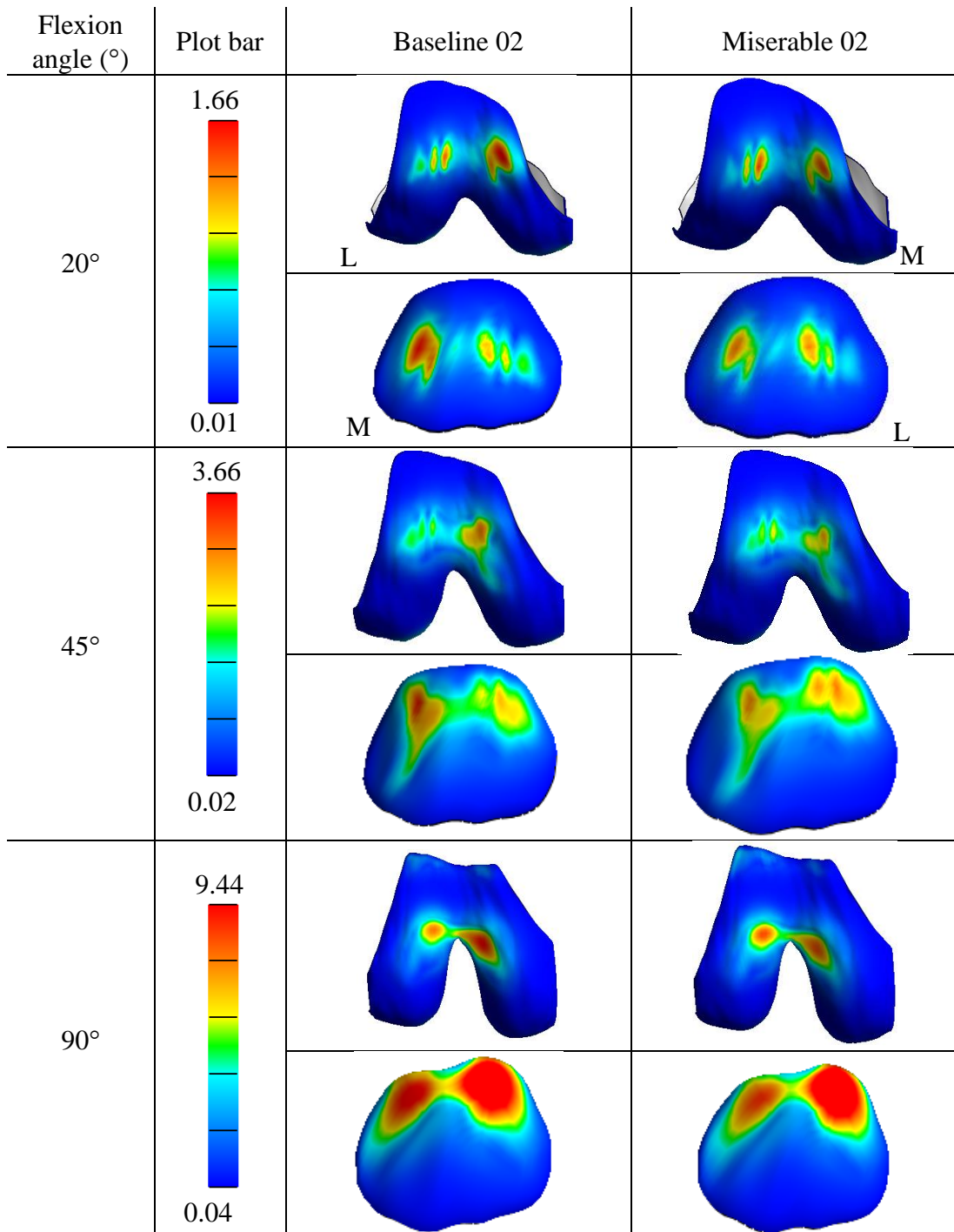
Figure 4.3.8b: Contact stress distributions in the patellofemoral joint during squatting at 20°, 45° and 90° in the baseline model (Baseline 02) and miserable malalignment model (Miserable 02) with A-A hip torsional spring stiffness of 1.12 Nm/deg.
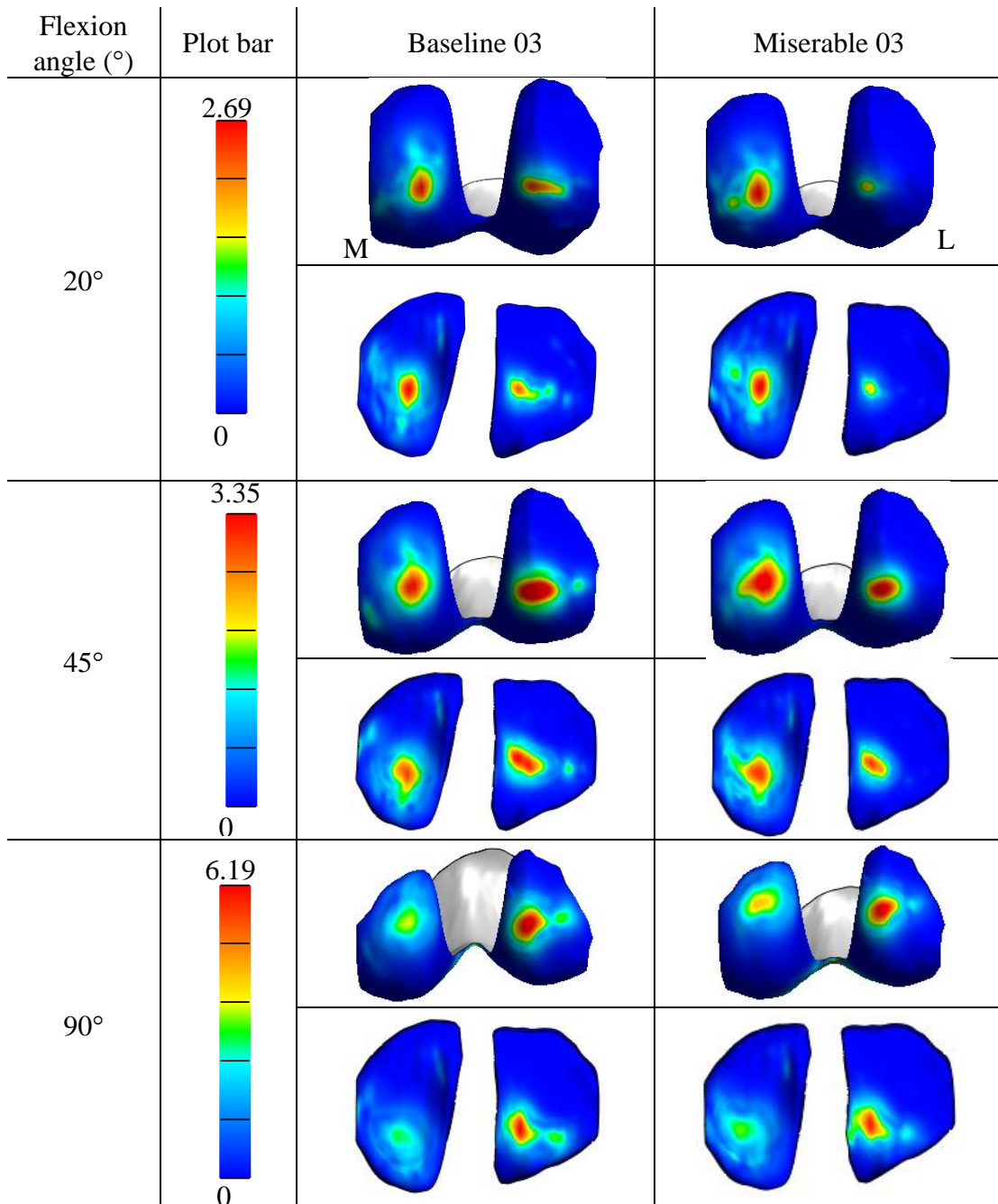
Figure 4.3.9a: Contact stress distributions in the tibiofemoral joint during squatting at 20°, 45° and 90° in the baseline model (Baseline 03) and miserable malalignment model (Miserable 03) with A-A hip torsional spring stiffness of 1.87 Nm/deg.
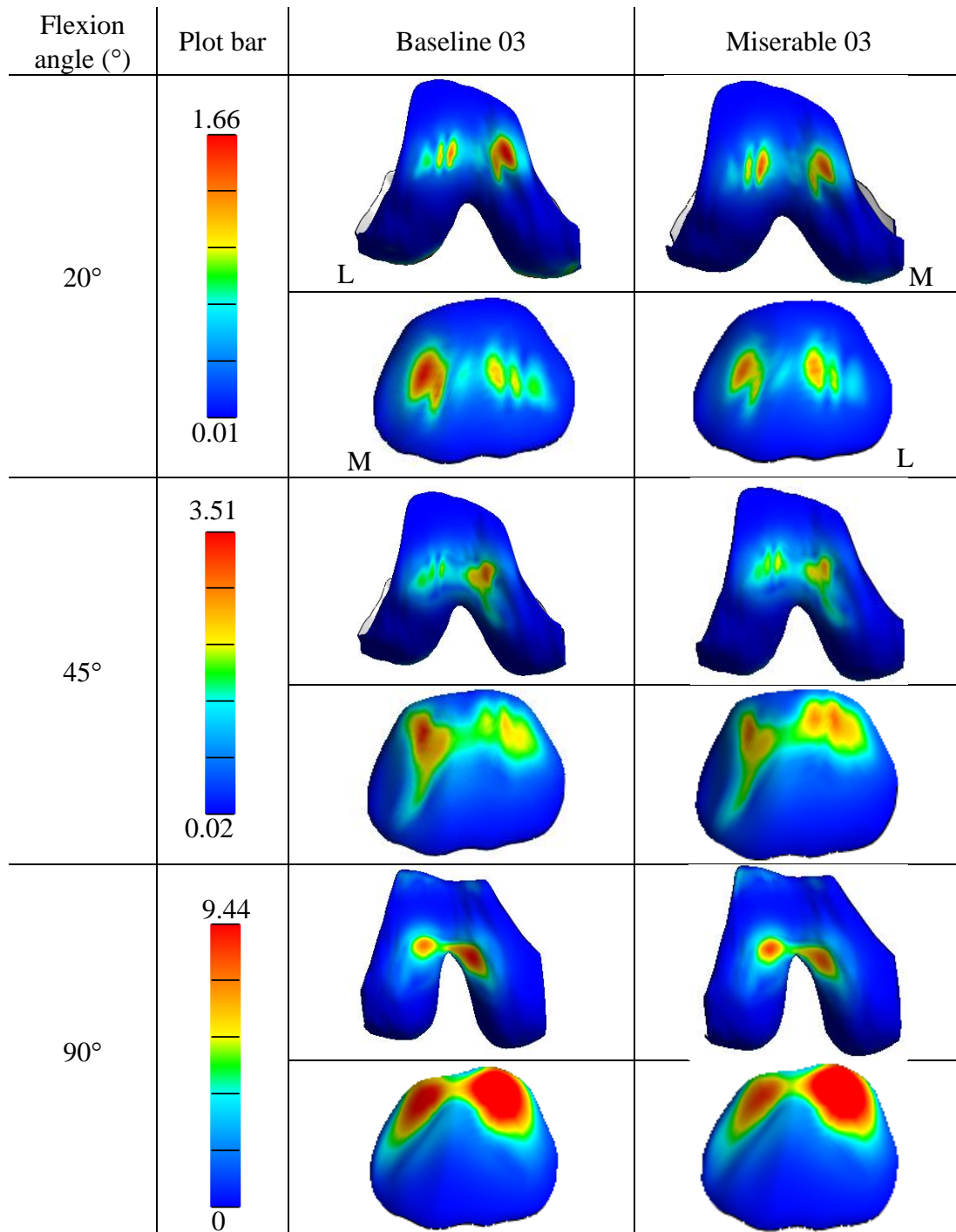
Figure 4.3.9b: Contact stress distributions in the patellofemoral joint during squatting at 20°, 45° and 90° in the baseline model (Baseline 03) and miserable malalignment model (Miserable 03) with A-A hip torsional spring stiffness of 1.87 Nm/deg.

angle (°)	Plot bar	Miserable 01	Miserable 02	Miserable 03
20°	2.70 ... 0			
45°	3.3 ... 0			
90°	6.0 ... 0			
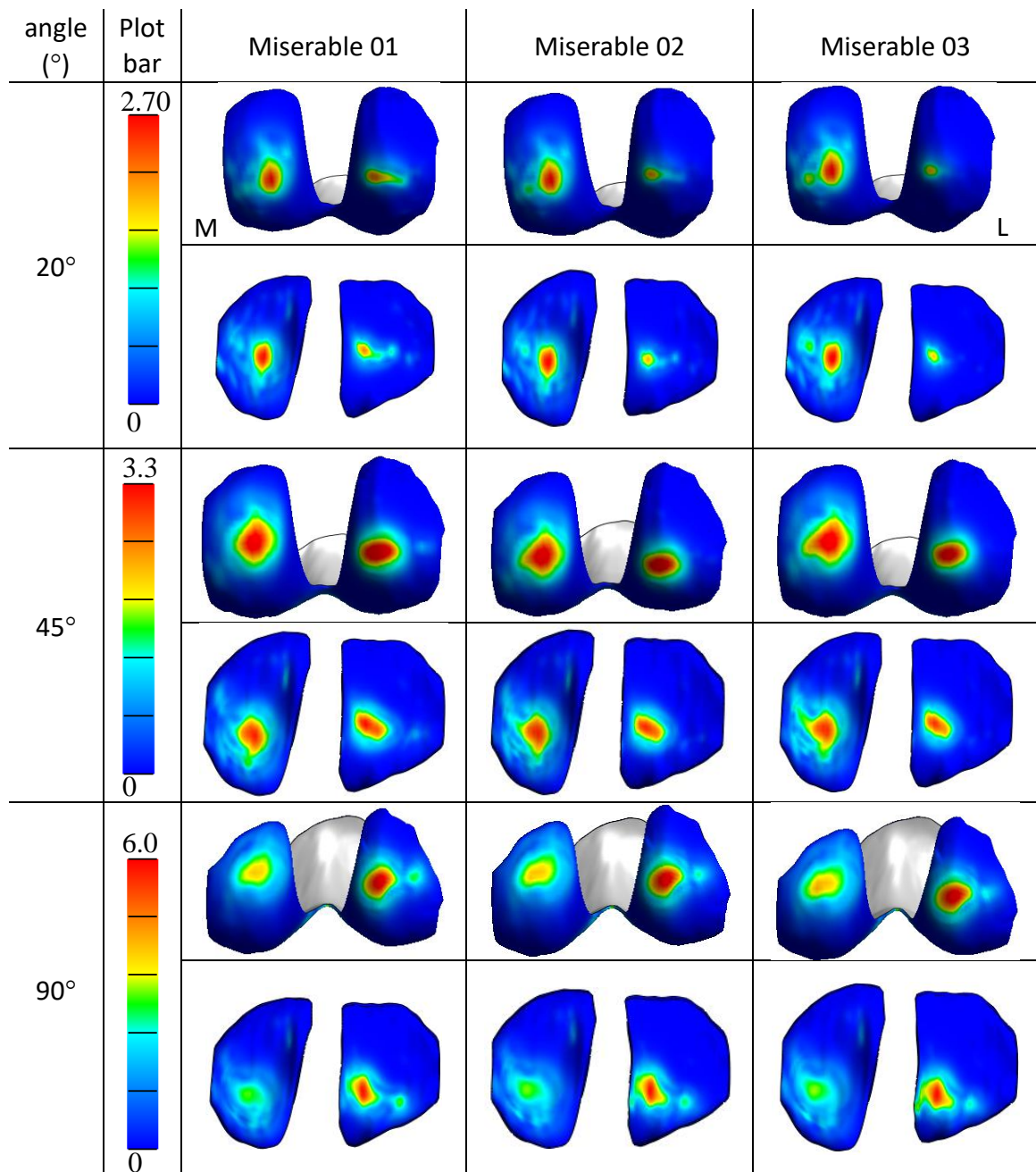
Figure 4.3.10a: Contact stress distributions in the tibiofemoral joint during squatting at 20°, 45° and 90° in miserable malalignment models with A-A hip torsional spring stiffness of (01) 0.37 Nm/deg; (02) 1.12Nm/deg; (03) 1.87 Nm/deg.
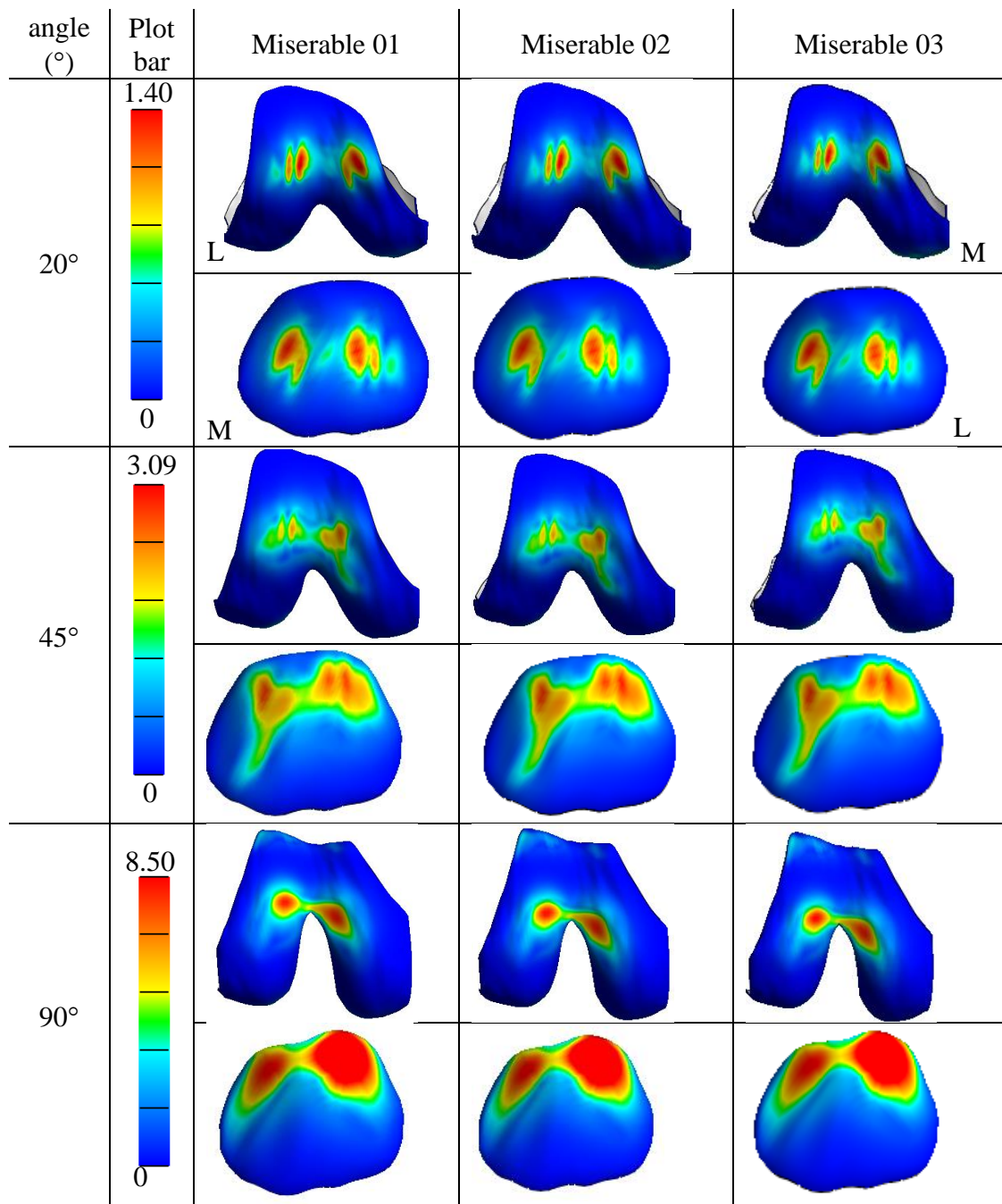
Figure 4.3.10b: Contact stress distributions in the patellofemoral joint during squatting at 20°, 45° and 90° in miserable malalignment models with A-A hip torsional spring stiffness of (01) 0.37 Nm/deg; (02) 1.12Nm/deg; (03) 1.87 Nm/deg.
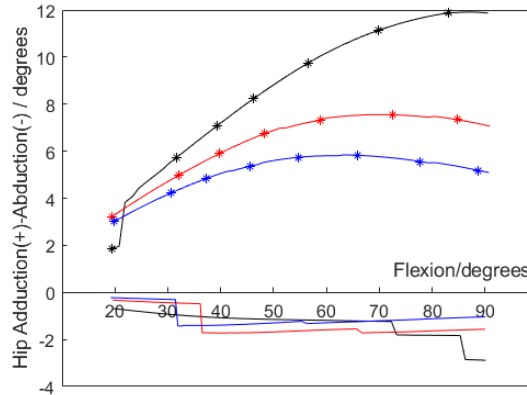
Figure 4.3.11: Adduction-abduction rotation angles of the hip joint in baseline models (solid lines) and miserable malalignment models (lines with stars) with different stiffness values: (1) 0.373 Nm/deg (black lines); (2) 1.12 Nm/deg (red lines); (3) 1.87 Nm/deg (blue lines).

The miserable alignment increased medial contact force compared to the baseline model with the same torsional spring, while it decreased the lateral contact force. This influence was more significant as the stiffness of the A-A torsional spring at the hip joint increased (Figure 4.3.12). The greatest difference between the baseline and miserable model was with a torsional stiffness of 1.87 Nm/deg. However, it weakly affected the total tibiofemoral contact force value with errors between models with the same torsional springs within 0.1x bodyweight (Figure 4.3.13a). Also, miserable malalignment had weak effects on the total patellofemoral contact force values with errors within 0.2x bodyweight (Figure 4.3.13b). Medial force ratio errors between the baseline and miserable malalignment models increased as the stiffness value of the A-A torsional spring at the hip joint increased (Figure 4.3.14).

(a)   (b)
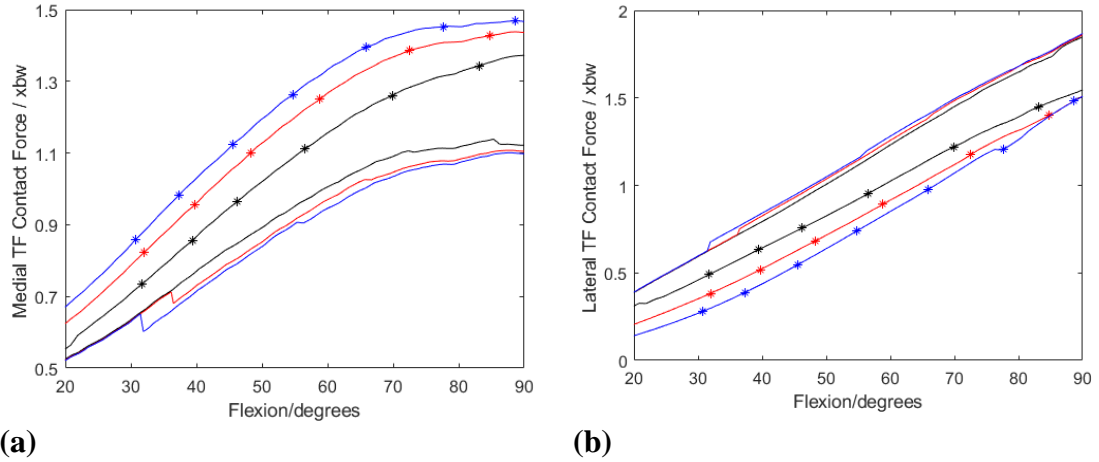
Figure 4.3.12: Medial (a) and lateral (b) contact force in baseline models (solid lines) and miserable malalignment models (lines with stars) with different stiffness values: (1) 0.373 Nm/deg (black lines); (2) 1.12 Nm/deg (red lines); (3) 1.87 Nm/deg (blue lines).

(a)

(b)
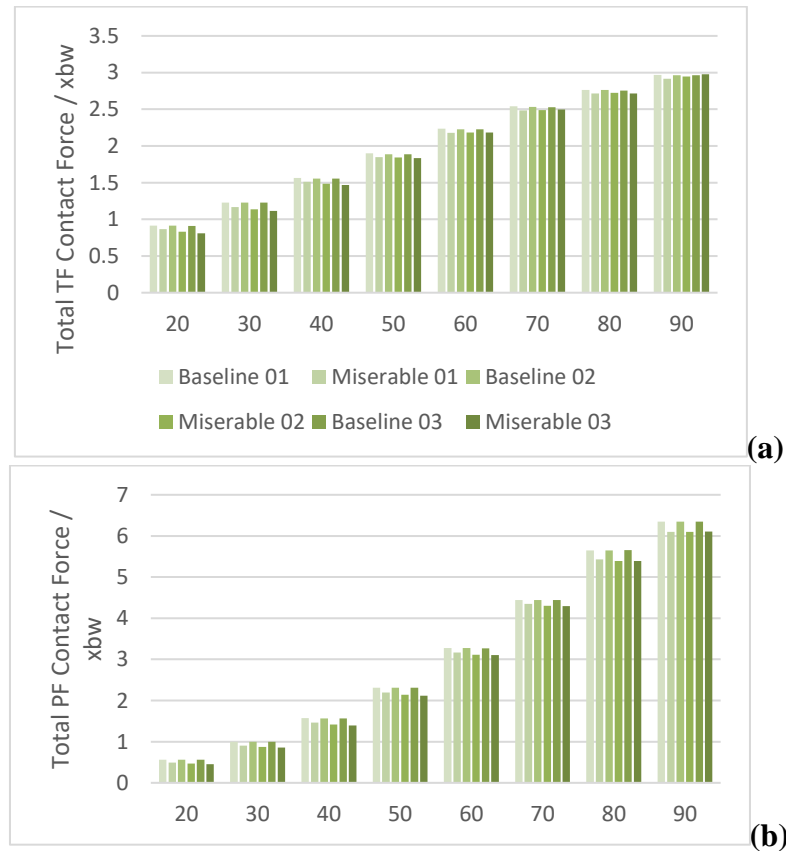
Figure 4.3.13: Total tibiofemoral (a) and patellofemoral (b) contact forces in baseline models and miserable malalignment models with different stiffness values: (01) 0.373 Nm/deg; (02) 1.12 Nm/deg; (03) 1.87 Nm/deg.
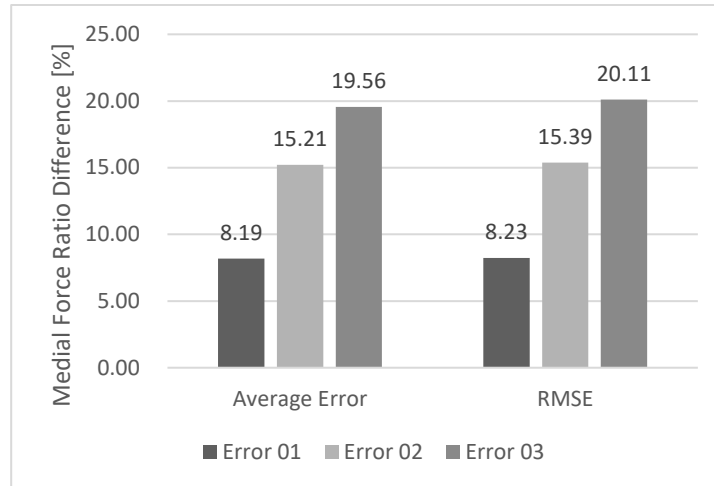
Figure 4.3.14: Average error and RMSE between the miserable malalignment and baseline models with the same torsional spring stiffness. Error 01: 0.373 Nm/deg; Error 02: 1.12 Nm/deg; Error 03: 1.87 Nm/deg.

Kinematics in the knee joint is shown in Figure 4.3.15. The knee adduction angle increased in the miserable malalignment models compared to the baseline models. The stiffness of the A-A torsional spring at the hip joint had weak effects in the baseline models, while it induced slightly increased adduction angles at low flexion angles (before 70 degrees) as the stiffness value increased. In addition, miserable malalignment induced greater internal rotation during squatting compared to the baseline models. Also, the stiffness of the A-A torsional spring at the hip joint significantly increased internal rotation in the miserable models, while it had weak effects on internal rotation in the baseline model. The most significant error was the internal rotation of 5.4° between the miserable malalignment and baseline models with an A-A torsional spring stiffness of 1.87 Nm/deg at the hip joint.

(a)   **(b)**
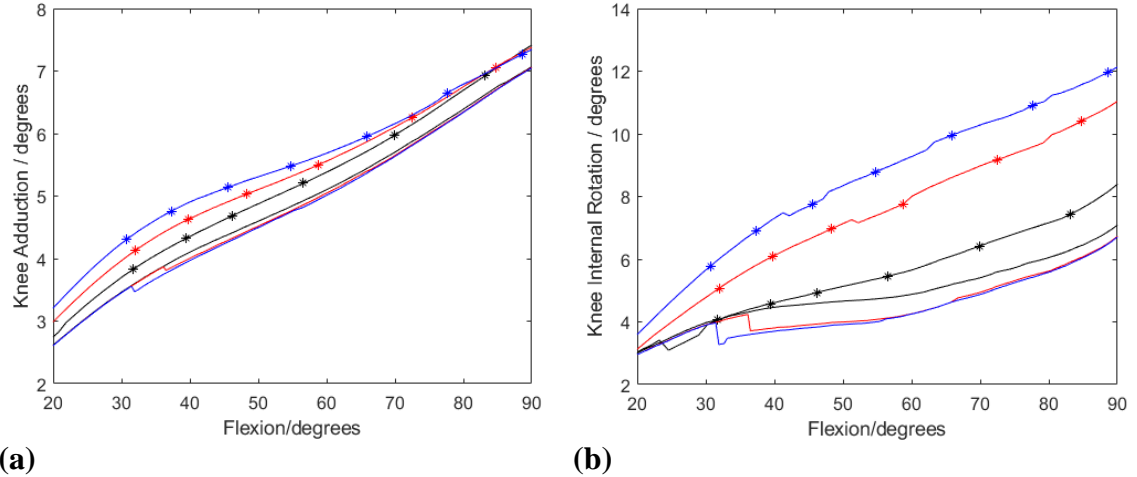
Figure 4.3.15: Knee joint adduction (a) and internal rotation (b) during squatting from 20 to 90 degrees in baseline models (solid lines) and miserable malalignment models (lines with stars) with different stiffness values: (1) 0.373 Nm/deg (black lines); (2) 1.12 Nm/deg (red lines); (3) 1.87 Nm/deg (blue lines).

4.4 Discussion

This chapter aimed to investigate the influence of frontal and axial malalignment on stress distributions in the tibiofemoral and patellofemoral joints, medial load, lateral load, and medial force ratio in the tibiofemoral joint. To achieve this aim, the hip center, ankle center, and proximal quadriceps were rotated ±8° valgus-varus around the knee center in the frontal plane while the geometries of the knee joint remained unchanged. Also, the distal femur and proximal tibia were rotated inward 30° in the axial plane to simulate miserable malalignment, adding adduction-abduction torsional spring with different level of stiffness at the hip joint to avoid knees knocking.

The sensitivity of the average medial force ratio error to the frontal alignment angle was -1.5 %/deg in valgus-aligned knees and +1.7 %/deg in varus-aligned knees, while the RMSE was around 1.9 %/deg. In valgus-aligned knees, the medial force magnitude decreased by 0.03 BW/deg, while the lateral force magnitude increased by 0.016 BW/deg. In varus-aligned knees, the medial force magnitude increased by 0.03 BW/deg, while the lateral force magnitude decreased by 0.027 BW/deg. This is difficult to directly compare with previous studies as most previous research studied the influence of frontal

malalignment during gait [12-14, 30-32]. The same tendency was found in these publications in that varus malalignment increases the medial load and decreases the lateral load, while valgus malalignment increases the lateral load and decreases the medial load. Specifically, Lener et al. (2015) found changes of -0.62x bodyweight and +0.37x bodyweight over 8° valgus malalignment during walking [13]. In addition, Smith et al. (2016) predicted changes of over 0.5x bodyweight in medial and lateral loads over ±4° valgus-varus alignment range. They also found that frontal malalignment had weak effects on net knee joint contact force, which is in line with the results of this study. According to our knowledge, only one previous publication [10] has studied the influence of varus and valgus alignment during activities including squatting. However, this study only reported the correlation between the frontal alignment angle and the medial force ratio through different activities. Although the sensitivity of the medial force ratio to the frontal alignment angle is unknown, the directly measured medial force ratio ranges 29% to 53% during knee bend with an average knee flexion angle of 93°(SD 11°) among patients with an alignment of 4.5° valgus and 7° varus. In this study, the medial force ratio was 37% in 4° valgus model and 45% in the 8° varus model at 90 degrees of flexion.

Lateral patellar contact pressure increased in the valgus malalignment model with an increased Q-angle, while medial patellar contact pressure increased in the varus malalignment model with decreased Q-angle, which is partially in agreement with a previous study [33]. Mizuno et al. (2001) [33] translated the proximal end of the quadriceps laterally and medially to simulate the increased and decreased Q-angle and concluded that increasing the Q-angle could increase lateral patellar contact pressures, while a Q-angle decrease may not shift the patellar contact pressures medially. However, they used *in vivo* experiments to investigate variations in tibiofemoral and patellofemoral kinematics instead of a direct investigation of the changes in contact mechanics under deviations of Q-angle. In this study, we investigated the increased lateral contact pressures in the miserable malalignment model, which had a Q-angle increase. The same correlation was reported in previous studies [8, 9, 34] that excessive femoral anteversion or medial femoral rotation may be present in patients with anterior knee pain associated

with an increased Q-angle, higher lateral patellar contact pressures and patella tilt. Bruce et al. [23] recommended that patients with anterior knee pain associated with miserable malalignment perform rotational osteotomies to relieve their pain.

Compared to the baseline model, the miserable malalignment models in this study had increased medial force and decreased lateral force, with the medial force ratio increasing at least 8% during squatting, controlling knees to avoid knocking. Previous studies [5-7] have found a positive relationship between the knee adduction moment (KAM) and excessive rotational deformity of the tibia, including both internal and external torsions in experiments. Although they did not directly measure medial loading, KAM has proven to be correlated with medial loading and the onset of medial knee osteoarthritis (KOA). Huang et al. (2021) [6] reported that external tibial torsion is positively associated with external KAM during squatting in patients with moderate KOA while Krackow et al. (2011) [5] demonstrated that medial KOA subjects with tibial torsion had greater mechanical axis varus and knee varus moment than medial KOA subjects without tibial torsion and control groups. Moreover, MacWilliams et al. (2010) [7] concluded that both excessive inward and outward tibial torsion adversely affect the frontal moments, measuring data from eight subjects with excessive inward tibial torsion and ten subjects with excessive outward tibial torsion.

In the miserable malalignment models in this study, while keeping the feet facing forward, the A-A rotation at the hip joint was controlled with a torsional spring to simulate the knees remaining apart. The stiffness of the torsional spring was varied higher to lower down the varus angle at the hip joint. As a result, a medial force ratio increase in the miserable malalignment model ranged from +8% to +20% as the stiffness increased from 0.373 Nm/deg to 1.87 Nm/deg. The medial force and medial force ratio increased as the varus angle at the hip joint decreased. A similar influence was found in a previous study [35]. In this study, Trepczynski et al. (2014) [35] tested external KAM and medial tibiofemoral contact force *in vivo* for patients with TKA and required patients to squat naturally or squeeze their knees together (valgus squat) or push their knees apart (varus squat), maintaining their feet approximately shoulder-width apart. Consequently, Trepczynski et al. (2014) [35] reported a lower medial force and KAM in squat valgus

and greater medial force and KAM in squat varus compared to the values in a natural squat.

Miserable malalignment and varus malignment models in this study showed greater tibial internal rotation with respect to the femur, while the valgus malalignment model decreased internal rotation compared to the baseline models. Also, the miserable alignment model with higher A-A torsional stiffness induced higher tibial internal rotation. In addition, knee deformity in the axial and frontal planes had weak effects on knee adduction-abduction rotation. To date, little is known from previous studies about the influence of knee deformity on kinematics. Souza et al. (2010) [34] reported that patients with patellofemoral pain (PFP) had lower medial femoral rotation as the angle of flexion decreased. The kinematics for this study were obtained from a vertically open magnetic resonance imaging system while subjects performed a single-limb squat. Powers et al. (2002) concluded that patients with patellofemoral pain (PFP) had less femoral internal rotation than control subjects during self-speed walking. On average, patients with PFP had 2.1° external femoral rotation, while subjects in the control group had 1.6° internal femoral rotation. The authors explained this difference as a compensatory strategy to decrease the Q-angle. However, this disagrees with the study of Mizuno et al. (2001) [33], who reported that a Q-angle increase did not influence the tibiofemoral rotational kinematics, including adduction-abduction and Internal-External, while a Q-angle decrease induced a lower tibial internal rotation. The data in this study were tested *in vitro* by translating the proximal quadriceps medially and laterally to increase and decrease the Q-angle. In this study, the model with a greater medial force ratio had higher internal tibial rotation, which is speculated to be a strategy to compensate the knee varus orientation. Stief et al. (2014) [37] studied the influence of lower limb malalignment based on *in vivo* measurements of subjects with a pathological varus malalignment of the knee and founded a linear relationship between lower extremity varus malalignment and internal tibial rotation. In addition, previous studies [6, 7] demonstrated the excessive tibial external torsion leaded to an increased adduction moment in the coronal plane during gait analysis.

4.5 Conclusion

This chapter aimed to investigate the influence of knee malalignment in the frontal plane and axial plane on (1) contact mechanics, including medial and lateral tibiofemoral contact force, medial force ratio in the tibiofemoral joint, stress distributions and total contact loads in tibiofemoral and patellofemoral joints and (2) rotational kinematics, including adduction-abduction and Internal-External.

For frontal plane malalignment, valgus malalignment induced a greater medial force ratio and lateral patellar contact pressures, while varus malalignment induced a smaller medial force ratio and medial patellar contact pressures. The sensitivity of the average medial force ratio error to the frontal alignment angle was -1.5 %/deg in valgus-aligned knees and +1.7 %/deg in varus-aligned knees, while the RMSE was around 1.9 %/deg. For axial plane malalignment, the miserable malalignment (combined excessive femoral anteversion and tibial external torsion) increased the medial force ratio and lateral patellar contact pressures. With the hip adduction angle constrained by a torsional spring, the lower hip adduction angle significantly increased medial tibiofemoral load. An increase of the medial force ratio in the miserable malalignment model ranged from +8% to +20% as the stiffness increased from 0.373 Nm/deg to 1.87 Nm/deg. However, the influence of the constrained hip adduction angle on patellofemoral contact redistribution was not observed in this study.

Models with a greater medial force ratio had a higher internal tibial rotation, which is speculated to be a compensatory motion to lower the knee varus orientation. In contrast, knee deformity was found to have weak effects on adduction-abduction rotation in this study.

References

[1] Johnson F, Leitl S, Waugh W. The distribution of load across the knee. J Bone *Joint Surg*. 1980;67-B:346–349.

[2] Cerejo, R., D. D. Dunlop, S. Cahue, D. Channin, J. Song, and L. Sharma. The influence of alignment on risk of knee osteoarthritis progression according to baseline stage of disease. *Arthritis Rheum*. 2002;46:2632–2636.

[3] Ford, K. R., G. D. Myer, and T. E. Hewett. Valgus knee motion during landing in high school female and male basketball players. *Med. Sci. Sports Exerc*. 2003;35:1745–1750.

[4] Sharma, L., J. Song, D. T. Felson, S. Cahue, E. Shamiyeh, and D. D. Dunlop. The role of knee alignment in disease progression and functional decline in knee osteoarthritis. *JAMA*. 2001;286:188-195.

[5] Krackow KA, Mandeville DS, Rachala SR, Bayers-Thering M, Osternig LR. Torsion deformity and joint loading for medial knee osteoarthritis. *Gait Posture*. 2011;33(4):625-629.

[6] Huang C, Chan PK, Chiu KY, et al. Knee joint loadings are related to tibial torsional alignments in people with radiographic medial knee osteoarthritis. *PLoS One*. 2021;16(7 July):1-11.

[7] MacWilliams BA, McMulkin ML, Baird GO, Stevens PM. Distal tibial rotation osteotomies normalize frontal plane knee moments. *J Bone Jt Surg - Ser A*. 2010;92(17):2835-2842.

[8] Eckhoff DG, Montgomery WK, Kicoyne RF, et al. Femoral morphometry and anterior knee pain. *Clin Orthop*. 1994;302:64–68.

[9] Lee TQ, Anzel SH, Bennett KA, Pang D, Kim WC. The influence of fixed rotational deformities of the femur on the patellofemoral contact pressures in human cadaver knees. *Clin Orthop Relat Res*. 1994;302(302):69-74.

[10] Kutzner I, Bender A, Dymke J, Duda G, von Roth P, Bergmann G. Mediolateral force distribution at the knee joint shifts across activities and is driven by tibiofemoral alignment. Bone Joint J. 2017;99-B(6):779-787.

[11] Bergmann G, Bender A, Graichen F, et al. Standardized loads acting in knee implants. *PLoS One*. 2014;9(1).

[12] Smith CR, Vignos MF, Lenhart RL, Kaiser J, Thelen DG. The influence of component alignment and ligament properties on tibiofemoral contact forces in total knee replacement. *J Biomech Eng*. 2016;138(2).

[13] Lerner ZF, DeMers MS, Delp SL, Browning RC. How tibiofemoral alignment and contact locations affect predictions of medial and lateral tibiofemoral contact forces. *J Biomech*. 2015;48(4):644-650.

[14] Van Rossom S, Wesseling M, Smith CR, et al. The influence of knee joint geometry and alignment on the tibiofemoral load distribution: A computational study. *Knee*. 2019;26(4):813-823.

[15] Liao TC, Yin L, Powers CM. The influence of isolated femur and tibia rotations on patella cartilage stress: a sensitivity analysis. *Clin Biomech*. 2018;54(March):125-131.

[16] Barink M, De Waal Malefijt M, Celada P, Vena P, Van Kampen A, Verdonschot N. A mechanical comparison of high-flexion and conventional total knee arthroplasty. *Proc Inst Mech Eng Part H J Eng Med*. 2008;222(3):297-307. doi:10.1243/09544119JEIM353

[17] Adouni M, Shirazi-Adl A. Knee joint biomechanics in closed-kinetic-chain exercises. *Comput Methods Biomech Biomed Engin*. 2009;12(6):661-670. doi:10.1080/10255840902828375

[18] Bellemans J, Colyn W, Vandenneucker H, Victor J. The chitranjan ranawat award. *Clin Orthop Relat Res*. 2012;470(1):45-53. doi:10.1007/s11999-011-1936-5

[19] Cooke D, Scudamore A, Li J, Wyss U, Bryant T, Costigan P. Axial lower-limb alignment: comparison of knee geometry in normal volunteers and osteoarthritis patients. *Osteoarthritis Cartilage*. 1997;5(1):39-47. doi:10.1016/s1063-4584(97)80030-1

[20] León-Muñoz VJ, Manca S, López-López M, Martínez-Martínez F, Santonja-Medina F. Coronal and axial alignment relationship in Caucasian patients with osteoarthritis of the knee. *Sci Rep*. 2021;11(1):1-8.

[21] Turner MS, Smillie IS. The effect of tibial torsion of the pathology of the knee. *J Bone Joint Surg*. 1981;63-B(3):396–398

[22] James SL. Chondromalacia of the patella in the adolescent. In: Kennedy JC, ed. The Injured Adolescent Knee. Baltimore: Williams & Wilkins; 1979:205–251.

[23] Bruce WD, Stevens PM. Surgical Correction of Miserable Malalignment Syndrome. *J Pediatr Orthop*. 2004;24(4):392-396. doi:10.1097/00004694-200407000-00009

[24] Erkocak OF, Altan E, Altintas M, Turkmen F, Aydin BK, Bayar A. Lower extremity rotational deformities and patellofemoral alignment parameters in patients with anterior knee pain. *Knee Surg Sports Traumatol Arthrosc*. 2016;24(9):3011-3020. doi:10.1007/s00167-015-3611-y

[25] Kuo TY, Skedros JG, Bloebaum RD. Measurement of femoral anteversion by biplane radiography and computed tomography imaging: comparison with an anatomic reference. *Invest Radiol*. 2003;38(4):221-229. doi:10.1097/01.RLI.0000059542.90854.EF

[26] Seber S, Hazer B, Köse N, Göktürk E, Günal I, Turgut A. Rotational profile of the lower extremity and foot progression angle: computerized tomographic examination of 50 male adults. *Arch Orthop Trauma Surg*. 2000;120(5-6):255-258. doi:10.1007/s004020050459

[27] Clementz BG, Magnusson A. Fluoroscopic measurement of tibial torsion in adults. A comparison of three methods. *Arch Orthop Trauma Surg*. 1989;108(3):150-153. doi:10.1007/BF00934258

[28] Lee TQ, Anzel SH, Bennett KA, Pang D, Kim WC. The influence of fixed rotational deformities of the femur on the patellofemoral contact pressures in human cadaver knees. *Clin Orthop Relat Res*. 1994;302(302):69-74.

[29] Stevens PM, Gililland JM, Anderson LA, Mickelson JB, Nielson J, Klatt JW. Success of torsional correction surgery after failed surgeries for patellofemoral pain and instability. *Strateg Trauma Limb Reconstr*. 2014;9(1):5-12.

[30] Saliba CM, Brandon SCE, Deluzio KJ. Sensitivity of medial and lateral knee contact force predictions to frontal plane alignment and contact locations. *J Biomech*. 2017;57:125-130. doi:10.1016/j.jbiomech.2017.03.005

[31] Adouni M, Shirazi-Adl A. Partitioning of knee joint internal forces in gait is dictated by the knee adduction angle and not by the knee adduction moment. *J Biomech*. 2014;47(7):1696-1703. doi:10.1016/j.jbiomech.2014.02.028

[32] Kutzner I, Trepczynski A, Heller MO, Bergmann G. Knee adduction moment and medial contact force-facts about their correlation during gait. *PLoS One*. 2013;8(12):8-15. doi:10.1371/journal.pone.0081036

[33] Mizuno Y, Kumagai M, Mattessich SM, et al. Q-angle influences tibiofemoral and patellofemoral kinematics. *J Orthop Res*. 2001;19(5):834-840. doi:10.1016/S0736-0266(01)00008-0

[34] Souza RB, Draper CE, Fredericson M, Powers CM. Femur rotation and patellofemoral joint kinematics: A weight-bearing magnetic resonance imaging analysis. *J Orthop Sports Phys Ther*. 2010;40(5):277-285. doi:10.2519/jospt.2010.3215

[35] Trepczynski A, Kutzner I, Bergmann G, Taylor WR, Heller MO. Modulation of the relationship between external knee adduction moments and medial joint contact forces across subjects and activities. *Arthritis Rheumatol*. 2014;66(5):1218-1227. doi:10.1002/art.38374

[36] Powers CM, Chen PY, Reischl SF, Perry J. Comparison of foot pronation and lower extremity rotation in persons with and without patellofemoral pain. *Foot Ankle Int*. 2002;23(7):634-640. doi:10.1177/107110070202300709

[37] Stief F, Böhm H, Dussa CU, et al. Effect of lower limb malalignment in the frontal plane on transverse plane mechanics during gait in young individuals with varus knee alignment. *Knee*. 2014;21(3):688-693. doi:10.1016/j.knee.2014.03.004

Chapter 5

5   Summary and Future Work

5.1   Summary

This thesis developed a full-leg squatting FE model based on a general FE knee joint model (OpenKnee model) and musculoskeletal model (Lenhart 2015) and validated it by comparing the contact loads with published data. This model was used to investigate the influence of knee deformities in the frontal plane and axial plane on contact mechanics in both tibiofemoral and patellofemoral joints and knee joint rotational kinematics during squatting.

In Chapter 3, the development and validation of a full-leg squat model were reported. The LCL and lateral tibiofemoral cartilage were modified for better numerical converge of FE simulation where the Openknee model was hard to converge in higher flexion angle. The model with pre-strain has shown realistic kinematics and contact loads with more negligible differences to published data. The parametric analysis was performed to investigate outputs (contact and muscle loads) under the inputs (tibiofemoral alignment, patella thickness and patella superior-inferior position) in variations. The model with the lowest difference to the published data was chosen as the baseline model in this study.

Chapter 4 outlines the influence of frontal malalignment and miserable malalignment during squatting. The medial force ratio (medial force/total force) significantly increased in the varus-aligned and miserable malalignment model. In contrast, it decreased in the valgus-aligned model. However, the knee deformities had weak effects on total tibiofemoral and patellofemoral contact loads. Higher lateral patellar contact pressures were investigated in the varus and miserable malalignment modes, while the higher medial patellar contact pressures were presented in the valgus model. With the squat varus (controlling knees apart), lower hip adduction angle induced a higher medial force ratio in the miserable malalignment model. The model with a higher medial force ratio had a higher internal tibial rotation, which was speculated as a compensatory motion to reduce the varus orientation.

5.2   Limitations and Future Work

The FE model in this study predicted the medial/total tibiofemoral contact force with reasonable accuracy to *in vivo* experimental studies but over-estimated the magnitude of total contact loads. However, as this model was used to investigate the influence of knee deformities, knee deformities have shown weak effects on values of total contact forces, while knee deformities have shown significant influence on force and stress distributions. Like other Oxford rigs, the quadriceps tendon in this study is an individual meshed part with a single line of action instead of separated tendons, as in reality. The tendon forces therefore do not exactly match previous data. Thus, data in this study were deemed validated based on their similar tendency to previous studies, however absolute comparisons were not made due to different loading scenarios. Furthermore, the primary consideration for continued work with this FE model is additional simulations for comparisons with more experimental studies of the knee joint.

Hip and ankle joints in this study did not have bone shapes and soft tissues, and they were unable to simulate motions in reality. Thus, a separate simulation of external tibial torsion was unable to perform in this study due to the lack of anatomical hip joint. Excessive internal hip rotation with respect to the foot facing forward should be performed in the anatomical hip joint in the case of external tibial torsion. However, kinematics data in hip and ankle joints can be calculated in a subject-specific musculoskeletal model based on *in vivo* experiments. The FE model in this study could use these kinematic data as boundary conditions to simulate subject-specific analysis of daily activities.

Pre-strains were taken from previous literature, and the values were in a wide range according to different studies. In this study, we only discussed the effect of average pre-strain values and values of zero during varus and valgus rotations. An interesting future application of this FE model is to observe the sensitivity of contact mechanics to pre-strain values in a wide range taken from previous publications. Higher values of pre-strains can simulate tight ligaments and muscles as they lead to limited knee motions, while lower values of pre-strain can observe the influence of lax ligaments and muscles as they induce knee instability and osteoarthritis.

5.3 Significance

This thesis presents a finite element study based on open-resource models for observing the influence of knee deformities on knee contact force distributions. This is the first study including both frontal and axial plane deformities and their effects on both tibiofemoral and patellofemoral joints. To achieve this, the Openknee model was revised and validated based on previous literature to develop a full-leg squatting model. Through revision and validation, the model can predict the contact force distributions in the knee joint to corresponded to lower limb alignment during squatting from 20 to 90 degrees. Furthermore, general models were used to represent the knee alignment, so it is still possible to reproduce the same trends in results basing the FE model on a new cadaver.

Appendices

Appendix A: The design of simulations for SA

Runs	Hip offset (mm)	Quadriceps offset (mm)	Ankle offset (mm)	Medial force ratio during 20 to 90 degrees of flexion							
				20º	30º	40º	50º	60º	70º	80º	90º
1	5	5	5	41.93	41.07	41.29	39.97	38.35	36.56	35.36	34.29
2	5	10	10	44.06	42.66	42.49	40.87	38.74	36.86	35.55	34.34
3	5	15	15	46.13	44.22	43.76	41.71	39.23	37.16	35.75	34.45
4	5	20	20	48.20	45.96	44.88	42.63	39.72	37.54	35.97	34.51
5	5	25	25	50.12	47.22	46.17	43.47	40.27	37.95	36.18	34.72
6	5	30	30	51.98	48.47	47.17	44.45	40.92	38.43	36.46	34.86
7	5	35	35	53.97	49.94	48.07	45.29	41.56	38.86	36.75	34.93
8	10	5	10	47.11	44.94	44.36	42.40	40.10	38.09	36.71	35.53
9	10	10	15	49.10	46.45	45.54	43.23	40.56	38.37	36.91	35.60
10	10	15	20	51.11	48.11	46.63	44.07	41.01	38.72	37.09	35.67
11	10	20	25	52.84	49.24	47.88	44.92	41.53	39.14	37.30	35.85
12	10	25	30	54.66	50.45	48.77	45.87	42.16	39.58	37.55	35.93
13	10	30	35	56.58	51.85	49.56	46.64	42.77	39.99	37.83	35.99
14	10	35	5	43.16	41.85	41.76	40.40	38.62	36.91	35.71	34.63
15	15	5	15	52.14	48.77	47.31	44.77	41.87	39.56	38.06	36.79
16	15	10	20	53.98	50.19	48.43	45.54	42.31	39.91	38.24	36.83
17	15	15	25	55.66	51.29	49.56	46.43	42.81	40.30	38.43	36.97
18	15	20	30	57.39	52.48	50.38	47.29	43.42	40.72	38.66	43.42
19	15	25	35	59.28	53.83	51.11	47.99	44.00	41.14	38.91	37.06
20	15	30	5	46.10	44.04	43.56	41.89	39.94	38.10	36.87	35.76
21	15	35	10	48.45	45.81	44.84	42.76	40.41	38.43	37.06	35.86
22	20	5	20	56.85	52.28	50.27	47.01	43.62	41.12	39.37	38.01
23	20	10	25	58.48	53.38	51.24	47.89	44.10	41.48	39.55	38.08
24	20	15	30	60.22	54.56	52.00	48.71	44.67	41.88	39.76	38.18
25	20	20	35	62.02	55.87	52.68	49.38	45.24	42.27	39.99	38.15
26	20	25	5	49.09	46.26	45.36	43.37	41.24	39.32	38.01	36.91

27	20	30	10	51.30	47.96	46.64	44.24	41.70	39.62	38.19	36.99
28	20	35	15	53.62	49.77	47.86	45.16	42.20	39.96	38.41	37.13
29	25	5	25	61.38	55.47	52.90	49.37	45.39	42.67	40.69	39.19
30	25	10	30	63.08	56.65	53.64	50.13	45.94	43.04	40.86	39.24
31	25	15	35	64.83	57.95	54.30	50.78	46.47	43.43	41.09	39.22
32	25	20	5	52.12	48.55	47.16	44.88	42.56	40.51	39.16	38.05
33	25	25	10	54.28	50.16	48.44	45.71	42.98	40.79	39.31	38.13
34	25	30	15	56.45	51.95	49.55	46.64	43.45	41.13	39.53	38.22
35	25	35	20	58.42	53.35	50.93	47.45	44.00	41.55	39.74	38.42
36	30	5	30	65.97	58.79	55.26	51.56	47.21	44.19	41.99	40.37
37	30	10	35	67.72	60.06	55.94	52.15	47.71	44.56	42.18	40.29
38	30	15	5	55.17	50.80	48.98	46.40	43.88	41.72	40.31	39.21
39	30	20	10	57.27	52.41	50.22	47.19	44.27	41.99	40.42	39.30
40	30	25	15	59.31	54.07	51.34	48.07	44.72	42.29	40.64	39.29
41	30	30	20	61.17	55.33	52.61	48.87	45.23	42.70	40.84	39.52
42	30	35	25	63.07	56.73	53.58	49.87	45.81	43.13	41.12	39.63
43	35	5	35	70.64	62.22	57.59	53.54	48.96	45.72	43.29	41.38
44	35	10	5	57.90	53.08	50.88	47.91	45.21	42.91	41.45	40.34
45	35	15	10	60.26	54.67	51.98	48.73	45.57	43.17	41.56	40.45
46	35	20	15	62.12	56.13	53.10	49.51	46.00	43.51	41.77	40.47
47	35	25	20	63.92	57.41	54.27	50.32	46.47	43.86	41.92	40.61
48	35	30	25	64.20	58.72	55.18	51.26	47.05	44.26	42.18	40.71
49	35	35	30	65.56	60.22	56.04	52.10	47.68	44.73	40.99	40.83

Appendix B: The results of simulations for SA

Runs	RMSE	Average difference
1	9.43	-9.31
2	8.54	-8.47
3	7.70	-7.61
4	6.91	-6.74
5	6.23	-5.90
6	5.63	-5.07
7	5.17	-4.24
8	6.84	-6.76
9	6.10	-5.95
10	5.45	-5.11
11	4.93	-4.33
12	4.55	-3.54
13	4.35	-2.76
14	8.87	-8.78
15	4.62	-4.26
16	4.20	-3.48
17	3.93	-2.73
18	3.00	-1.19
19	4.02	-1.25
20	7.19	-7.13
21	6.30	-6.21
22	3.38	-1.85
23	3.50	-1.14
24	3.81	-0.42
25	4.32	0.28
26	5.54	-5.47
27	4.79	-4.59

28	4.19	-3.65
29	3.86	0.47
30	4.48	1.16
31	5.18	1.84
32	3.99	-3.79
33	3.49	-2.94
34	3.29	-2.05
35	3.37	-1.18
36	5.59	2.75
37	6.38	3.41
38	2.74	-2.11
39	2.76	-1.28
40	3.14	-0.45
41	3.68	0.37
42	4.38	1.20
43	7.79	5.00
44	2.33	-0.46
45	3.04	0.38
46	3.80	1.16
47	4.61	1.93
48	5.06	2.53
49	5.92	3.10

Appendix C: The optimum sequences and corresponding results

Runs	Hip offset/mm	Quadriceps offset/mm	Ankle offset/mm	RMSE	Average difference
Optimum sequence 1	30	15	15	4.29	1.41
Optimum sequence 2	30	20	35	6.22	3.18

Appendix D: Copyright Approval

📙 Anatomy of the human body
by Gray, Henry, 1825-1861; Lewis, Warren H. (Warren Harmon), 1870-1964

Publication date	1924
Usage	Public Domain Mark 1.0 ⓒ Ⓢ
Topics	Anatomy of the human body / by Henry Gray., Human anatomy, Anatomy
Publisher	Philadelphia and New York : Lea & Febiger
Collection	opensource
Language	English

Thou shalt not varus: still applicable in total knee arthroplasty?

H. B. Waterson, J. R. A. Philips, V. I. Mandalia, A. D. Toms

3D Automatic Feature Construction System for Lower Limb Alignment

Publisher: IEEE   Cite This   PDF

Qi Xing ; Wenzhen Yang ; Mark M. Theiss ; Jihui Li ; Qiang Peng ; Jim X. Chen   **All Authors**

Coronal and axial alignment relationship in Caucasian patients with osteoarthritis of the knee

Vicente J. León-Muñoz ✉, Silvio Manca, Mirian López-López, Francisco Martínez-Martínez & Fernando Santonja-Medina

744 Accesses | 3 Altmetric | Metrics

Patellofemoral Stresses during Open and Closed Kinetic Chain Exercises: An Analysis Using Computer Simulation

Zohara A. Cohen, MS, Hrvoje Roglic, MS, Ronald P. Grelsamer, MD, Jack H. Henry, MD, William N. Levine, MD, C. Van Mow, PhD, Gerard A. Ateshian, PhD   Show less ∧

117
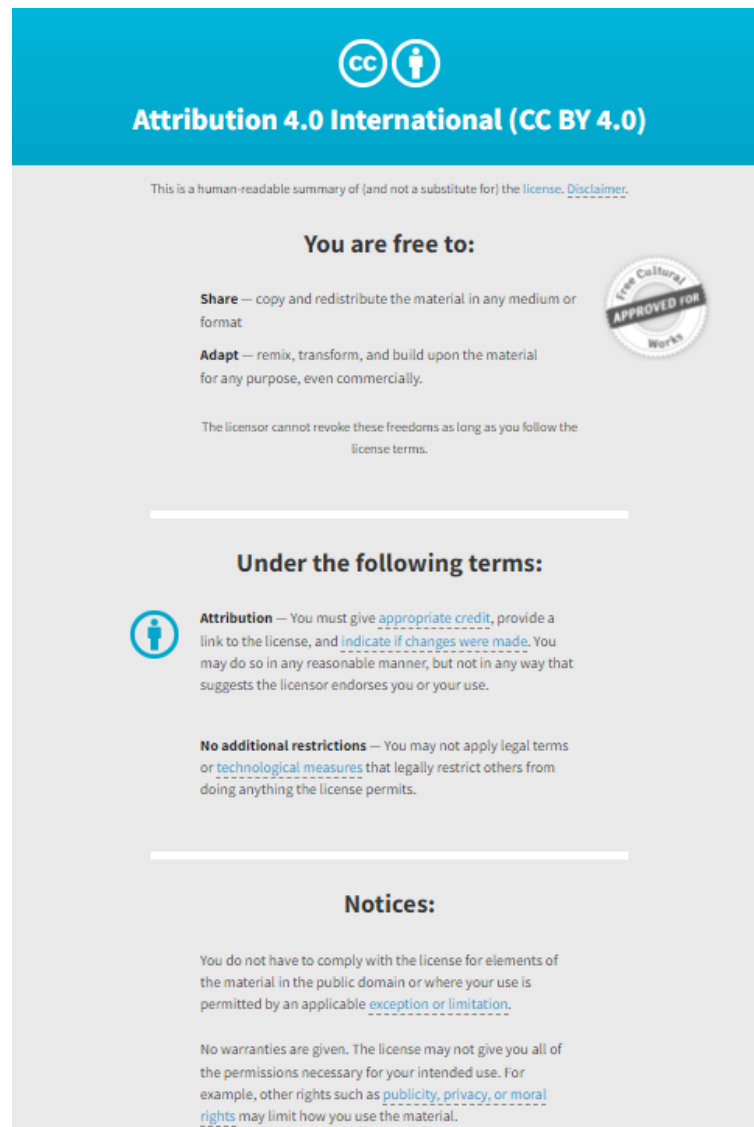
This Agreement between Western University, Canada -- Yidan Xu ("You") and
Elsevier ("Elsevier") consists of your license details and the terms and
conditions provided by Elsevier and Copyright Clearance Center.

License Number	5267640682982
License date	Mar 14, 2022
Licensed Content Publisher	Elsevier
Licensed Content Publication	Gait & Posture
Licensed Content Title	Tibiofemoral joint contact forces and knee kinematics during squatting
Licensed Content Author	Stacey M. Smith,Robert A. Cockburn,Andrea Hemmerich,Rebecca M. Li,Urs P. Wyss
Licensed Content Date	Apr 1, 2008
Licensed Content Volume	27
Licensed Content Issue	3
Licensed Content Pages	11
Start Page	376
End Page	386
Type of Use	reuse in a thesis/dissertation
Portion	figures/tables/illustrations
Number of figures/tables/illustrations	1
Format	both print and electronic
Are you the author of this Elsevier article?	No
Will you be translating?	No
Title	The Influence of Frontal and Axial plane Deformities on Contact Mechanics during Squatting: A Finite Element Study
Institution name	Western University, Canada
Expected presentation date	Apr 2022
Order reference number	1
Portions	Figure 2 right
Requestor Location	Yidan Xu 1151 Richmond St London, ON N6A 3K7 Canada Attn: Western University, Canada
Publisher Tax ID	GB 494 6272 12

118

License Number	5267640980047
License date	Mar 14, 2022
Licensed Content Publisher	Elsevier
Licensed Content Publication	Journal of the Mechanical Behavior of Biomedical Materials
Licensed Content Title	A general framework for application of prestrain to computational models of biological materials
Licensed Content Author	Steve A. Maas,Ahmet Erdemir,Jason P. Halloran,Jeffrey A. Weiss
Licensed Content Date	Aug 1, 2016
Licensed Content Volume	61
Licensed Content Issue	n/a
Licensed Content Pages	12
Start Page	499
End Page	510
Type of Use	reuse in a thesis/dissertation
Portion	figures/tables/illustrations
Number of figures/tables/illustrations	1
Format	both print and electronic
Are you the author of this Elsevier article?	No
Will you be translating?	No
Title	The Influence of Frontal and Axial plane Deformities on Contact Mechanics during Squatting: A Finite Element Study
Institution name	Western University, Canada
Expected presentation date	Apr 2022
Order reference number	1
Portions	Figure 1
Requestor Location	Yidan Xu 1151 Richmond St London, ON N6A 3K7 Canada Attn: Western University, Canada
Publisher Tax ID	GB 494 6272 12

119

Anatomy and Kinematics of the Lateral Collateral Ligament of the Knee

Brad R. Meister, MD, Stanley P. Michael, MD, Ray A. Moyer, MD, John D. Kelly, MD, Carson D. Schneck, MD, PhD   Show less ⌃

SAGE
Publishing

Anatomy and Kinematics of the Lateral Collateral Ligament of the Knee

Author: Brad R. Meister, Stanley P. Michael, Ray A. Moyer, et al
Publication: American Journal of Sports Medicine
Publisher: SAGE Publications
Date: 11/01/2000

Gratis Reuse

Permission is granted at no cost for use of content in a Master's Thesis and/or Doctoral Dissertation, subject to the following limitations. You may use a single excerpt or up to 3 figures tables. If you use more than those limits, or intend to distribute or sell your Master's Thesis/Doctoral Dissertation to the general public through print or website publication, please return to the previous page and select 'Republish in a Book/Journal' or 'Post on intranet/password-protected website' to complete your request.

BACK   CLOSE WINDOW

Curriculum Vitae

Name: Yidan Xu

Post-secondary Harbin Engineering University
Education and   Harbin, Heilongjiang, China
Degrees: 2015-2019 B.A.

          The University of Western Ontario
          London, Ontario, Canada
          2019-2021 MESc

Related Work   Teaching Assistant
Experience   The University of Western Ontario
          2020-2021